THE INFINITE ORDER SUDDEN APPROXIMATION AND THE DELTA-SHELL POTENTIAL

by

STEPHEN JOHN DANCHO
B.Sc., The University of Winnipeg, 1981

A THESIS SUBMITTED IN PARTIAL FULFILLMENT OF
THE REQUIREMENTS FOR THE DEGREE OF
MASTER OF SCIENCE
in
THE FACULTY OF GRADUATE STUDIES
DEPARTMENT OF CHEMISTRY

We accept this thesis as conforming
to the required standard

.....

.....

.....

.....

.....

.....

.....

THE UNIVERSITY OF BRITISH COLUMBIA
October 1992

In presenting this thesis in partial fulfilment of the requirements for an advanced degree at the University of British Columbia, I agree that the Library shall make it freely available for reference and study. I further agree that permission for extensive copying of this thesis for scholarly purposes may be granted by the head of my department or by his or her representatives. It is understood that copying or publication of this thesis for financial gain shall not be allowed without my written permission.

(Signatu

Department of CHEMISTRY

The University of British Columbia
Vancouver, Canada

Date OCT 13/92

DE-6 (2/88)

The Infinite Order Sudden Approximation and the Delta-Shell Potential

Abstract

The Infinite Order Sudden (IOS) approximation is applied to the collision of an atom with a diatom where the intermolecular potential is given by a delta-shell. It is shown that modelling the potential as such allows for a simpler calculation of the close-coupled equations, and using the IOS results in even further savings in calculations. Exact and IOS calculations at 300K and 1000K are compared and it is found that the IOS overestimates inelastic cross sections for both temperatures. A variety of corrections to the IOS are considered and the Energy Corrected IOS (ECIOS) approximation is shown to be the best of those studied. Other possible improvements to the IOS are proposed.

Contents

List of Tables

List of Figures

Acknowledgement

This project is actually the completion of some work that was originally started in 1984 and worked on until 1985. The work was resumed last year and it has only been with the help of some very exceptional and special people that I have been able to finish the thesis. I would like to express thanks:

To my parents Joan and John for their love and support, to Sheryl and Vince for helping me through the toughest time, to Cathy and Nigel and Connie and Dave for the phone calls and letters, to Heather and Jennifer for their drawings which I have on the wall at the office, to my Grandmother Stella who taught for 41 years in the Manitoba public school system and to my other Grandmother Catherine who I wish could be with me for this graduation.

To my friends Daniel and Jaleel for helping me keep perspective while I worked on this research, and to Valerie and Colleen.

To my Aunt Rita and Uncle Don for helping me on my move to Vancouver, to my godparents Aunt Margaret and Uncle Ed for their hospitality on my many trips between Winnipeg and Vancouver, and to my cousins and Toni and my godchild Marie.

To my students Vanessa, Leora, Nicol, Julie, Mark, Linda, Arlann, Ian, Jaye, Michael, Dave, Bron, Amie, Cathy, Christina and Carol-Anne who showed me that Science can explain a lot more than I thought it could.

To my teachers Dr. R. Wasylishen, Dr. C. Campbell, Dr. W. Mabb, Dr. H. Hutton, Dr. H. E. Duckworth, Mr. M. Selby, Mr. J. Dobrovolny, Dr. Kerr, Dr. D. Topper, Dr. C. Ridd, Dr. E. A. Ogryzlo, Dr. D. G. Fleming, Dr. M. C. L. Gerry, to my references Mr. P. K. Bingham, Mr. T. Kostynyk and Mr. C. Buffie, to my customers at Eatons', Mr. D. Feinberg, Mr. H. Delorme and Mr. D. Sloan, to my colleagues Mr. Guowei Wei, Mr. Pat Duffy and Mr. Dan Berard for help on Quantum Mechanics, DOS real mode and Unix, and to the professors in the UBC Theoretical Chemistry group,

Dr. D. P. Chong, Dr. J.A.R. Coope, Dr. G.N. Patey and Dr. B. Shizgal, for their examples of excellence in teaching and research.

To the doctors who have kept me healthy, Dr. B. Jones and Dr. G. Laws and to all the researchers in neurochemistry.

To the administration at UBC for assisting me this year, Dr. Legzdins, Head, Dept. of Chemistry, Ms. Tilly Schreinders, Graduate Secretary, Mr. Alnoor Aziz, Finance Department, Ms. Anne Grierson, Graduate Studies.

For the generous financial support from NSERC.

To Dr. R. Pincock, Graduate Admissions, Dept. of Chemistry, for giving me the chance to finish this work and for his constant assistance throughout the year.

And finally to my supervisor Dr. R. F. Snider for suggesting this fascinating topic, a topic that has kept me intrigued and confused for the last 8 years and probably will for the rest of my life. I owe a great deal of thanks to him for all the encouragement, patience and enlightening conversations throughout the years. And especially for giving me the freedom to discover this part of the world in my own way. It is indeed a pleasure to work with such a gifted educator and scientist.

1. INTRODUCTION

The study of molecular collisions is the basis for understanding a large number of chemical phenomena such as chemical reactions, gas viscosity and pressure broadening. Specifically, the equation used to describe molecular collisions is the Schrödinger equation. The aim of this thesis is to further investigate an approximation used to numerically solve the Schrödinger equation — the Infinite Order Sudden (IOS) approximation — on the scattering problem where the interaction potential between an atom and diatom is given by a delta-shell. This chapter gives a brief introduction to and describes the development of both the IOS and the delta-shell potential.

The description of the collision of an atom and a diatom requires consideration of the process before, during and after the collision. Before the collision, it is necessary to set the initial conditions, that is, to describe the state of the free atom and free diatom. The collision itself involves a choice of intermolecular potential and a set of coordinates suitable for the mathematical description of the collision process. Finally one must identify the amplitude and relative probability for the products of the collision as they are separating at infinite distance from each other. Here the latter are reported only in terms of the total degeneracy

averaged cross section into each of the allowed states. In setting up the problem, attention is paid to how the calculation can be performed with computational efficiency. [1].

The system to be studied is the collision of a homonuclear diatom, treated as a rigid rotor, with an atom. Later on, the description will be more specific and the molecular parameters will be chosen to model the argon (Ar) - nitrogen (N_2) system. Until that is done, the description is for the general collision of an atom with a rigid rotor.

A detailed description of rotational excitation caused by the collision of two molecules requires the solution of a set of close coupled equations [2]. Approximation techniques have been developed over the last 20 years in order to reduce the amount of computation required to solve these equations. The approximation technique of interest in this thesis is the IOS.

The close coupled equations are equivalent to the Schrödinger equation. The solution of the Schrödinger equation for inelastic processes involves the proper treatment of both the angular and radial motion. Depending on the basis set used, the equations are coupled via angular momentum operators or the interaction potential. The first type of operator, responsible for directional coupling, is the interaction potential, which is generally diagonal in orientation representation but non-diagonal in angular momentum representation. The second type of operator includes the orbital angular momentum operator and the translational energy operator, which, in contrast to the potential, are diagonal in angular mo-

mentum representation and non-diagonal in orientation representation. Hence, in either representation — angular momentum or orientation representation — the Schrödinger equation will couple direction dependent states.

The IOS approximation replaces the quantum numbers for rotational and centrifugal angular momentum with constant values, decoupling the set of equations in an orientational basis. This has the computational advantage of decoupling the angular and radial motion, treating the former as a constant and the Schrödinger equation then reduces to motion in one dimension (the radial motion). A standard further simplification is to use the WKB approximation [3]. An alternate approach is to look for a potential that simplifies the radial motion. In particular, the Schrödinger equation for the delta-shell potential can be reduced to treating the radial motion by matching inner and outer solutions. For the exact close coupled equations, this leaves the angular motion to be treated by matrix methods. In the IOS approximation the solution is obtained analytically so that not even matrix methods are required.

The IOS is a combination of two approximations – the Energy Sudden (ES) [4, 5] and Centrifugal Sudden (CS) [6, 7, 8, 9, 10, 11] approximations.

The Energy Sudden approximation is equivalent to assuming the rotor's orientation is fixed for the duration of the collision, but exact solutions to collision problems involving a homonuclear diatom (rotor) and an atom take into account the fact that the rotor's orientation changes during the collision process. The ES, which involves treating all rotational states as degenerate, was first used

by Drozdov [4] and Chase [5], according to an IOS history given by Parker and Pack [12].

The CS approximation involves treating the centrifugal potentials as degenerate. There were two approaches taken leading to this approximation method. One approach, taken by Pack and co-workers [6, 7, 8, 9, 10], was to treat all centrifugal potentials as degenerate *as well* as incorporating the ES in a space fixed frame of reference. The other approach, that of McGuire and Kouri [11], was to treat all centrifugal potentials as degenerate in a body fixed frame of reference.

The approach taken by Pack and collaborators was first proposed in 1963 by Takayanagi [13]. In 1970 Tsien and Pack [6] applied Takayanagi's approximation and tested it numerically on an $He - N_2$ system. The results proved encouraging and further work by Pack and co-workers [7, 8, 9, 10] led to what is now called the IOS approximation. In 1974 Pack [3] then extended his work to a body-fixed coordinate system and chose to replace the centrifugal potential operator with a single centrifugal potential which he identified as the *total* angular momentum. He termed this the CS-J approximation.

In 1972 Rabitz [14] developed an effective Hamiltonian method which succeeded in decoupling orbital and rotor angular momentum. An alternative way of achieving this decoupling was presented in 1974 by McGuire and Kouri [11]. In their work they fixed the centrifugal potential as a *final orbital angular momentum* and termed it the Coupled States (CS) approximation.

The CS of McGuire and Kouri and the CS-J of Pack were shown to be equivalent in 1977 by Parker and Pack [15] when they identified the single centrifugal potential in the CS-J as labelled with a final orbital, rather than total, angular momentum. Simultaneously Shimoni and Kouri [16, 17, 18] found that the cross sections for Pack's CS-J approximation were greatly improved when a similar substitution was made.

An equivalent approximation to the IOS is assuming constant orientations for the duration of the collision. This idea had been used as early as 1961 by Monchick and Mason [19] when it was applied as an approximation for classical scattering. In 1975 Secrest [20] and Hunter [21] simultaneously succeeded in formalizing the IOS from a fixed-angle approach. Hunter [21] further pointed out that this approach was similar to an approach taken by Curtiss in 1968 [22] who, while developing a formalism describing molecule-molecule collisions, presented an approximation where all orientations of both molecules are fixed.

The IOS is expected to be a valid approximation when the collision is sudden, that is, when the collision process occurs over such a short time duration that only negligible rotations of the molecular system can take place. To enhance its range of applicability, a variety of corrections have been considered. In this thesis, the IOS and some of the methods of correcting it are applied to a system which has a delta-shell potential – a potential having an infinite height extending over an infinitesimal width at some distance from the origin. As a basis for comparison, the degeneracy averaged cross sections of $Ar - N_2$ collisions of the

exact, IOS and IOS-corrected solutions are studied.

It would be expected that a delta-shell potential would make for conditions where the IOS approximation is valid. An interaction described by a delta-shell potential would have only an infinitesimal distance in which to act, which implies an interaction taking very little time — the basic concept of a sudden collision.

The delta-shell is first investigated in its simplest form — as a spherical potential. Then an angular dependence for the potential is introduced. The resulting exact and IOS degeneracy averaged cross sections for this potential are then derived and studied.

The savings in calculation noted above merits further investigation into whether more accurate modelling of potentials with one or more delta-shells can be accomplished.

While this thesis uses the delta shell as an interaction potential between two molecules, most work with the delta-shell has been in nuclear physics. One study found that two terms of a spin-angle expansion of an effective neutron-proton potential for deuteron-proton reactions to be well approximated using delta-shells [23]. Kok et. al. have found the delta-shell potential useful in calculating phase shifts for proton-proton and N$-\alpha$ scattering [24]. Other applications for the delta-shell have been in molecular physics [25] (studying hyperfine interactions) and in solid state physics [26] (calculating band structures).

Chapter 2 outlines the theory for the exact and IOS calculations of cross sections. Chapter 3 describes the calculational details required to obtain these

cross sections with first a spherical delta-shell and then a non-spherical delta-shell. Chapter 4 describes the parameters used, lists the cross sections obtained, and compares the values calculated for the exact, IOS, and IOS-corrected cross sections. A brief discussion of computer time saved by using the IOS, current work on the IOS, and possible future work for the delta-shell potential then follows in Chapter 5. Finally Chapter 6 concludes with a summary of the main points of this thesis.

2. ATOM-DIATOM COLLISION THEORY

2.1 Uncoupled Angular Momentum Representation

The dynamics of the collision process are governed by the Schrödinger equation. Since the collision process starts and ends with two free particles (in this case, an atom and a diatom) a positive energy solution for the Schrödinger equation is required. As well, a centre of mass co-ordinate system is chosen so only relative motion between the particles need be considered. The Schrödinger equation is

$$H\Psi(\hat{r},\mathbf{R}) = E\Psi(\hat{r},\mathbf{R}) \tag{1}$$

where H is the Hamiltonian, $\Psi(\hat{r},\mathbf{R})$ is the wave function of the system, and E is the energy.

This section solves (1) in an uncoupled representation — both the rotational angular momentum of the rotor and orbital angular momentum of the relative motion between the atom and diatom are treated independently. In the next section a coupled representation is introduced, allowing for some simplifications in both notation and in manipulation of terms.

To set up the mathematical description of an atom colliding with a diatom it is necessary to first define a set of coordinates. For this study, a space fixed centre of mass coordinate system is chosen. With reference to Figure 1 on page 10 , $\mathbf{R}$ is the position vector describing the distance from the diatom (rotor) centre of mass to the atom centre of mass, $\mathbf{r}$ is the vector between atoms in the diatom and θ is the relative angle between $\mathbf{R}$ and $\mathbf{r}$. In this paper, three-dimensional vectors will be designated in bold and the following convention will be used:

$$\begin{aligned} \mathbf{r} &= r\hat{r} \\ \mathbf{R} &= R\hat{R} \end{aligned} \tag{2}$$

where r, R denote the magnitude of vectors $\mathbf{r}, \mathbf{R}$ and $\hat{r}, \hat{R}$ denote the direction unit vectors of $\mathbf{r}, \mathbf{R}$ respectively.

In order to solve this equation, a specification of the Hamiltonian H is needed. We are interested only in the rotational aspects of the diatom so the rigid rotor approximation for the diatom is assumed, with both electronic and vibrational contributions being neglected. Since the rotor is rigid, the magnitude of $\mathbf{r}$ will not change so the potential will be only a function of $\mathbf{R}$ and the direction $\hat{r}$.

There are thus two types of motion to be considered for the Hamiltonian. The first is that of the spinning rotor and the second is the relative motion of the atom with respect to the diatom centre of mass. The Hamiltonian H_1 for the rotor is

$$H_1 = \frac{J_r^2}{2I} \tag{3}$$

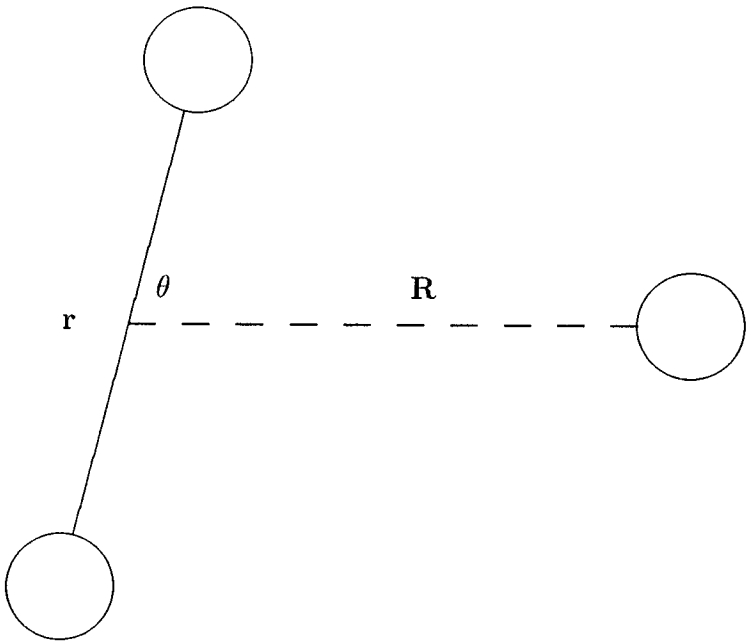

FIGURE 1: Coordinates used for diatom-atom collision problem.

where J_r is the angular momentum operator of the rotor and I is the moment of inertia of the rotor. Next, an appropriate complete set of states for the expansion of Ψ is chosen. Since in free motion, the spinning rotor motion is independent of that of the orbital motion of the atom around the diatom, Ψ can be expanded in a complete set of rotational eigenfunctions, each expressed as a product of eigenfunctions of the two rotational motions. These comprise a discrete, as opposed to continuous, basis. The eigenvectors of J_r^2 are the spherical harmonics $Y_{jm}(\hat{r})$ and so

$$J_r^2 Y_{jm}(\hat{r}) = j(j+1)\hbar^2 Y_{jm}(\hat{r}) \tag{4}$$

where j is the quantum number for magnitude of rotor angular momenta and m is the quantum number representing its component along the z-axis.

The Hamiltonian H_2 for the atom-diatom relative motion is

$$H_2 = -\frac{\hbar^2}{2\mu}\nabla_{\mathbf{R}}^2 \tag{5}$$

where μ is the reduced mass. In the Ar-N_2 system the reduced mass μ is

$$\mu = \frac{m_{Ar} m_{N_2}}{(m_{Ar} + m_{N_2})}, \tag{6}$$

m_{Ar} being the atomic mass of Ar, m_{N_2} the molecular mass of N_2.

The eigenvectors of H_2 are $e^{i\mathbf{k}\cdot\mathbf{R}}$ so that

$$H_2 e^{i\mathbf{k}\cdot\mathbf{R}} = \frac{\hbar^2 k^2}{2\mu} e^{i\mathbf{k}\cdot\mathbf{R}} \tag{7}$$

where $e^{i\mathbf{k}\cdot\mathbf{R}}$ is a plane wave of momentum $\hbar\mathbf{k}$. For the scattering problem to be studied, one assumes an incoming plane wave in initial momentum state $\hbar\mathbf{k}'$ and rotor state $j'm'$.

The expression for the total Hamiltonian H can be written

$$H = H_1 + H_2 + V(\hat{r}, \mathbf{R}) \tag{8}$$

where $V(\hat{r}, \mathbf{R})$ is the atom-diatom potential. This potential can be written in the form

$$V(\hat{r}, \mathbf{R}) = \sum_L V_L(R) P_L(\cos\theta) \tag{9}$$

where P_L is the Lth Legendre function and $V_L(R)$ its expansion coefficient.

Converting $\nabla^2_{\mathbf{R}}$ to polar co-ordinates R, φ and ϕ, the total Hamiltonian H given by (8) becomes:

$$H = \frac{-\hbar^2}{2\mu}\left[\frac{1}{R^2}\frac{\partial}{\partial R}R^2\frac{\partial}{\partial R} - \frac{\Lambda^2}{\hbar^2 R^2}\right] + \frac{J_r^2}{2I} + V(\hat{r}, \mathbf{R}) \tag{10}$$

where Λ^2 is the operator for the square of the orbital angular momentum, which is, in orientation representation:

$$\Lambda^2 = -\hbar^2\left[\frac{1}{\sin\varphi}\frac{\partial}{\partial\varphi}\left(\sin\varphi\frac{\partial}{\partial\varphi}\right) + \frac{1}{\sin^2\theta}\frac{\partial^2}{\partial\phi^2}\right]. \tag{11}$$

The eigenvectors of Λ^2 are the spherical harmonics $Y_{\lambda s}(\hat{r})$, λ being the quantum number of angular momentum magnitude for the orbital angular momenta and s is its component along the z-axis. Hence

$$\Lambda^2 Y_{\lambda s}(\hat{R}) = \lambda(\lambda+1) Y_{\lambda s}(\hat{R}). \tag{12}$$

In the orientation representation it is required to solve (1) for Ψ. With the expansion as given by (12) and (4), Ψ can now be written:

$$\Psi(\hat{r}, \mathbf{R}) = \sum_{jm\lambda s} Y_{jm}(\hat{r}) Y_{\lambda s}(\hat{R}) \psi_{\alpha\alpha'}(R) \tag{13}$$

where α is an abbreviation for the set of quantum numbers j, m, λ and s, α' the initial set of quantum numbers and $\psi_{\alpha\alpha'}(R)$ is the coefficient for this expansion for a given α and α'.

Putting (13) and (10) into (1) and operating on the left of each equation by

$$\int\int Y^*_{jm}(\hat{r})Y^*_{\lambda s}(\hat{R})d\hat{r}d\hat{R} \tag{14}$$

gives the set of close coupled equations in an uncoupled angular momentum representation:

$$\frac{\hbar^2}{2\mu}\left[\frac{d^2}{dR^2}+\frac{2}{R}\frac{d}{dR}+k_j^2-\frac{\lambda(\lambda+1)}{R^2}\right]\psi_{\alpha\alpha'}(R)=\sum_{\alpha''}V_{\alpha\alpha''}\psi_{\alpha''\alpha'}(R) \tag{15}$$

where

$$k_j^2=\frac{2\mu}{\hbar^2}\left[E-\frac{j(j+1)\hbar^2}{2I}\right] \tag{16}$$

and

$$V_{\alpha\alpha''}=\int\int Y^*_{jm}(\hat{r})Y^*_{\lambda s}(\hat{R})V(\hat{r},\mathbf{R})Y_{j''m''}(\hat{r})Y_{\lambda''s''}(\hat{R})d\hat{r}d\hat{R}. \tag{17}$$

Next the boundary conditions are set for Ψ and its expansion coefficients $\psi_{\alpha\alpha'}$. As well, Ψ and all the $\psi_{\alpha\alpha'}$'s must be regular at the origin. Finally the $\psi_{\alpha\alpha'}$'s must be chosen so that Ψ satisfies the incoming wave condition, ie., the solution of (1) starting with planar motion in rotational state $j', m', \mathbf{k}'$ (eigenstates of H_1 and H_2). So

$$\Psi=e^{i\mathbf{k}'\cdot\mathbf{R}}Y_{j'm'}(\hat{r})+\Psi_{\text{scatt}}. \tag{18}$$

where Ψ_{scatt} is the scattered part of Ψ. The experimental observable to be examined in this thesis is the cross section (which will be defined in Section 2.3).

In order to calculate the cross section it is necessary to determine the amplitude $f_{jm\,;j'm'}(\hat{R})$ of the spherical wave in the final state jm. (18) is rewritten as

$$\Psi \sim e^{i\mathbf{k}'\cdot\mathbf{R}}Y_{jm}(\hat{r}) + \sum_{jm} Y_{jm}(\hat{r}) f_{jm\,;j'm'}(\hat{R})\frac{e^{ik_jR}}{R}, \quad R \to \infty. \tag{19}$$

We make a spherical harmonic expansion of the initial plane wave,

$$e^{i\mathbf{k}'\cdot\mathbf{R}} = 4\pi \sum_{\lambda s} i^{\lambda} j_{\lambda}(k'R) Y_{\lambda s}(\hat{R}) Y^*_{\lambda s}(\hat{k}') \tag{20}$$

where $j_\lambda(k'R)$ is a Bessel function of order λ, and k' is shorthand for $k_{j'}$.

Thus the wave function with appropriate initial conditions is expanded as in (13) with expansion coefficients

$$\psi_{\alpha\alpha'}(R) = 4\pi \sum_{\lambda' s'} i^{\lambda'} \chi_{\alpha\alpha'}(R) Y^*_{\lambda' s'}(\hat{k}'). \tag{21}$$

The $\chi_{\alpha\alpha'}(R)$ functions at large R satisfy the coupled equations (15) with boundary conditions

$$\chi_{\alpha\alpha'}(R) \sim j_{\lambda'}(k'R)\delta_{\alpha\alpha'} - \frac{1}{2}\sqrt{\frac{k_j}{k_{j'}}} T_{\alpha\alpha'} h_\lambda(k_j R) \tag{22}$$

where $\delta_{\alpha\alpha'}$ is the Kronecker symbol, to match the incoming plane wave and the outgoing spherical wave of equation (18) in terms of the transition matrix element $T_{\alpha\alpha'}$. $h_\lambda(kR)$ is the Hankel function and its asymptotic solution as $R \to \infty$ is given by:

$$h_\lambda(k_j R) \sim -\frac{i}{k_j R} e^{i(k_j R - \lambda\pi/2)}, \qquad R \to \infty. \tag{23}$$

Using (23) in (22) yields

$$\chi_{\alpha\alpha'}(R) \sim j_{\lambda'}(k'R)\delta_{\alpha\alpha'} + \frac{i}{2\sqrt{k_j k'}} T_{\alpha\alpha'} \frac{e^{i(k_j R - \lambda\pi/2)}}{R} \tag{24}$$

so that comparison of (19) and (24) leads to the following relationship between $f_{\alpha\alpha'}$ and $T_{\alpha\alpha'}$:

$$f_{\alpha\alpha'} = \frac{2\pi i}{\sqrt{k_j k'}} T_{\alpha\alpha'}. \tag{25}$$

In conclusion it is noted that to attain the goal of a calculation of the atom-diatom collision cross section, it is necessary to solve the set of differential equations (15) which are coupled by potential matrix elements $V_{\alpha\alpha'}$, subject to the boundary conditions of being regular at the origin and asymptotically of the form of (22).

2.2 The Total-J Representation

Since H is invariant with respect to a rotation of the co-ordinate system, the total angular momentum is conserved. Hence states having a *total* angular momentum J are not coupled to states with a different total angular momentum J' and the Schrödinger equation is decoupled into different total angular momentum components.

The total angular momentum operator $J = \Lambda + J_r$ has eigenfunctions

$$Y_{j\lambda}^{JM}(\hat{r}, \hat{R}) = \sum_m \sum_s (jm\lambda s \mid j\lambda JM) Y_{jm}(\hat{r}) Y_{\lambda s}(\hat{R}) \tag{26}$$

where $(jm\lambda s \mid j\lambda JM)$ is a Clebsch-Gordan coefficient[27].

The expansion coefficients $\chi_{j\lambda;j'\lambda'}^{JM}(R)$ of the scattering wave function (22) in this angular momentum representation satisfy

$$\hbar\Psi_{\hbar\mathbf{k}'j'm'}(\hat{r},\mathbf{R}) = 4\pi \sum_{\substack{j\lambda JM \\ \lambda' s'}} i^{\lambda} Y_{j\lambda}^{JM}(\hat{r},\hat{R}) \chi_{j\lambda;j'\lambda'}^{J}(R) \times (j'\lambda' JM \mid j'm'\lambda' s') Y_{\lambda' s'}^{*}(\hat{k}'). \tag{27}$$

Performing a similar set of operations as outlined in the previous section only this time operating on the left of each equation by

$$\int\int Y_{j'''\lambda'''}^{*JM}(\hat{r},\hat{R}) d\hat{r} d\hat{R} \tag{28}$$

gives the set of close coupled equations in the coupled angular momentum representation:

$$\frac{\hbar^2}{2\mu}\left[\frac{d^2}{dR^2} + \frac{2}{R}\frac{d}{dR} + k_j^2 - \frac{\lambda(\lambda+1)}{R^2}\right] \chi_{j\lambda;j'\lambda'}^{J}(R) = \sum_{j''\lambda''} V_{j\lambda;j''\lambda''}^{J} \chi_{j''\lambda'';j'\lambda'}^{J}(R) \tag{29}$$

where

$$V_{j\lambda;j''\lambda''}^{J} = \int\int Y_{j\lambda}^{*JM}(\hat{r},\hat{R}) V(\hat{r},\mathbf{R}) Y_{j''\lambda''}^{JM}(\hat{r},\hat{R}) d\hat{r} d\hat{R}. \tag{30}$$

For the potential of (9) we are interested in determining an angular momentum representation. First the expression for the uncoupled representation, that is, for the V-matrix element $\left\langle jm\lambda s \middle| V \middle| j'm'\lambda' s' \right\rangle$ is determined. This quantity is then transformed into a total-J representation. It is then shown that rotational invariance of the potential allows certain simplifications in the total-J representation.

The potential given by (9) is in an orientation representation. The *angular momentum* representation of V,given in terms of the orientation representation,

is:

$$\left\langle jm\lambda s\middle|V\middle|j'm'\lambda's'\right\rangle = \int\int\int\int\left\langle jm\lambda s\middle|\hat{r};\hat{R}\right\rangle\left\langle\hat{r};\hat{R}\middle|V(R)\middle|\hat{r}';\hat{R}'\right\rangle\left\langle\hat{r}';\hat{R}'\middle|j'm'\lambda's'\right\rangle d\hat{r}d\hat{R}d\hat{r}'d\hat{R}'. \tag{31}$$

Using 4.6.6 of Edmonds[27], ie.,

$$P_L(\cos\theta) = \frac{4\pi}{2L+1}\sum_{\mu} Y_{L\mu}(\hat{r})Y^*_{L\mu}(\hat{R}) \tag{32}$$

(9) can be written as

$$\langle\hat{r};\hat{R}|V(R)|\hat{r}';\hat{R}'\rangle = \sum_{L\mu} V_L(R)\frac{4\pi}{2L+1}Y_{L\mu}(\hat{r})Y^*_{L\mu}(\hat{R})\delta(\hat{R}-\hat{R}')\delta(\hat{r}-\hat{r}'). \tag{33}$$

Using the following defined phase conventions [28]

$$\left\langle jm\lambda s\middle|\hat{r};\hat{R}\right\rangle = (-i)^j Y^*_{jm}(\hat{r})(-i)^{\lambda}Y^*_{\lambda s}(\hat{R}) \tag{34}$$

and substituting (33) into (31), one obtains the following equation:

$$\left\langle jm\lambda s\middle|V\middle|j'm'\lambda's'\right\rangle = \int\int(-i)^j Y^*_{jm}(\hat{r})(-i)^{\lambda}Y^*_{\lambda s}(\hat{R}) \times\sum_{L\mu} V_L(R)\frac{4\pi}{2L+1}Y_{L\mu}(\hat{r})Y^*_{L\mu}(\hat{R})i^{j'}Y_{j'm'}(\hat{r})(i)^{\lambda'}Y_{\lambda's'}(\hat{R})d\hat{r}d\hat{R}. \tag{35}$$

By using the following two properties of the spherical harmonics, (equations 2.5.6 and 4.6.3 of Edmonds [27])

$$Y^*_{L\mu}(\hat{R}) = (-)^{\mu}Y_{L-\mu}(\hat{R}) \tag{36}$$

and

$$\int Y_{j-m}(\hat{r})Y_{L\mu}(\hat{r})Y_{j'm'}(\hat{r})d\hat{r} =$$
$$\sqrt{\frac{(2j+1)(2L+1)(2j'+1)}{4\pi}}\begin{pmatrix} j & L & j' \\ -m & \mu & m' \end{pmatrix}\begin{pmatrix} j & L & j' \\ 0 & 0 & 0 \end{pmatrix}, \quad (37)$$

(35) can be written as

$$\left\langle jm\lambda s\middle|V(R)\middle|j'm'\lambda's'\right\rangle = i^{j'+\lambda'-j-\lambda}\sqrt{(2j+1)(2j'+1)(2\lambda+1)(2\lambda'+1)}$$
$$\times\sum_{L\mu}(-)^{-\mu-m-s}V_L(R)\begin{pmatrix} j & L & j' \\ 0 & 0 & 0 \end{pmatrix}\begin{pmatrix} \lambda & L & \lambda' \\ 0 & 0 & 0 \end{pmatrix}$$
$$\times\begin{pmatrix} j & L & j' \\ -m & \mu & m' \end{pmatrix}\begin{pmatrix} \lambda & L & \lambda' \\ -s & -\mu & s' \end{pmatrix}. \quad (38)$$

Equation (38) is the expression for the V-matrix element in the uncoupled representation. Eight quantum numbers, $j, m, \lambda, s, j', m', \lambda'$ and s' are required to label each element. The total-J representation, however, can reduce the number of labels needed to five, ie., J, j, λ, j' and λ', as will be shown. In order to arrive at an expression for the total-J V-matrix element, the uncoupled V-matrix expression is converted to the coupled expression through the following transformation:

$$\left\langle j\lambda JM\middle|V(R)\middle|j'\lambda'J'M'\right\rangle =$$
$$\sum_{msm''s''}\left\langle j\lambda JM\middle|jm\lambda s\right\rangle\left\langle jm\lambda s\middle|V(R)\middle|j''m''\lambda''s''\right\rangle\left\langle j''m''\lambda''s''\middle|j'\lambda'J'M'\right\rangle. \quad (39)$$

Using the phase convention given by equation 3.7.3 of Edmonds [27] which relates the Clebsch-Gordan coefficients with the 3-j symbols through the following:

$$\left\langle j\lambda JM\middle|jm\lambda s\right\rangle = (-)^{j-\lambda+M}\begin{pmatrix} j & \lambda & J \\ m & s & -M \end{pmatrix}\sqrt{2J+1} \quad (40)$$

and using (38) for $\left\langle jm\lambda s\middle|V(R)\middle|j'm'\lambda's'\right\rangle$, (39) can be written

$$\left\langle j\lambda JM\middle|V(R)\middle|j'\lambda'J'M'\right\rangle = \sum_{msm's'}(-)^{j-\lambda+M}\sqrt{2J+1}\begin{pmatrix} j & \lambda & J \\ m & s & -M \end{pmatrix}$$
$$\times i^{j'+\lambda'-j-\lambda}\sqrt{(2j+1)(2j'+1)(2\lambda+1)(2\lambda'+1)}$$
$$\times\sum_{L\mu}V_L(R)\begin{pmatrix} j & L & j' \\ 0 & 0 & 0 \end{pmatrix}\begin{pmatrix} \lambda & L & \lambda' \\ 0 & 0 & 0 \end{pmatrix}\begin{pmatrix} j & L & j' \\ -m & \mu & m' \end{pmatrix}\begin{pmatrix} \lambda & L & \lambda' \\ -s & -\mu & s' \end{pmatrix}$$
$$\times(-)^{-\mu-m-s}(-)^{j'-\lambda'+M'}\sqrt{2J'+1}\begin{pmatrix} j' & \lambda' & J' \\ m' & s' & -M' \end{pmatrix}. \qquad (41)$$

Two symmetry property of the 3-j symbols, given by equations 3.7.6 and 3.7.5 of Edmonds [27], ie.,

$$\begin{pmatrix} j' & \lambda' & J' \\ m' & s' & -M' \end{pmatrix} = (-)^{j'+\lambda'+J'}\begin{pmatrix} j' & \lambda' & J' \\ -m' & -s' & M' \end{pmatrix} \qquad (42)$$

and

$$\begin{pmatrix} j & L & j' \\ -m & \mu & m' \end{pmatrix} = (-)^{j+L+j'}\begin{pmatrix} j & j' & L \\ -m & m' & \mu \end{pmatrix} \qquad (43)$$

allows (41) to be written as

$$\left\langle j\lambda JM\middle|V(R)\middle|j'\lambda'J'M'\right\rangle = \sqrt{(2j+1)(2j'+1)(2\lambda+1)(2\lambda'+1)(2J+1)(2J'+1)}$$
$$\times\sum_{L}i^{j'+\lambda'-j-\lambda}V_L(R)\begin{pmatrix} j & L & j' \\ 0 & 0 & 0 \end{pmatrix}\begin{pmatrix} \lambda & L & \lambda' \\ 0 & 0 & 0 \end{pmatrix}$$
$$\times\sum_{m's'}(-)^{j+j'+J'+M+M'}\begin{pmatrix} j' & \lambda' & J' \\ -m' & -s' & M' \end{pmatrix}$$
$$\times\sum_{\mu ms}(-)^{m-s+\mu+j+\lambda+L}\begin{pmatrix} \lambda' & \lambda & L \\ s' & -s & -\mu \end{pmatrix}\begin{pmatrix} j & j' & L \\ -m & m' & \mu \end{pmatrix}\begin{pmatrix} j & \lambda & J \\ m & s & -M \end{pmatrix}. \qquad (44)$$

Further simplification in (44) is possible by considering equation 6.2.8 from

Edmonds [27], where

$$\sum_{\mu_1\mu_2\mu_3}(-)^{\mu_1+\mu_2+\mu_3+l_1+l_2+l_3}\begin{pmatrix} j_1 & l_2 & l_3 \\ m_1 & \mu_2 & -\mu_3 \end{pmatrix} \times\begin{pmatrix} l_1 & j_2 & l_3 \\ -\mu_1 & m_2 & \mu_3 \end{pmatrix}\begin{pmatrix} l_1 & l_2 & j_3 \\ \mu_1 & -\mu_2 & m_3 \end{pmatrix} = \begin{Bmatrix} j_1 & j_2 & j_3 \\ l_1 & l_2 & l_3 \end{Bmatrix}\begin{pmatrix} j_1 & j_2 & j_3 \\ m_1 & m_2 & m_3 \end{pmatrix} \tag{45}$$

where $j_1, j_2, j_3, m_1, m_2, m_3, l_1, l_2$ and l_3 are the arbitrary indices used in Edmonds [27] and

$$\begin{Bmatrix} j_1 & j_2 & j_3 \\ l_1 & l_2 & l_3 \end{Bmatrix} \tag{46}$$

is the 6-j symbol defined by Edmonds [27]. (44) can be written

$$\begin{aligned}\left\langle j\lambda JM\middle|V(R)\middle|j'\lambda' J'M'\right\rangle &= \sqrt{(2j+1)(2j'+1)(2\lambda+1)(2\lambda'+1)(2J+1)(2J'+1)} \\ &\times\sum_L i^{j'+\lambda'-j-\lambda}V_L(R)\begin{pmatrix} j & L & j' \\ 0 & 0 & 0 \end{pmatrix}\begin{pmatrix} \lambda & L & \lambda' \\ 0 & 0 & 0 \end{pmatrix} \\ &\times\sum_{m's'}(-)^{j+j'+J'+M+M'}\begin{Bmatrix} \lambda' & j' & J \\ j & \lambda & L \end{Bmatrix}\begin{pmatrix} j' & \lambda' & J' \\ -m' & -s' & M' \end{pmatrix}\begin{pmatrix} \lambda' & j' & J \\ s' & m' & -M \end{pmatrix}.\end{aligned} \tag{47}$$

Using (42) and equation 3.7.8 from Edmonds [27], ie. ,

$$\sum_{m_1m_2}\begin{pmatrix} j_1 & j_2 & j_3 \\ m_1 & m_2 & m_3 \end{pmatrix}\begin{pmatrix} j_1 & j_2 & j_3' \\ m_1 & m_2 & m_3' \end{pmatrix} = (2j_3+1)^{-1}\delta_{m_3m_3'}\delta_{j_3j_3'}\delta_{j_1j_2j_3} \tag{48}$$

where $\delta_{j_1j_2j_3}=1$ if j_1, j_2 and j_3 satisfy the triangular conditions and $\delta_{j_1j_2j_3}=0$ otherwise, (47) is further reduced to

$$\left\langle j\lambda JM\middle|V(R)\middle|j'\lambda'J'M'\right\rangle = \sqrt{(2j+1)(2j'+1)(2\lambda+1)(2\lambda'+1)(2J+1)(2J'+1)}$$
$$\times\sum_L i^{j'+\lambda'-j-\lambda}V_L(R)\begin{pmatrix} j & L & j' \\ 0 & 0 & 0\end{pmatrix}\begin{pmatrix} \lambda & L & \lambda' \\ 0 & 0 & 0\end{pmatrix}$$
$$\times(-)^{j+j'+J+M+M'}(2J+1)^{-1}\delta_{JJ'}\delta_{MM'}\begin{Bmatrix} \lambda' & j' & J \\ j & \lambda & L\end{Bmatrix}. \qquad (49)$$

Finally, using the symmetry of the 6-j symbols as given by equation 6.2.4 of Edmonds [27],

$$\begin{Bmatrix} j_1 & j_2 & j_3 \\ j_4 & j_5 & j_6\end{Bmatrix} = \begin{Bmatrix} j_3 & j_1 & j_2 \\ j_6 & j_4 & j_5\end{Bmatrix} \qquad (50)$$

the following expression is obtained:

$$\left\langle j\lambda JM\middle|V(R)\middle|j'\lambda'J'M'\right\rangle = i^{j'+\lambda'-j-\lambda}\sqrt{(2j+1)(2j'+1)(2\lambda+1)(2\lambda'+1)}$$
$$\times\sum_L V_L(R)(-)^{J+j+j'}\begin{pmatrix} j & L & j' \\ 0 & 0 & 0\end{pmatrix}\begin{pmatrix} \lambda & L & \lambda' \\ 0 & 0 & 0\end{pmatrix}\begin{Bmatrix} J & \lambda' & j' \\ L & j & \lambda\end{Bmatrix}. \qquad (51)$$

Note that the V matrix element is independent of M, the projection of the total angular momentum on the z-axis. This is expected of any rotationally invariant (scalar) quantity such as the interaction between atom and diatom. Secondly it is noted that the total angular momentum J is the same in the initial and final state. For this reason J need not appear in *both* initial and final states but can be denoted as a superscript on the operator V, ie., V^J.

Hence the V-matrix element $\left\langle j\lambda JM\middle|V(R)\middle|j'\lambda'J'M'\right\rangle$ may be written as $\langle j\lambda|V^J|j'\lambda'\rangle$. This new representation, having taken advantage of the simplifications made possible by the rotational invariance of the interaction potential, now requires only five indices instead of the original eight.

As done in (22), an incoming plane wave of constant flux in initial momentum state $\hbar\mathbf{k}'$ and rotor state $j'm'$ is assumed for the boundary conditions for Ψ. It is also required that the solution be regular at the origin and have the asymptotic form

$$\chi^J_{j\lambda\,;j'\lambda'}(R) \sim j_{\lambda'}(k'R)\delta_{jj'}\delta_{\lambda\lambda'} + \frac{i}{2\sqrt{kk'}}\frac{e^{ikR}}{R}T^J_{j\lambda;j'\lambda'}, \quad R \to \infty. \tag{52}$$

2.3 Cross Sections in the Total-J Representation

The cross section is defined as the ratio of outgoing spherical flux to incoming planar flux. Planar flux is defined as the number of incident particles crossing a unit surface area placed perpendicular to the direction of propagation per unit time while spherical flux is defined as the number of outgoing particles scattering through solid angle $d\Omega$ per unit time.

The incoming plane wave $e^{i\mathbf{k}'\cdot\mathbf{R}}$ has flux F_{incoming} [29]

$$F_{\text{incoming}} = \frac{\hbar k'}{\mu} \tag{53}$$

Putting (22) in (21) and then into (13), and substituting $\hat{k}$ for $\hat{R}$ results in the following expression for the spherical flux F_{outgoing} for the outgoing spherical wave e^{ikR}/R [29]:

$$F_{\text{outgoing}} = \frac{\hbar k'}{\mu}\left|(4\pi)\frac{i}{2\sqrt{k_j k_{j'}}}\sum_{\lambda s\lambda' s'} Y_{\lambda s}(\hat{k})T_{jm\lambda s\,;j'm'\lambda' s'}Y^*_{\lambda' s'}(\hat{k}')\right|^2 d\Omega \tag{54}$$

From (53) and (54) the differential cross section $\sigma_{jm\leftarrow j'm'}(\hat{k})$ is:

$$\sigma_{jm\leftarrow j'm'}(\hat{k}) = \frac{4\pi^2}{k_{j'}^2}\left|\sum_{\lambda s\lambda' s'} Y_{\lambda s}(\hat{k}) T_{jm\lambda s\,;\,j'm'\lambda' s'} Y^*_{\lambda' s'}(\hat{k}')\right|^2 \tag{55}$$

In this work only the ***total*** *degeneracy averaged* cross section, $\sigma^{\rm TDA}_{j\leftarrow j'}$, ie., the differential cross section integrated over all angles and summed over all m's,

$$\sigma^{\rm TDA}_{j\leftarrow j'} = \frac{1}{2j'+1}\sum_{mm'}\int \sigma_{jm\leftarrow j'm'}(\hat{k})d\hat{k} \tag{56}$$

is to be calculated.

It is possible to simplify the resulting total cross section by choosing the incoming direction $\hat{k}'$ as the z-axis. Since

$$Y_{\lambda s}(\hat{k}') = Y_{\lambda s}(\hat{z}) = \sqrt{\frac{2\lambda+1}{4\pi}}\delta_{s0} \tag{57}$$

the expression for $\sigma^{\rm TDA}_{j\leftarrow j'}$ becomes:

$$\begin{aligned}\sigma^{\rm TDA}_{j\leftarrow j'} &= \frac{4\pi^2}{k'^2(2j'+1)}\sum_{mm'}\int\sum_{\lambda s\lambda'} T_{jm\lambda s\,;\,j'm'\lambda' 0}(E) Y_{\lambda s}(\hat{k})\sqrt{\frac{2\lambda'+1}{4\pi}} \\ &\quad\times\sum_{\lambda'' s''\lambda'''} Y^*_{\lambda'' s''}(\hat{k}) T^*_{jm\lambda'' s''\,;\,j'm'\lambda''' 0}(E)\sqrt{\frac{2\lambda'''+1}{4\pi}}d\hat{k}\end{aligned} \tag{58}$$

Using the orthonormality of the spherical harmonics,

$$\int Y_{\lambda s}(\hat{k}) Y^*_{\lambda'' s''}(\hat{k})d\hat{k} = \delta_{\lambda\lambda''}\delta_{ss''} \tag{59}$$

the expression for the total cross section now is

$$\sigma^{\rm TDA}_{j\leftarrow j'} = \frac{\pi}{k'^2(2j'+1)}\sum_{\lambda s\lambda' mm'}\left|T_{jm\lambda s\,;\,j'm'\lambda' 0}(E)\right|^2(2\lambda'+1) \tag{60}$$

Finally, then, we seek the appropriate form for $\sigma^{\rm TDA}_{j\leftarrow j'}$ in the total-J representation. Using the identity

$$\Big\langle jm\lambda s\Big|T(E)\Big|j'm'\lambda's'\Big\rangle = \sum_{JMJ'M'}\Big\langle jm\lambda s\Big|JMj\lambda\Big\rangle\Big\langle JMj\lambda\Big|T(E)\Big|J'M'j'\lambda'\Big\rangle\Big\langle J'M'j'\lambda'\Big|j'm'\lambda's'\Big\rangle \quad (61)$$

and (40), (60) in the total J representation is:

$$\sigma^{\rm TDA}_{j\leftarrow j'} = \frac{\pi}{k'^2(2j'+1)}\sum_{mm'}\sum_{\lambda s\lambda' s'}\Bigg|\sum_{JMJ'M'}(-)^{j+j'-\lambda'-\lambda}(2J+1) \times\begin{pmatrix} j & \lambda & J\\ m & s & -M\end{pmatrix}\begin{pmatrix} j' & \lambda' & J'\\ m' & s' & -M'\end{pmatrix}\Big\langle j\lambda\Big|T^{JM}\Big|j'\lambda'\Big\rangle\Bigg|^2$$

$$= \frac{\pi}{k'^2}\sum_{\lambda\lambda'}\sum_{JMJ'M'}(2J+1)^2\Big\langle j\lambda\Big|T^{JM}\Big|j'\lambda'\Big\rangle\Big\langle j'\lambda'\Big|T^{JM\dagger}\Big|j\lambda\Big\rangle \times\sum_{mm'ss'}\begin{pmatrix} j & \lambda & J\\ m & s & -M\end{pmatrix}\begin{pmatrix} j' & \lambda' & J'\\ m' & s' & -M'\end{pmatrix} \times\sum_{J''M''J'''M'''}\begin{pmatrix} j & \lambda & J''\\ m & s & -M''\end{pmatrix}\begin{pmatrix} j' & \lambda' & J'''\\ m' & s' & -M'''\end{pmatrix} \quad (62)$$

where the notation

$$\Big\langle j\lambda\Big|T^J\Big|j'\lambda'\Big\rangle = \Big\langle JMj\lambda\Big|T(E)\Big|J'M'j'\lambda'\Big\rangle\,\delta_{MM'} \quad (63)$$

has been introduced since $J = J'$ and $M = M'$ by conservation of angular momentum.

Using 3.7.8 from Edmonds[27], ie.,

$$\sum_{ss'}\begin{pmatrix} j & \lambda & J\\ m & s & -M\end{pmatrix}\begin{pmatrix} j & \lambda & J'\\ m & s & -M'\end{pmatrix} = \frac{1}{2J+1}\delta_{JJ'}\delta_{MM'} \quad (64)$$

the following expression for the degeneracy averaged cross section for the $j \leftarrow j'$ transition in the total-J representation is obtained:

$$\begin{aligned}\sigma^{\mathrm{TDA}}_{j\leftarrow j'} &= \frac{\pi}{k'^2(2j'+1)}\sum_{\lambda\lambda'}\sum_{JM}\left|\left\langle j\lambda\left|T^{JM}\right|j'\lambda'\right\rangle\right|^2 \\ &= \frac{\pi}{k'^2(2j'+1)}\sum_{\lambda\lambda'}\sum_{J}(2J+1)\left|\left\langle j\lambda\left|T^{J}\right|j'\lambda'\right\rangle\right|^2 \qquad (65)\end{aligned}$$

It is this quantity which will be used as the basis for both the exact and IOS results.

2.4 The IOS Approximation

The close coupled equations (29) consist of a set of coupled differential equations which must be simultaneously integrated to obtain a solution. For example, expanding (29) to 100 partial waves and ten rotor states leaves over a thousand coupled equations to solve. The IOS approximation is a drastic simplification since it decouples these equations (but in an orientational basis). This approximation assumes the collision to be sudden, allowing for a diagonalization in orientation representation. This is equivalent to replacing all k_j^2 and all λ with the constants k_o^2 and λ_o respectively in the coupled set. Actually, the IOS is a combination of two approximations, the Energy Sudden approximation (ES) and Centrifugal Sudden approximation (CS). These will be examined in turn.

The Energy Sudden approximation replaces the j dependent wave number k_j with a j independent effective value k_o. Since this approximation no longer treats the angular momentum of Λ and J_r equally, the uncoupled representation

(15) is used. Putting (21) in (15) and converting to Dirac notation gives the following equation:

$$\frac{\hbar^2}{2\mu}\left[\frac{d^2}{dR^2}+\frac{2}{R}\frac{d}{dR}+k_j^2-\frac{\lambda(\lambda+1)}{R^2}\right]\left\langle\alpha\middle|\chi_{\alpha'}(R)\right\rangle=\sum_{\alpha''}\left\langle\alpha\middle|V(R)\middle|\alpha''\right\rangle\left\langle\alpha''\middle|\chi_{\alpha'}(R)\right\rangle. \tag{66}$$

Replacing k_j^2 with k_o^2 leaves (66) in the form

$$\frac{\hbar^2}{2\mu}\left[\frac{d^2}{dR^2}+\frac{2}{R}\frac{d}{dR}+k_o^2-\frac{\lambda(\lambda+1)}{R^2}\right]\left\langle\alpha\middle|\chi_{\alpha'}(R)\right\rangle=\sum_{\alpha''}\left\langle\alpha\middle|V(R)\middle|\alpha''\right\rangle\left\langle\alpha''\middle|\chi_{\alpha'}(R)\right\rangle. \tag{67}$$

Operating on the left by $\sum_{jm}\left\langle\hat{r}\middle|jm\right\rangle$ gives

$$\begin{aligned}\sum_{jm}\left\langle\hat{r}\middle|jm\right\rangle&\left[\frac{d^2}{dR^2}+\frac{2}{R}\frac{d}{dR}+k_o^2-\frac{\lambda(\lambda+1)}{R^2}\right]\left\langle\lambda sjm\middle|\chi_{\alpha'}(R)\right\rangle\\&=\sum_{jm}\left\langle\hat{r}\middle|jm\right\rangle\frac{2\mu}{\hbar^2}\sum_{\alpha''}\left\langle\alpha\middle|V(R)\middle|\alpha''\right\rangle\left\langle\alpha''\middle|\chi_{\alpha'}(R)\right\rangle.\end{aligned} \tag{68}$$

Using

$$\sum_{jm}\left|jm\right\rangle k_o^2\left\langle jm\right|=k_o^2 \tag{69}$$

and

$$\sum_{\alpha''}\sum_{jm}\left\langle\hat{r}\middle|jm\right\rangle\left\langle\alpha\middle|V(R)\middle|\alpha''\right\rangle\left\langle\alpha''\middle|\chi_{\alpha'}(R)\right\rangle=\sum_{\lambda''s''}\left\langle\lambda s\middle|V(\hat{r},R)\middle|\lambda''s''\right\rangle\left\langle\lambda''s''\middle|\chi_{\alpha'}(\hat{r},R)\right\rangle \tag{70}$$

we finally get the ES equation:

$$\begin{aligned}\left[\frac{d^2}{dR^2}+\frac{2}{R}\frac{d}{dR}+k_o^2-\frac{\lambda(\lambda+1)}{R^2}\right]&\left\langle\lambda s\middle|\chi_{\lambda's'}(\hat{r},R)\right\rangle\\&=\frac{2\mu}{\hbar^2}\sum_{\lambda''s''}\left\langle\lambda s\middle|V(\hat{r},R)\middle|\lambda''s''\right\rangle\left\langle\lambda''s''\middle|\chi_{\lambda''s''}(\hat{r},R)\right\rangle.\end{aligned} \tag{71}$$

We note that the effect of replacing k_j^2 with the constant parameter k_o^2 allows the Schrödinger equation to be diagonalized in the rotor orientation. In other words, the collision process occurs with fixed rotor orientation.

A collision process which is fixed for a particular rotor orientation corresponds to a situation where the incoming atom has a velocity relative to the diatom centre of mass much larger than the angular velocity of the rotating diatom. Hence the ES approximation is expected to get better with larger translational kinetic energy of the incoming atom or slower angular velocity of the rotor.

In the CS approximation, λ is replaced with the constant parameter λ_o, so (29) now becomes:

$$\frac{\hbar^2}{2\mu}\left[\frac{d^2}{dR^2}+\frac{2}{R}\frac{d}{dR}+k_j^2-\frac{\lambda_o(\lambda_o+1)}{R^2}\right]\left\langle\alpha\middle|\chi_{\alpha'}(R)\right\rangle=\sum_{\alpha''}\left\langle\alpha\middle|V\middle|\alpha''\right\rangle\left\langle\alpha''\middle|\chi_{\alpha'}(R)\right\rangle. \tag{72}$$

Operating on the left by $\sum_{\lambda s}\left\langle\hat{R}\middle|\lambda s\right\rangle$ and transforming into the orientation representation by carrying out operations analogous to those discussed above for the ES approximation, we get

$$\left[\frac{d^2}{dR^2}+\frac{2}{R}\frac{d}{dR}+k_j^2-\frac{\lambda_o(\lambda_o+1)}{R^2}\right]\left\langle jm\middle|\chi_{j'm'}(\mathbf{R})\right\rangle = \frac{2\mu}{\hbar^2}\sum_{j''m''}\left\langle jm\middle|V(\mathbf{R})\middle|j''m''\right\rangle\left\langle j''m''\middle|\chi_{\alpha'}(\mathbf{R})\right\rangle. \tag{73}$$

Note that (73) has a fixed $\hat{R}$ orientation-the sudden approximation for large centrifugal energy.

One limitation of the CS approximation is that it breaks down in the region of the turning point [30]. Classically, the turning point is defined as the point

where the radial kinetic energy vanishes [31]. The rotor, however, is still rotating and thus collisions at the turning point could not be considered sudden.

As the energy of the collision increases, the CS improves [30]. An increase of energy would correspond to a small rotation of the rotor relative to the distance covered by an incoming atom with high velocity.

Finally the IOS combines both of the above approximations, replacing k_j^2 with k_o^2 *and* replacing λ with λ_o. We operate on the left by $\sum_\alpha \left\langle \hat{R}; \hat{r} \middle| \alpha \right\rangle$ and since the angular momentum operators are now merely parameters we can use closure of the $\left| \alpha \right\rangle$ states to give the IOS equation:

$$\left[\frac{d^2}{dR^2} + \frac{2}{R}\frac{d}{dR} + k_o^2 - \frac{\lambda_o(\lambda_o+1)}{R^2} \right] \chi_{\alpha'}(\hat{r}, \mathbf{R}) = \frac{2\mu}{\hbar^2} V(\hat{r}, \mathbf{R}) \chi_{\alpha'}(\hat{r}, \mathbf{R}). \quad (74)$$

Note the effect of replacing operators by numbers and the subsequent change of basis leaves the equations without any sum over intermediate states and all equations are decoupled.

2.4.1 IOS Cross Sections

The T-matrix was introduced in (22) in an uncoupled representation. As was noted in the previous section, the IOS decouples the Schrödinger equation in a basis with fixed orientation. Hence all quantities calculated from the IOS Schrödinger equation, such as the T-matrix, are diagonal in the orientation representation. The only rotationally invariant quantity that depends on the different possible orientations is the scalar product of the rotor orientation $\hat{r}$ and atom-diatom orientation $\hat{R}$. Thus T is a function of the angle θ between $\hat{r}$ and $\hat{R}$.

This can be expanded in Legendre polynomials:

$$T^{\lambda_0 k_0}(\hat{r}, \hat{R}) = \sum_L \sqrt{2L+1}\, T_L^{\lambda_0 k_0} P_L(\hat{r} \cdot \hat{R}). \tag{75}$$

where $P_L(\hat{r} \cdot \hat{R})$ is the Legendre polynomial of order L.

Equation (55) can be expressed in a different representation as:

$$\sigma_{jm \leftarrow j'm'}(\hat{k}) = \frac{4\pi^2}{k_{j'}^2} \left| \left\langle jm; \hat{k} \middle| T \middle| j'm'; \hat{k}' \right\rangle \right|^2. \tag{76}$$

For the IOS cross sections $\sigma^{\mathrm{IOS}}_{jm \leftarrow j'm'}(\hat{k})$ we have:

$$\begin{aligned} \sigma^{\mathrm{IOS}}_{jm \leftarrow j'm'}(\hat{k}) &= \frac{4\pi^2}{k_{j'}^2} \left| \int\int \left\langle jm; \hat{k} \middle| \hat{r}, \hat{R} \right\rangle T^{\lambda_0 k_0}(\hat{r}, \hat{R}) \left\langle \hat{r}, \hat{R} \middle| j'm'; \hat{k}' \right\rangle d\hat{r} d\hat{R} \right|^2 \\ &= \frac{4\pi^2}{k_{j'}^2} \left| \int\int \sum_{\lambda s \lambda' s'} Y_{\lambda s}(\hat{k}) i^{\lambda' + 3\lambda} Y^*_{\lambda' s'}(\hat{k}) Y^*_{jm}(\hat{r}) Y^*_{\lambda s}(\hat{R}) \right. \\ &\qquad \left. \times T^{\lambda_0 k_0}(\hat{r}, \hat{R}) Y_{j'm'}(\hat{r}) Y_{\lambda' s'}(\hat{R}) d\hat{r} d\hat{R} \right|^2. \end{aligned} \tag{77}$$

Using (75) and the expansion given by (32), the IOS expression for the degeneracy averaged differential cross sections, or $\sigma^{IOS}(\hbar \mathbf{k}', j' \rightarrow \hat{k}, j)$ is

$$\begin{aligned} \sigma^{IOS}(\hbar \mathbf{k}', j' \rightarrow \hat{k}, j) &= (2j+1) \frac{4\pi^2}{k'^2} \sum_{mm'} \left| \sum_{\lambda s \lambda' s'} Y_{\lambda s}(\hat{k}) i^{\lambda' + 3\lambda} \right. \\ &\times \sqrt{(2L+1)(2\lambda+1)(2\lambda'+1)}\, T_L^{\lambda_0 k_0} (-)^{m'+s} Y_{\lambda' s'}(\hat{k}') \\ &\left. \times \begin{pmatrix} j & L & j' \\ 0 & 0 & 0 \end{pmatrix} \begin{pmatrix} j & L & j' \\ -m & -\sigma & m \end{pmatrix} \begin{pmatrix} j & L & \lambda' \\ 0 & 0 & 0 \end{pmatrix} \begin{pmatrix} \lambda & L & \lambda \\ s & \sigma & s' \end{pmatrix} \right|^2. \end{aligned} \tag{78}$$

Equation (78) may also be written as

$$\sigma^{IOS}(\hbar \mathbf{k}', j' \rightarrow \hat{k}, j) = (2j+1) \sum_L \begin{pmatrix} j & L & j' \\ 0 & 0 & 0 \end{pmatrix}^2 \sigma(\hbar \mathbf{k}', 0 \rightarrow \hat{k}, L) \tag{79}$$

where

$$\sigma(\hbar\mathbf{k}', 0 \to \hat{k}, L) = \frac{4\pi^2}{k'^2} \sum_{\sigma} \Bigg| \sum_{\lambda s \lambda' s'} i^{\lambda'-\lambda} \sqrt{(2\lambda+1)(2\lambda'+1)} \times Y_{\lambda s}(\hat{k}) T_L^{\lambda_o k_o} (-)^s \begin{pmatrix} \lambda & L & \lambda' \\ 0 & 0 & 0 \end{pmatrix} \begin{pmatrix} \lambda & L & \lambda \\ s & \sigma & s' \end{pmatrix} Y_{\lambda' s'}(\hat{k}') \Bigg|^2 . \quad (80)$$

If the initial momentum direction $\hat{k}'$ is chosen as the z axis, there will not be any z projections of angular momentum for the initial state, so (57) holds.

Therefore

$$\begin{aligned} &\sigma^{IOS}(\hbar\mathbf{k}', j' \to \hat{k}, j) \\ &= (2j+1) \sum_L \frac{\pi}{k'^2} \begin{pmatrix} j & L & j \\ 0 & 0 & 0 \end{pmatrix}^2 \Bigg| \sum_{\lambda\lambda'} Y_{\lambda\sigma}(\hat{k}) i^{\lambda'-\lambda} \sqrt{(2\lambda+1)(2\lambda'+1)} \\ &\quad \times T_L^{\lambda_o k_o} (-)^s \begin{pmatrix} \lambda & L & \lambda' \\ 0 & 0 & 0 \end{pmatrix} \begin{pmatrix} \lambda & L & \lambda' \\ -\sigma & \sigma & 0 \end{pmatrix} \Bigg|^2 . \end{aligned} \quad (81)$$

To get the *total* cross section $\sigma_{L\leftarrow 0}$, (81) is integrated over all angles to give the following

$$\begin{aligned} \sigma_{L\leftarrow 0} &= \int_0^{2\pi} \int_0^{\pi} \sigma(\hbar\mathbf{k}', 0 \to \hat{k}, L) \sin\theta d\theta d\phi \\ &= \frac{\pi}{k'^2} \sum_{\sigma\lambda} \Bigg| \sum_{\lambda'} (2\lambda+1)(2\lambda'+1) T_L^{\lambda_o k_o} i^{\lambda'-\lambda} \begin{pmatrix} \lambda & L & \lambda' \\ 0 & 0 & 0 \end{pmatrix} \begin{pmatrix} \lambda & L & \lambda' \\ -\sigma & \sigma & 0 \end{pmatrix} \Bigg|^2 \\ &= \frac{\pi}{k'^2} \sum_{\lambda\lambda'} (2\lambda+1)(2\lambda'+1) \left| T_L^{\lambda_o k_o} i^{\lambda'-\lambda} \right|^2 \begin{pmatrix} \lambda & L & \lambda' \\ 0 & 0 & 0 \end{pmatrix}^2 . \end{aligned} \quad (82)$$

If the initial λ paramaterization for the IOS is assumed, ie., $\lambda = \lambda'$, (82) simplifies to

$$\sigma_{L\leftarrow 0} = \frac{\pi}{k'^2} \sum_{\lambda_o} (2L+1) \left| T_L^{\lambda_o k_o} \right|^2 . \quad (83)$$

For total cross section $\sigma_{j\leftarrow j'}^{IOS}$, (79) is integrated over all angles to give the following IOS scaling law:

$$\sigma_{j\leftarrow j'}^{IOS} = (2j+1)\sum_{L}\begin{pmatrix} j & L & j' \\ 0 & 0 & 0 \end{pmatrix}^2 \sigma_{L\leftarrow 0}^{IOS}. \tag{84}$$

2.4.2 Energy Corrected IOS Cross Sections

The scaling law given by (84) can be modified in a manner such that it takes into account a collision time τ. (Recall the IOS assumes a sudden collision, ie, $\tau \approx 0$.) DePristo et. al. [32] have proposed a scaling law called the Energy Corrected Sudden (ECS) approximation which incorporates the collision time τ as a correction to the IOS approximation in the form of a simple multiplicative factor.

DePristo [32] corrects for the S-matrix, but since the S- and T-matrices differ only by the identity matrix and some phase and the correction factor does not change the identity matrix we relate the T-matrices by the same correction factor:

$$T_{jj'}^{ECIOS}(E_k+\epsilon_{j'}) = \frac{6}{6+(\epsilon_{j'}-\epsilon_j)^2\tau^2/(2\hbar)^2} T_{jj'}^{IOS}(E_k+\epsilon_{j'}). \tag{85}$$

where E_k is the translational energy, ϵ_j is the rotor energy of the jth rotor state and τ is the collision time.

In this study the centrifugal sudden approximation is also assumed so that the correction factor is applied to the IOS T-matrices, giving an "Energy Corrected IOS" T-matrix, or $T_{jj'}^{ECIOS}$:

Since by (76) cross sections are proportional to the square of the T-matrices, and assuming that τ is independent of λ and λ', the following simple scaling rule is obtained:

$$\sigma^{ECIOS}_{j\leftarrow j'} = \left[\frac{24\hbar^2}{24\hbar^2 + (\epsilon_{j'} - \epsilon_j)^2\tau^2}\right]^2 \sigma^{IOS}_{j\leftarrow j'}. \tag{86}$$

τ shall be treated as a parameter to help fit the cross sections from this scaling to the cross sections from the exact calculations. DePristo [32] gives a method of estimating τ and this is then compared in a later section to the τ value which gives the best agreement with the exact results.

2.4.3 General S-Matrix Cross Sections

One of the interesting results arising from the IOS treatment of cross sections is that all $j \leftarrow j'$ transitions can be calculated from a single set of cross section values using (84). DePristo et. al. [32] have taken this property of the IOS to investigate whether the *exact* cross sections follow the same scaling laws.

The General S-Matrix (GSM) scaling relationship is a way of calculating a set of cross sections from another set of cross sections with different energies and transitions. The relationship makes use of some IOS properties which allow these connections, but the GSM scaling relationship is actually a relationship between *exact* cross section values.

The IOS implies that the $L \leftarrow 0$ and $j \leftarrow j'$ S-matrices are related by [32]

$$S^{IOS}_{j\leftarrow j'}(E_k + \epsilon_{j'}) = \sum_L \begin{pmatrix} j & j' & L \\ 0 & 0 & 0 \end{pmatrix} S^{IOS}_{L\leftarrow 0}(E_k + \epsilon_L). \tag{87}$$

Using the factor in (85) to relate $S^{IOS}_{j\leftarrow j'}$ with $S^{\text{Exact}}_{j\leftarrow j'}$ *and* to relate $S^{IOS}_{L\leftarrow 0}$ with $S^{\text{Exact}}_{L\leftarrow 0}$ and then using (87) allows for the $L \leftarrow 0$ and $j \leftarrow j'$ exact S-matrices to be related by

$$S^{GSM}_{j\leftarrow j'}(E_k+\epsilon_{j'}) = \sum_L \frac{24\hbar^2 + (\epsilon_L - \epsilon_0)^2\tau^2}{24\hbar^2 + (\epsilon_{j'} - \epsilon_j)^2\tau^2} \begin{pmatrix} j & j' & L \\ 0 & 0 & 0 \end{pmatrix} S^{\text{Exact}}_{L\leftarrow 0}(E_k+\epsilon_L). \quad (88)$$

Here ϵ_L is the rotational energy associated with the Lth rotor state. Then, in order to get a cross section relation, DePristo et. al. [32] make an assumption similar to that made in the previous section, ie., that τ is independent of λ and λ'. They arrive at the following scaling law for the GSM $\sigma_{j\leftarrow j'}$:

$$\sigma^{GSM}_{j\leftarrow j'}(E_k+\epsilon_{j'}) = (2j+1)\sum_L \left[\frac{24\hbar^2 + (\epsilon_L - \epsilon_0)^2\tau^2}{24\hbar^2 + (\epsilon_{j'} - \epsilon_j)^2\tau^2}\right]^2 \begin{pmatrix} j & j' & L \\ 0 & 0 & 0 \end{pmatrix}^2 \sigma^{\text{Exact}}_{L\leftarrow 0}(E_k+\epsilon_L). \quad (89)$$

The above scaling law will be used with $\sigma^{\text{Exact}}_{L\leftarrow 0}$ values to calculate $\sigma_{j\leftarrow j'}$ values and these will be compared with the actual $\sigma^{\text{Exact}}_{j\leftarrow j'}$ values to determine whether the above scaling law is valid.

As well, the scaling law shall be used with $\sigma^{IOS}_{L\leftarrow 0}$ to determine which of the scaling laws, (86) or (89) leads to a more useful manner of correcting the IOS cross sections.

2.4.4 Accessible States Scaling Law

DePristo and Rabitz [33] arrive at an expression for the cross section which does not involve 3-j symbols. To get this expression, they make the following 3 assumptions:

- angular coupling coefficients are mainly a function of difference $|j' - j|$ only
- quantum tunneling is unimportant, so the main energy dependence corresponds to the criterion of determining the outermost turning point.
- the transition probability is inversely proportional to the number of accessible states

The result of the first assumption is that cross sections are a function of $|j' - j|$. The result of the second assumption, that tunneling is not important, allows the cross section to be evaluated at the kinetic energy corresponding to the highest rotor level (where the kinetic energy is the least and where tunneling is least effective). Combining these two assumptions with the third allows the Accessible States (AS) cross section $\sigma^{\mathrm{AS}}_{j \leftarrow j'}(E)$ to be written as

$$\sigma^{\mathrm{AS}}_{j \leftarrow j'}(E) = f\Big(|j' - j|, E - \epsilon_{j_{\max}}\Big) N(E)^{-1} \tag{90}$$

where f is a function of $|j' - j|$ and $E - \epsilon_{j_{\max}}$. $\epsilon_{j_{\max}}$ is the energy of the rotor for the maximum allowed j value, and $N(E)$ is the number of available rotor states for a given energy E.

The assumed functional properties of the f function implies a relationship between cross sections which have the same $|j' - j|$ and $E - \epsilon_{j_{\max}}$ values, namely

$$\sigma^{\mathrm{AS}}_{j \leftarrow j'}(E_k + \epsilon_{j'}) = \frac{[2j+1][2(j'-j)+1]}{[2j'+1]} \frac{N(E_k + \epsilon_{j'-j})}{N(E_k + \epsilon_{j'})} \sigma_{0 \leftarrow j'-j}(E_k + \epsilon_{j'-j}), \quad j' > j. \tag{91}$$

(The form of (91) is equation (4.9) of [32] which was first presented in a different form in [33].)

The scaling law given by (91) is here referred to as the AS scaling law, referring to the $N(E_k + \epsilon_{j'-j})/N(E_k + \epsilon_{j'}$ term, which actually describes only one of the three approximations made.

Note that in contrast to the previous scaling laws, (91) relates cross sections of different *total* energies, ie, $\sigma^{\mathrm{AS}}_{j\leftarrow j'}(E_k + \epsilon_{j'})$ with $\sigma_{0\leftarrow j'-j}(E_k + \epsilon_{j'-j})$. A set of *exact* $\sigma_{j\leftarrow j'}$ and $\sigma_{0\leftarrow j'-j}$ values are related by a given *total* energy. Although there is a question in the exact case as to which *total* energy to use, this study will show that this choice is not a significant factor determining cross section values.

However, in this study we will use (91) to determine its validity as a scaling law for the IOS approximation. Since the IOS treats all rotor states as having the same energy, $\sigma^{IOS}_{j\leftarrow j'}(E_k + \epsilon_{j'})$ and $\sigma^{IOS}_{0\leftarrow j'-j}(E_k + \epsilon_{j'-j})$ should actually be written as $\sigma^{IOS}_{j\leftarrow j'}(E_{k_o})$ and $\sigma^{IOS}_{0\leftarrow j'-j}(E_{k'_o})$ where k_o and k'_o are those wave numbers corresponding to the parameters chosen to replace the k_j value and ϵ_{k_o} is the energy associated with the k_o wave number. It is this aspect of the IOS approximation - the incorporation of rotor and translational energies into one effective wave number - which makes (91) lose some of its specificity when applied to the IOS results. It will be shown later that this loss of energy dependence does not significantly affect the accuracy of the scaling law given by (91).

3. THE DELTA-SHELL POTENTIAL

3.1 Scattering From a Spherical Delta Shell Potential

In its simplest form the delta shell potential is

$$V(R) = V_\delta \, \delta(R - a) \tag{92}$$

where V_δ is a potential strength parameter having units of energy times distance, a is the distance from the origin at which the potential acts and $\delta(R-a)$ is the Dirac delta function.

If the collision involves only a spherical potential, rotor states are unchanged in the collision process and need not be considered further. The form for the Hamiltonian H is thus

$$H = -\frac{\hbar^2}{2\mu}\left[\frac{1}{R^2}\frac{\partial}{\partial R}R^2\frac{\partial}{\partial R} - \frac{\Lambda^2}{R^2}\right] + V(R) \tag{93}$$

where Λ^2 is given by (11).

The Schrödinger equation now takes the form

$$\frac{\hbar^2}{2\mu}\left[\frac{1}{R^2}\frac{\partial}{\partial R}R^2\frac{\partial}{\partial R} - \frac{\Lambda^2}{R^2} + \frac{2\mu}{\hbar^2}E\right]\Psi(\mathbf{R}) = V(R)\Psi(\mathbf{R}) \tag{94}$$

where $\Psi(\mathbf{R})$ is the wave function for a spherical delta shell.

Using the partial wave expansion of the wave function $\Psi(\mathbf{R})$

$$\Psi(\mathbf{R}) = \sum_{\lambda s} Y_{\lambda s}(\hat{R})\psi_{\lambda s}(R) \tag{95}$$

where

$$\psi_{\lambda s}(R) = 4\pi i^{\lambda}\chi_{\lambda}(R)Y^{*}_{\lambda s}(\hat{k}') \tag{96}$$

and using equation (92) for $V(R)$ and introducing the dimensionless variable $x = kR$ where $k^2 = 2\mu E/\hbar^2$ we now can write (94) as

$$\frac{\hbar^2}{2\mu}\left[\frac{2}{x}\frac{\partial}{\partial x} + \frac{\partial^2}{\partial x^2} - \frac{\lambda(\lambda+1)}{x^2} + 1\right]\chi_{\lambda} = \frac{V_{\delta}}{k}\delta(x-ka)\chi_{\lambda} \tag{97}$$

where the following property of the delta function [34] has been used:

$$\delta(R-a) = k\delta(x-ka) \tag{98}$$

For $x \neq ka$, there is no potential and the partial wave solutions are the well known spherical Bessel and Hankel functions [35]. With the constraint that χ_{λ} must be well behaved at the origin, the solution of (97) is given up to a constant by

$$\begin{aligned} \chi_{\lambda} &= j_{\lambda}(x) - \tfrac{1}{2}T_{\lambda}h_{\lambda}(x), \quad x > ka \\ \chi_{\lambda} &= B_{\lambda}j_{\lambda}(x), \qquad\qquad\quad x < ka \end{aligned} \tag{99}$$

where the j_{λ}'s are the regular Bessel functions and the h_{λ}'s are the Hankel functions. The expansion coefficients T_{λ} and B_{λ} are to be determined by appropriate matching conditions at $x = ka$.

Defining

$$\begin{aligned} ka^- &\equiv ka - \varepsilon \\ ka^+ &\equiv ka + \varepsilon, \quad \varepsilon \to 0 \end{aligned} \tag{100}$$

and integrating (97) over x from ka^- to ka^+ and requiring χ_λ to be continuous at ka gives

$$\left.\frac{\partial \chi_\lambda}{\partial x}\right|_{ka-}^{ka^+} - \left.\frac{2\chi_\lambda}{ka}\right|_{ka-}^{ka^+} = \frac{2\mu}{\hbar^2 k} V_\delta \chi_\lambda. \tag{101}$$

Since χ_λ is continuous,

$$\frac{\partial}{\partial x}\chi_\lambda(ka^+) - \frac{\partial}{\partial x}\chi_\lambda(ka^-) = \frac{2\mu}{\hbar^2 k} V_\delta \chi_\lambda. \tag{102}$$

Using (99) in (102) gives

$$j'_\lambda(ka^+) - \frac{1}{2}T_\lambda h'_\lambda(ka^+) - B_\lambda j'_\lambda(ka^-) = \frac{2\mu}{\hbar^2 k} V_\delta j_\lambda(ka) B_\lambda \tag{103}$$

where

$$\begin{aligned} j'_\lambda(x) &= \frac{d}{dx} j_\lambda(x) \\ h'_\lambda(x) &= \frac{d}{dx} h_\lambda(x). \end{aligned} \tag{104}$$

Since χ_λ is continuous at ka,

$$\chi_\lambda(ka^+) = \chi_\lambda(ka^-) \tag{105}$$

and so

$$j_\lambda(ka) - \frac{1}{2}T_\lambda h_\lambda(ka) = B_\lambda j_\lambda(ka). \tag{106}$$

Allowing $\varepsilon \to 0$ and multiplying (103) by $h_\lambda(ka)$, (106) by $h'_\lambda(ka)$ and then using the following property of the Wronskian W of the Bessel and Hankel functions [35]:

$$W = j'_\lambda(x)h_\lambda(x) - j_\lambda(x)h'_\lambda(x) = \frac{1}{ix^2} \tag{107}$$

an expression for B_λ is obtained:

$$B_\lambda = \frac{1}{1 - i\xi g j_\lambda h_\lambda} \tag{108}$$

where j_λ is shorthand for $j_\lambda(ka)$, h_λ for $h_\lambda(ka)$,

$$\xi = ka \tag{109}$$

and

$$g = -\frac{2\mu V_\delta a}{\hbar^2}. \tag{110}$$

Finally, multiplying (103) by j_λ, (106) by j'_λ, and using (107) and (108) gives the following expression for T_λ:

$$T_\lambda = -\frac{2i\xi g j_\lambda^2}{1 - i\xi g j_\lambda h_\lambda}. \tag{111}$$

With T_λ and B_λ solved, we are interested in the behaviour of χ_λ at $R \gg a$. From the asymptotic behaviour of the Bessels and Hankels given in (23) the expression for χ_λ as $R \to \infty$ is now

$$\chi_\lambda \sim -\frac{1}{2ika}\left[e^{-i(ka-\lambda\pi/2)} - (1 - T_\lambda)e^{i(ka-\lambda\pi/2)}\right]. \tag{112}$$

Using (60) and assuming $j' = 0$ (ie, no rotor states) the total cross section is

$$\sigma^{\text{total}} = \frac{\pi}{k^2}\sum_\lambda (2\lambda + 1)\left|T_\lambda\right|^2. \tag{113}$$

Hence a calculation of the cross section for a spherical delta shell potential requires the wave number k, the parameter strength V_δ and the distance a of the delta shell from the origin. After evaluating the j_λ's and h_λ's at ka, the total cross section for the spherical delta shell potential is obtained from (111) and (113).

3.2 Scattering From a Non-Spherical Delta Shell Potential

For the system being studied — an atom-diatom — the fact that the scattering centre is non-spherical (ie., the potential between the atom and diatom is θ dependent) means that the angular momentum of the diatom can couple with the orbital angular momentum of the atom. It is the θ dependence in the potential which is responsible for angular momentum transfer between rotor angular momentum and orbital angular momentum.

A θ dependent potential can be expanded in Legendre functions. Since we are studying a *homo*nuclear system, only even Legendre functions appear in the expansion. Here only the zeroth and second order Legendre functions are retained to give a potential in the form

$$V(\theta) = V_\delta \left[1 + b_2 P_2(\cos\theta)\right] \delta(R - a) \tag{114}$$

where b_2 is a constant. Explicitly, the second order Legendre is

$$P_2(\cos\theta) = \frac{1}{2}(3\cos^2\theta - 1) \tag{115}$$

With a spherical potential there is no coupling between orbital and rotor angular momentum and therefore it is not necessary to designate initial and final angular momenta – they are always the same. With a non-spherical potential, transfer of angular momentum may occur between the two types of angular momentum. This implies that the initial state, designated by quantum numbers j', m', λ' and s', can be different from the final state, designated by quantum numbers j, m, λ and s. Since Ψ must then be described by an initial and final state, a notation is introduced where the vector wave function χ is represented as a *matrix* $\boldsymbol{\chi}$. (Matrices will be indicated with bold type.) As well, since the rotor operator k, orbital angular momentum operator Λ and potential operator V all must be parameterized by indices corresponding to the ket and bra states, they too will be represented by a similar matrix notation, ie., $\mathbf{k}$, $\boldsymbol{\Lambda}$ and $\mathbf{V}$ respectively.

In a previous section it was shown how a total-J coupling scheme can separate the V-matrix elements into blocks having the same total-J. Since by (133) the only non-diagonal matrix that $\mathbf{T}$ depends on is $\mathbf{V}$ it is possible to separate the calculation of the T-matrix as well into blocks with the same total-J. With this in mind, and using the above notation, (29) is actually one matrix element of a matrix equation and can be generalized as

$$\frac{\hbar^2}{2\mu}\left[\frac{d^2}{dR^2}+\frac{2}{R}\frac{d}{dR}+\mathbf{k}^2-\frac{\boldsymbol{\Lambda}^2}{\hbar^2R^2}\right]\boldsymbol{\chi}^J=\mathbf{V}^J\boldsymbol{\chi}^J \tag{116}$$

where $\mathbf{k}^2$ and $\boldsymbol{\Lambda}^2$ are diagonal matrices whose elements in the angular momentum representation are defined by

$$\mathbf{k}_{jj'} = k_j \delta_{jj'} = \left(\frac{2\mu}{\hbar^2}\right)^{\frac{1}{2}} \left[E - \frac{j(j+1)\hbar^2}{2I}\right]^{\frac{1}{2}} \delta_{jj'}\delta_{\lambda\lambda'} \tag{117}$$

and

$$\mathbf{\Lambda}^2_{\lambda\lambda'} = \lambda(\lambda+1)\hbar^2 \delta_{\lambda\lambda'}\delta_{jj'} \tag{118}$$

The form of (116) corresponding to matrix element $\left\langle j\lambda \middle| \chi^J \middle| j'\lambda' \right\rangle$ is then

$$\frac{\hbar^2}{2\mu}\left[\frac{d^2}{dR^2} + \frac{2}{R}\frac{d}{dR} + k_j^2 - \frac{\lambda(\lambda+1)}{\hbar^2 R^2}\right]\left\langle j\lambda \middle| \chi^J(R) \middle| j\lambda \right\rangle = \sum_{j'''\lambda'''} \left\langle j\lambda \middle| V^J \middle| j''\lambda'' \right\rangle \delta(R-a) \left\langle j''\lambda'' \middle| \chi^J(R) \middle| j'\lambda' \right\rangle \tag{119}$$

This is similar in form to (97). In the same manner as we solved (97), we choose solutions

$$\begin{aligned} &\left\langle j\lambda \middle| \chi^J \middle| j'\lambda' \right\rangle \\ &= j_\lambda(k_j R) - \frac{1}{2} h_\lambda(k_j R) k_j^{\frac{1}{2}} \left\langle j\lambda \middle| T^J \middle| j'\lambda' \right\rangle k_{j'}^{-\frac{1}{2}}, \quad R > a \\ &= \left\langle j\lambda \middle| B^J \middle| j'\lambda' \right\rangle j_\lambda(k_j R), \quad R < a \end{aligned} \tag{120}$$

where the coefficients T and B are no longer simply parameterized by λ but must be matrices themselves corresponding to the representation of χ. If the matrices $\mathbf{j}$ and $\mathbf{h}$ are now introduced, their matrix elements are given by

$$\begin{aligned} \left\langle j\lambda \middle| j(k_j R) \middle| j'\lambda' \right\rangle &= j_\lambda(k_j R)\delta_{jj'}\delta_{\lambda\lambda'} \\ \left\langle j\lambda \middle| h(k_j R) \middle| j'\lambda' \right\rangle &= h_\lambda(k_j R)\delta_{jj'}\delta_{\lambda\lambda'} \end{aligned} \tag{121}$$

(120) can be written in matrix notation as

$$\begin{aligned} \chi &= \mathbf{j} - \frac{1}{2}\mathbf{h}\mathbf{k}^{\frac{1}{2}}\mathbf{T}\mathbf{k}^{-\frac{1}{2}}, \quad R > a \\ &= \mathbf{j}\mathbf{B}, \quad R < a \end{aligned} \tag{122}$$

$\mathbf{j}$ represents the prepared incoming state; $\frac{1}{2}\mathbf{h}\mathbf{k}^{\frac{1}{2}}\mathbf{T}\mathbf{k}^{-\frac{1}{2}}$ represents the scattered outgoing wave and $\mathbf{jB}$ represents the part of the incoming wave that has tunneled through the potential barrier.

Next (119) is integrated with respect to R from $\mathbf{k}a^-$ to $\mathbf{k}a^+$ where

$$\begin{aligned} \mathbf{k}a^+ &= \mathbf{k}a + \varepsilon \\ \mathbf{k}a^- &= \mathbf{k}a - \varepsilon, \quad \varepsilon \to 0 \end{aligned} \tag{123}$$

The requirement of continuity of χ, ie.,

$$\chi(k_j a^+) = \chi(k_j a^-), \tag{124}$$

is used to get

$$\frac{d}{d\mathbf{y}}\chi(k_j a^+) - \frac{d}{d\mathbf{y}}\chi(k_j a^-) = \frac{2\mu}{\hbar^2}\mathbf{k}^{-1}\mathbf{V}\chi \tag{125}$$

where

$$\mathbf{y} = \mathbf{k}R. \tag{126}$$

Again the requirement of continuity for the wave function χ at $R = a$ implies

$$\mathbf{jB} = \mathbf{j} - \frac{1}{2}\mathbf{h}\mathbf{k}^{\frac{1}{2}}\mathbf{T}\mathbf{k}^{-\frac{1}{2}}, \qquad R = a \tag{127}$$

Inserting the expression for χ given by (122) into (125) gives

$$\frac{d\mathbf{j}}{d\mathbf{y}}\mathbf{B} + \frac{2\mu}{\hbar^2}\mathbf{k}^{-\frac{1}{2}}\mathbf{V}\left(\mathbf{j} - \frac{1}{2}\mathbf{h}\mathbf{k}^{\frac{1}{2}}\mathbf{T}\mathbf{k}^{-\frac{1}{2}}\right) = \frac{d\mathbf{j}}{d\mathbf{y}} - \frac{1}{2}\frac{d\mathbf{h}}{d\mathbf{y}}\mathbf{k}^{\frac{1}{2}}\mathbf{T}\mathbf{k}^{-\frac{1}{2}} \tag{128}$$

Operating on the left of (127) by $-(d/d\mathbf{y})\mathbf{j}$, on the left of (128) by $\mathbf{j}$ and then adding the two resulting equations gives

$$\frac{2\mu}{\hbar^2}\mathbf{k}^{-1}\mathbf{j}\mathbf{V}\left(\mathbf{j} - \frac{1}{2}\mathbf{h}\mathbf{k}^{\frac{1}{2}}\mathbf{T}\mathbf{k}^{-\frac{1}{2}}\right) = \frac{1}{2}\left(\frac{d\mathbf{j}}{d\mathbf{y}}\mathbf{h} - \mathbf{j}\frac{d\mathbf{h}}{d\mathbf{y}}\right)\mathbf{k}^{\frac{1}{2}}\mathbf{T}\mathbf{k}^{-\frac{1}{2}} \tag{129}$$

Using the matrix version of the Wronskian given by (107), ie.,

$$\mathbf{W} = \frac{d\mathbf{j}}{d\mathbf{y}}\mathbf{h} - \mathbf{j}\frac{d\mathbf{h}}{d\mathbf{y}} = \frac{1}{i(\mathbf{k}R)^2} \tag{130}$$

allows (129) to be written as

$$\frac{4a^2 i\mu}{\hbar^2}\mathbf{kjV}\left(\mathbf{j} - \frac{1}{2}\mathbf{hk}^{\frac{1}{2}}\mathbf{Tk}^{-\frac{1}{2}}\right) = \mathbf{k}^{\frac{1}{2}}\mathbf{Tk}^{-\frac{1}{2}} \tag{131}$$

or, rearranging,

$$\frac{4i\mu a^2}{\hbar^2}\mathbf{kjVj} = \mathbf{k}^{\frac{1}{2}}\left[\frac{2i\mu a^2}{\hbar^2}\mathbf{k}^{\frac{1}{2}}\mathbf{jVhk}^{\frac{1}{2}} + 1\right]\mathbf{Tk}^{-\frac{1}{2}} \tag{132}$$

so that finally an expression for $\mathbf{T}$ is obtained:

$$\mathbf{T} = \left[1 + \frac{2i\mu a^2}{\hbar^2}\mathbf{k}^{\frac{1}{2}}\mathbf{jVhk}^{\frac{1}{2}}\right]^{-1}\frac{4i\mu a^2}{\hbar^2}\mathbf{k}^{\frac{1}{2}}\mathbf{jVjk}^{\frac{1}{2}} \tag{133}$$

Another important point to mention regarding the separation of the T matrix into smaller blocks comes from the form of the potential used. The potential is expanded so that there are only two parameters for the $V_L(R)$'s, ie., V_0 and V_2. Hence $L = 0$ or $L = 2$. Equation (51) reveals that the potential matrix element is expanded in 3-j symbols $\begin{pmatrix} j & L & j' \\ 0 & 0 & 0 \end{pmatrix}\begin{pmatrix} \lambda & L & \lambda' \\ 0 & 0 & 0 \end{pmatrix}$ which are 0 if $j + L + j'$ or $\lambda + L + \lambda'$ is odd by equation (3.7.14) of Edmonds [27]. This means that j and j' must both be even or they must both be odd. The same is true for λ and λ'. Hence the V-matrix can be broken down into blocks categorized by:

1) total-J

2) even or odd λ

3) even or odd j.

And since **T** is a function of **V** then **T** as well can be broken down into these blocks.

One important difference between **T** and **V** is in the range of parameter off-diagonality that is allowed, that is, the difference allowed between j and j' and between λ and λ'. The V matrix, because of the $\begin{pmatrix} j & L & j' \\ 0 & 0 & 0 \end{pmatrix}\begin{pmatrix} \lambda & L & \lambda' \\ 0 & 0 & 0 \end{pmatrix}$ terms, can only couple λ and λ' states that differ by 0 or by 2. The T-matrix, however, allows for any even transitions. The reason for this is that the T-matrix depends on **V** not only linearly but on arbitrary products of **V** as well since (133) has an inverse of **V** in it.

With the above in mind the study was further restricted to even j states. The calculations were done by choosing a total-J value, then calculating cross sections for even λ and then odd λ. This was done for J ranging from 0 to its maximum value, $\lambda_{\max} + j_{\max}$.

Though one wave number κ and an initial j' value are chosen, (and a total energy value E_{total} is obtained from these values) other matrix elements having the same E_{total} but different j' (and therefore different wavelengths as well) must be calculated. That is, there is no way in the total-J coupling scheme to separate the various initial j states. Hence if the T-matrix elements are calculated

for $E_{\text{total}} = 5.820 \times 10^{-21}$J., so that the initial translational state corresponds to a temperature of 300K and the initial rotor state corresponds to a value of $j' = 6$, T-matrix elements corresponding to this same total energy but having different initial conditions are also calculated. For example, the initial conditions of $j' = 0$ and $k = 16.92 \times 10^{10}\text{m.}^{-1}$ correspond as well to a total energy of 5.820×10^{-21}J. So too do $j' = 2$ and $k = 16.57 \times 10^{10}\text{m.}^{-1}$, etc., all the way to $j' = 10$ and $k = 8.37 \times 10^{10}\text{m.}^{-1}$ Thus the sum of appropriate T-matrix elements will give cross sections not only for the intended initial conditions but for all other combinations of initial conditions having the same total energy.

3.3 Simplification Using Only Open States

Generally, in the solution of the T-matrix, the wave function must be expanded in a complete set of basis functions. This implies that internal states with energy greater than the total energy must also be considered in the expansion which leads to imaginary k values. These closed channel states are coupled to the initial and final scattering states by the intermolecular potential. In a physical sense, what this means is that the interaction perturbs the internal states and some of these energy forbidden internal states are necessary to represent the eigenstates of the perturbed system [36].

As a first approximation only real k values were used in the calculation. That is, only the energetically accessible (open) channels were used in the calculation of the T-matrix. The theory to include closed states is developed in the next

section.

For ease in computation, it is desirable to avoid inversion of a complex matrix. With this in mind, we define

$$\mathbf{h} = i\mathbf{n} + \mathbf{j} \tag{134}$$

where $\mathbf{n}$ is the matrix of Neumann functions. Equation (133) may be written as

$$\mathbf{T} = \frac{2i}{\mathbf{1} - \mathbf{N} + i\mathbf{J}}\mathbf{J} \tag{135}$$

where

$$\mathbf{J} \equiv \frac{2\mu a^2}{\hbar^2}\mathbf{k}^{\frac{1}{2}}\mathbf{j}\mathbf{V}\mathbf{j}\mathbf{k}^{\frac{1}{2}} \tag{136}$$

$$\mathbf{N} \equiv \frac{2\mu a^2}{\hbar^2}\mathbf{k}^{\frac{1}{2}}\mathbf{j}\mathbf{V}\mathbf{n}\mathbf{k}^{\frac{1}{2}} \tag{137}$$

and so that $\mathbf{J}$ and $\mathbf{N}$ are always real. Equation (135) can be expressed in another form:

$$\begin{aligned}
\mathbf{T} &= [\mathbf{N} - \mathbf{1} + i\mathbf{J}]^{-1}[\mathbf{N} - \mathbf{1}][\mathbf{N} - \mathbf{1}]^{-1}[-2i\mathbf{J}] \\
&= \left[[\mathbf{N} - \mathbf{1}]^{-1}[\mathbf{N} - \mathbf{1} - i\mathbf{J}]\right]^{-1}\left[-\frac{2i}{\mathbf{N} - \mathbf{1}}[\mathbf{J}]\right] \\
&= \left[\mathbf{1} - \frac{i}{\mathbf{N} - \mathbf{1}}[\mathbf{J}]\right]^{-1}\left[-\frac{2i}{\mathbf{N} - \mathbf{1}}[\mathbf{J}]\right] \\
&= [\mathbf{1} - i\mathbf{K}]^{-1}[-2i\mathbf{K}]
\end{aligned} \tag{138}$$

where

$$\mathbf{K} \equiv \frac{1}{\mathbf{N} - \mathbf{1}}[\mathbf{J}] \tag{139}$$

and $\mathbf{K}$ is always real. The following expression is obtained upon further expanding (139):

$$\begin{aligned}
\mathbf{T} &= \frac{1}{\mathbf{1}-i\mathbf{K}}\left[\mathbf{1}+i\mathbf{K}\right]^{-1}\left[\mathbf{1}+i\mathbf{K}\right]\left[-2i\mathbf{K}\right] \\
&= \frac{1}{\mathbf{1}+\mathbf{K}^2}\left[-2i\mathbf{K}+2\mathbf{K}^2\right] \\
&= \frac{1}{\mathbf{1}+\mathbf{K}^2}\left[2\mathbf{K}^2\right]-\frac{2i}{\mathbf{1}+\mathbf{K}^2}\left[\mathbf{K}\right]. \qquad (140)
\end{aligned}$$

Since $\mathbf{1}+\mathbf{K}^2$ is real, it is now possible to calculate both the real and imaginary part of $\mathbf{T}$ without using complex inversion.

For further ease of computation, it was investigated whether a symmetric form for the calculation of $\mathbf{K}$ could be found. Letting

$$\mathbf{W} \equiv \frac{2\mu a^2}{\hbar^2}\mathbf{k}^{\frac{1}{2}}\mathbf{V}\mathbf{k}^{\frac{1}{2}} \qquad (141)$$

allows $\mathbf{K}$ to be expanded as follows:

$$\begin{aligned}
\mathbf{K} &= \frac{1}{\mathbf{N}-\mathbf{1}}\left[\mathbf{J}\right] = \frac{1}{\mathbf{jWn}-\mathbf{1}}\left[\mathbf{jWj}\right] \\
&= \frac{1}{(\mathbf{j}/\mathbf{n})\left[\mathbf{nWn}-(\mathbf{n}/\mathbf{j})\right]}\left[\mathbf{jWn}\right]\left[\frac{\mathbf{j}}{\mathbf{n}}\right] \\
&= \frac{1}{\mathbf{nWn}-(\mathbf{n}/\mathbf{j})}\left[\frac{\mathbf{n}}{\mathbf{j}}\right]\left[\mathbf{jWn}-\mathbf{1}+\mathbf{1}\right]\left[\frac{\mathbf{j}}{\mathbf{n}}\right] \\
&= \frac{\mathbf{j}}{\mathbf{n}}+\frac{1}{\mathbf{nWn}-(\mathbf{n}/\mathbf{j})}. \qquad (142)
\end{aligned}$$

Since the $\mathbf{j}$'s and $\mathbf{n}$'s are diagonal matrices and $\mathbf{W}$ is a symmetric matrix, only a symmetric matrix inversion routine is needed in order to evaluate $\mathbf{K}$.

Problems, however, arose with this procedure. Neumann functions for sufficiently small values of ka at large λ approach ∞ as given by [35], ie.,

$$\mathsf{n}_\lambda \sim \frac{(2\lambda-1)!!}{(ka)^{\lambda+1}}. \tag{143}$$

Using Stirling's approximation for large N

$$N! = \left(\frac{N}{e}\right)^N \tag{144}$$

and

$$(2\lambda-1)!! = \frac{(2\lambda-1)!}{2^{\lambda-1}(\lambda-1)!} \tag{145}$$

and approximating $2\lambda-1$ as 2λ and $\lambda-1$ as λ for large λ, the Neumann functions become, as $ka \to 0$,

$$\mathsf{n}_\lambda \approx \frac{1}{ka}\left(\frac{2\lambda}{kae}\right)^\lambda, \qquad ka \to 0. \tag{146}$$

Treating the limiting behaviour of the Bessel functions in an analogous manner as $ka \to 0$ gives the limit

$$\mathsf{j}_\lambda \approx \frac{(ka)^\lambda}{(2\lambda+1)!!} \approx \frac{e}{2\lambda}\left(\frac{kae}{2\lambda}\right)^\lambda, \qquad ka \to 0. \tag{147}$$

Hence the $(\mathbf{n}/\mathbf{j})$ term in (142) is of the order of

$$\frac{\mathsf{n}_\lambda}{\mathsf{j}_\lambda} \approx \frac{\frac{1}{ka}\left(\frac{2\lambda}{kae}\right)^\lambda}{\frac{e}{2\lambda}\left(\frac{kae}{2\lambda}\right)^\lambda} = \left(\frac{2\lambda}{kae}\right)^{2\lambda+1}, \quad ka \to 0. \tag{148}$$

When the actual run was made, exponential overflow occurred in the inversion routine for (142) for initial rotor state j'=8, λ=74, j=12, ka=34 so that

$$\frac{\mathsf{n}_{74}(34)}{\mathsf{j}_{74}(34)} \approx \left[\frac{148}{34e}\right]^{149} \approx 3 \times 10^{30}. \tag{149}$$

Solving for an inverse of a matrix requires the multiplication of matrix elements; three terms of the order of (149) would be sufficient for an exponential overflow [37] on the Amdahl.

Thus another form for the **K** matrix was needed., Equation (142) can be rewritten in the form

$$\begin{aligned} \mathbf{K} &= \frac{\mathbf{j}}{\mathbf{n}} + \frac{1}{\mathbf{jWn} - \mathbf{1}} \left[\frac{\mathbf{j}}{\mathbf{n}}\right] \\ &= \frac{\mathbf{j}}{\mathbf{n}} + \frac{1}{\mathbf{j}[\mathbf{W} - (1/\mathbf{jn})]\,\mathbf{n}} \left[\frac{\mathbf{j}}{\mathbf{n}}\right] \\ &= \frac{\mathbf{j}}{\mathbf{n}} + \left[\frac{1}{\mathbf{n}}\right] \frac{1}{\mathbf{W} - (1/\mathbf{jn})} \left[\frac{1}{\mathbf{n}}\right]. \end{aligned} \tag{150}$$

In this rewritten form, the magnitude of the numbers were much more manageable. The $(1/\mathbf{jn})$ term was, for the parameters previously mentioned, of the order of

$$\frac{1}{\mathsf{j}_\lambda \mathsf{n}_\lambda} \sim \frac{2\lambda ka}{e} \approx \frac{2(74)34}{2.303} \approx 10^3, \qquad ka \to 0. \tag{151}$$

The **W** term [1] ranged from 4×10^4 to 2×10^8 and an exponential overflow was avoided using this form. (The only possibility of an overflow is for $\mathbf{W} = (1/\mathbf{jn})$ but this did not occur as $(1/\mathbf{jn})$ was evaluated at a small number of specific ka points; for the cases studied here $\mathbf{W} - (1/\mathbf{jn})$ never got close enough to 0 to cause overflow problems.)

[1]The range for **W** was calculated by recognizing that the term $(2\mu a/\hbar^2)\mathsf{V}_\delta$ is of the order of 100 while the actual V-matrix element, as given by (51) depends on 3-j and 6-j symbols, which, by their unitary nature [27], take on a maximum value of 1. Finally, the k values used in this study ranged from $5 \times 10^{10} m.^{-1}$ to $30 \times 10^{10} m.^{-1}$

3.4 Inclusion of Closed States

One approximation made in the previous section was limiting the basis set to energetically allowed states. We seek now a more general solution that includes "closed" channels, those channels (states) which are not physically allowed as final states for the collision process but nonetheless may affect the calculations.

Treatment of the problem with the inclusion of closed states is similar to that presented in (116) to (133), the only difference is that the incoming prepared state is designated $\mathbf{P_o j}$ where $\mathbf{P_o}$ is the projection operator onto open channels. The resulting equation is similar in form to (133) except for the projection operator at the end:

$$\mathbf{T} = \left[\mathbf{1} + \frac{2i\mu a^2}{\hbar^2}\mathbf{k}^{\frac{1}{2}}\mathbf{jVhk}^{\frac{1}{2}}\right]^{-1}\left[\frac{4i\mu a^2}{\hbar^2}\mathbf{k}^{\frac{1}{2}}\mathbf{jVjk}^{\frac{1}{2}}\mathbf{P_o}\right]. \tag{152}$$

With the following definitions

$$\mathbf{H} \equiv \frac{2\mu a^2}{\hbar^2}\mathbf{k}^{\frac{1}{2}}\mathbf{jVhk}^{\frac{1}{2}} = \mathbf{jWh} \tag{153}$$

and

$$\mathbf{J} \equiv \frac{2\mu a^2}{\hbar^2}\mathbf{k}^{\frac{1}{2}}\mathbf{jVjk}^{\frac{1}{2}} = \mathbf{jWj} \tag{154}$$

(where $\mathbf{W}$ is defined in (141)), the T-matrix can be written

$$\mathbf{T} = \left[\frac{\mathbf{1}}{\mathbf{1} + i\mathbf{H}}\right] 2i\mathbf{JP_o}. \tag{155}$$

For the calculation of the scattering cross section, only the open state part $\mathbf{T_{oo}}$ of the T-matrix is required:

$$\mathbf{T_{oo}} = \mathbf{P_o T} = \mathbf{P_o}\left[\frac{\mathbf{1}}{\mathbf{1} + i\mathbf{H}}\right] 2i\mathbf{JP_o}. \tag{156}$$

The term $\mathbf{P}_o[\mathbf{1}/(\mathbf{1}+i\mathbf{H})]$ can be broken up into open, closed and open-closed coupling contributions

$$\mathbf{P}_o\left[\frac{\mathbf{1}}{\mathbf{1}+i\mathbf{H}}\right] = \mathbf{P}_o\left[\frac{\mathbf{1}}{\mathbf{1}+i\mathbf{H}_o}\right]\left[\mathbf{1}+i\Big[\mathbf{H}-\mathbf{H}_1-\mathbf{H}_c\Big]\right]\left[\frac{\mathbf{1}}{\mathbf{1}+i\mathbf{H}}\right] \tag{157}$$

where

$$\mathbf{H}_o \equiv \mathbf{P}_o\mathbf{H}\mathbf{P}_o, \tag{158}$$

$$\mathbf{H}_1 \equiv \mathbf{P}_o\mathbf{H}\mathbf{P}_c + \mathbf{P}_c\mathbf{H}\mathbf{P}_o, \tag{159}$$

$\mathbf{P}_c$ being the projection operator on closed states, defined by

$$\mathbf{P}_c = \mathbf{1} - \mathbf{P}_o \tag{160}$$

and finally,

$$\mathbf{H}_c \equiv \mathbf{P}_c\mathbf{H}\mathbf{P}_c. \tag{161}$$

The following calculations can be performed: (non-contributing terms are marked with slashes)

$$\begin{aligned}
\mathbf{P}_o\left[\frac{\mathbf{1}}{\mathbf{1}+i\mathbf{H}}\right] &= \mathbf{P}_o\left[\frac{\mathbf{1}}{\mathbf{1}+i\mathbf{H}_o}\right] - i\mathbf{P}_o\left[\frac{\mathbf{1}}{\mathbf{1}+i\mathbf{H}_o}\right]\left[\mathbf{H}_1 + \cancel{\mathbf{H}_c}\right]\left[\frac{\mathbf{1}}{\mathbf{1}+i\mathbf{H}}\right] \\
&= \mathbf{P}_o\left[\frac{\mathbf{1}}{\mathbf{1}+i\mathbf{H}_o}\right] - i\left[\frac{\mathbf{1}}{\mathbf{1}+i\mathbf{H}_o}\right]\mathbf{P}_o\mathbf{H}_1\mathbf{P}_c\left[\frac{\mathbf{1}}{\mathbf{1}+i\mathbf{H}_c}\right] \\
&\quad \times\left[\mathbf{1}+i\left[\mathbf{H}-\cancel{\mathbf{H}_o}-\mathbf{H}_1\right]\right]\left[\frac{\mathbf{1}}{\mathbf{1}+i\mathbf{H}}\right] \\
&= \mathbf{P}_o\left[\frac{\mathbf{1}}{\mathbf{1}+i\mathbf{H}_o}\right] - i\left[\frac{\mathbf{1}}{\mathbf{1}+i\mathbf{H}_o}\right]\mathbf{P}_o\mathbf{H}_1\mathbf{P}_c\left[\frac{\mathbf{1}}{\mathbf{1}+i\mathbf{H}_c}\right] \\
&\quad -\left[\frac{\mathbf{1}}{\mathbf{1}+i\mathbf{H}_o}\right]\mathbf{P}_o\mathbf{H}_1\mathbf{P}_c\left[\frac{\mathbf{1}}{\mathbf{1}+i\mathbf{H}_c}\right]\mathbf{P}_c\mathbf{H}_1\mathbf{P}_o\left[\frac{\mathbf{1}}{\mathbf{1}+i\mathbf{H}}\right]. \qquad (162)
\end{aligned}$$

So

$$\left[1+\left[\frac{1}{1+i\mathsf{H}_o}\right]\mathsf{P}_o\mathsf{H}_1\mathsf{P}_c\left[\frac{1}{1+i\mathsf{H}_c}\right]\mathsf{P}_c\mathsf{H}_1\mathsf{P}_o\right]\mathsf{P}_o\left[\frac{1}{1+i\mathsf{H}}\right]=$$

$$\mathsf{P}_o\left[\frac{1}{1+i\mathsf{H}_o}\right]\left[1-i\mathsf{P}_o\mathsf{H}_1\mathsf{P}_c\left(\frac{1}{1+i\mathsf{H}_c}\right)\right]. \qquad (163)$$

If the above is multiplied on the left by $[1+i\mathsf{H}_o]$, the following is obtained:

$$\mathsf{P}_o\left[\frac{1}{1+i\mathsf{H}}\right] = \left[1+i\mathsf{H}_o+\mathsf{P}_o\mathsf{H}_1\mathsf{P}_c\left[\frac{1}{1+i\mathsf{H}_c}\right]\mathsf{P}_c\mathsf{H}_1\mathsf{P}_o\right]^{-1}$$
$$\times\mathsf{P}_o\left[1-i\mathsf{P}_o\mathsf{H}_1\mathsf{P}_c\left(\frac{1}{1+i\mathsf{H}_c}\right)\right]. \qquad (164)$$

The T-matrix can be written:

$$\mathsf{T}_{oo} = 2i\left[1+i\mathsf{H}_o+\mathsf{P}_o\mathsf{H}_1\mathsf{P}_c\left[\frac{1}{1+i\mathsf{H}_c}\right]\mathsf{P}_c\mathsf{H}_1\mathsf{P}_o\right]^{-1}$$
$$\times\left[\mathsf{P}_o\mathsf{J}\mathsf{P}_o-i\mathsf{P}_o\mathsf{H}_1\mathsf{P}_c\left[\frac{1}{1+i\mathsf{H}_c}\right]\mathsf{P}_c\mathsf{J}\mathsf{P}_o\right] \qquad (165)$$

or

$$\mathsf{T}_{oo} = \mathsf{P}_o-\left[\mathsf{P}_o+i\mathsf{H}_o+\mathsf{P}_o\mathsf{H}_1\mathsf{P}_c\left[\frac{1}{1+i\mathsf{H}_c}\right]\mathsf{P}_c\mathsf{H}_1\mathsf{P}_o\right]^{-1}$$
$$\times\left[\mathsf{P}_o+i\left[\mathsf{H}_o-2\mathsf{J}_o\right]+\mathsf{P}_o\mathsf{H}_1\mathsf{P}_c\left[\frac{1}{1+i\mathsf{H}_c}\right]\mathsf{P}_c\left(\mathsf{H}_1-2\mathsf{J}\right)\mathsf{P}_o\right] \qquad (166)$$

where

$$\mathsf{J}_o\equiv\mathsf{P}_o\mathsf{j}\mathsf{W}\mathsf{j}\mathsf{P}_o. \qquad (167)$$

Using

$$\begin{aligned} \mathbf{H}-2\mathbf{J} &= \frac{2\mu a^2}{\hbar^2}\mathbf{k}^{\frac{1}{2}}\mathbf{j}\mathbf{V}\left[\mathbf{h}-2\mathbf{j}\right]\mathbf{k}^{\frac{1}{2}} \\ &= \frac{2\mu a^2}{\hbar^2}\mathbf{k}^{\frac{1}{2}}\mathbf{j}\mathbf{V}\left[i\mathbf{n}-\mathbf{j}\right]\mathbf{k}^{\frac{1}{2}} \\ &= -\frac{2\mu a^2}{\hbar^2}\mathbf{k}^{\frac{1}{2}}\mathbf{j}\mathbf{V}\mathbf{h}^{(2)}\mathbf{k}^{\frac{1}{2}} \end{aligned} \tag{168}$$

or since for open channels $\mathbf{h}^{(2)} = \mathbf{h}^*$

$$\left[\mathbf{H}-2\mathbf{J}\right]\mathbf{P}_o = -\frac{2\mu a^2}{\hbar^2}\mathbf{k}^{\frac{1}{2}}\mathbf{j}\mathbf{V}\mathbf{h}^*\mathbf{k}^{\frac{1}{2}}\mathbf{P}_o, \tag{169}$$

the following expression for the $\mathbf{T}_{oo}$ matrix is obtained:

$$\begin{aligned} \mathbf{T}_{oo} &= \mathbf{P}_o - \mathbf{P}_o\left[\mathbf{1}+i\mathbf{H}_o+\mathbf{P}_o\mathbf{H}_1\mathbf{P}_c\left[\frac{\mathbf{1}}{\mathbf{1}+i\mathbf{H}_c}\right]\mathbf{P}_c\mathbf{H}_1\mathbf{P}_o\right]^{-1} \\ &\quad\times\left[\mathbf{P}_o - i\left(\mathbf{J}_o - i\mathbf{N}_o\right) - \mathbf{P}_o\mathbf{H}_1\mathbf{P}_c\left[\frac{\mathbf{1}}{\mathbf{1}+i\mathbf{H}_c}\right]\mathbf{P}_c\left(\mathbf{J}-i\mathbf{N}\right)\mathbf{P}_o\right] \end{aligned} \tag{170}$$

where

$$\mathbf{N}_o \equiv \mathbf{P}_o\mathbf{j}\mathbf{W}\mathbf{n}\mathbf{P}_o. \tag{171}$$

We define

$$\mathbf{R}_o \equiv \mathbf{P}_o\mathbf{W}\mathbf{P}_c\mathbf{h}\left[\frac{\mathbf{1}}{\mathbf{1}+i\mathbf{H}_c}\right]\mathbf{j}\mathbf{P}_c\mathbf{W}\mathbf{P}_o \tag{172}$$

where $\mathbf{W}$ has been defined in (141). Using (159) and (153) we can now write

$$
\begin{aligned}
\mathbf{P_o H_1 P_c}\left[\frac{\mathbf{1}}{\mathbf{1}+i\mathbf{H_c}}\right]\mathbf{P_c H_1 P_o} &= \mathbf{P_o}\left[\mathbf{P_o H P_c}+\mathbf{P_c H P_o}\right]\mathbf{P_c}\left[\frac{\mathbf{1}}{\mathbf{1}+i\mathbf{H_c}}\right] \\
&\quad \times \mathbf{P_c}\left[\mathbf{P_o H P_c}+\mathbf{P_c H P_o}\right]\mathbf{P_o} \\
&= \mathbf{P_o H P_c}\left[\frac{\mathbf{1}}{\mathbf{1}+i\mathbf{H_c}}\right]\mathbf{P_c H P_o} \\
&= \mathbf{P_o jWh P_c}\left[\frac{\mathbf{1}}{\mathbf{1}+i\mathbf{H_c}}\right]\mathbf{P_c jWh P_o} \\
&= \mathbf{jR_o h} \\
&= \mathbf{jR_o j}+i\mathbf{jR_o n} \\
&= i\left[\mathbf{J}_1+i\mathbf{N}_1\right] \qquad (173)
\end{aligned}
$$

where

$$\mathbf{J}_1 \equiv -i\mathbf{jR_o j} \qquad (174)$$

and

$$\mathbf{N}_1 \equiv -i\mathbf{jR_o n}. \qquad (175)$$

With the following definitions

$$\mathbf{H_o} \equiv \mathbf{J_o}+i\mathbf{N_o}, \qquad (176)$$

$$\overline{\mathbf{J}} \equiv \mathbf{J_o}+\mathbf{J}_1 \qquad (177)$$

and

$$\overline{\mathbf{N}} \equiv \mathbf{N_o}+\mathbf{N}_1, \qquad (178)$$

the $\mathbf{T_{oo}}$ matrix can be written

$$
\begin{aligned}
\mathbf{T}_{oo} &= \mathbf{P}_o - \frac{\mathbf{P}_o}{\mathbf{1} + i\overline{\mathbf{J}} - \overline{\mathbf{N}}}\left[\mathbf{1} - i\overline{\mathbf{J}} - \overline{\mathbf{N}}\right] \\
&= \mathbf{P}_o - \frac{\mathbf{P}_o}{\left[\mathbf{1} - \overline{\mathbf{N}}\right]\left[\mathbf{1} + \left[i/\left(\mathbf{1} - \overline{\mathbf{N}}\right)\right]\overline{\mathbf{J}}\right]}\left[\frac{\mathbf{1}}{\mathbf{1} - \overline{\mathbf{N}}}\right]\left[\mathbf{1} - \frac{i}{\mathbf{1} - \overline{\mathbf{N}}}\,\overline{\mathbf{J}}\right] \\
&= \mathbf{P}_o - \frac{\mathbf{P}_o}{\mathbf{1} + \left[i/\left(\mathbf{1} - \overline{\mathbf{N}}\right)\right]\overline{\mathbf{J}}}\left[\mathbf{1} - \frac{i}{\mathbf{1} - \overline{\mathbf{N}}}\,\overline{\mathbf{J}}\right] \qquad (179)
\end{aligned}
$$

or

$$
\mathbf{T}_{oo} = \mathbf{P}_o - \frac{\mathbf{P}_o}{\mathbf{1} - i\overline{\mathbf{K}}}\left[\mathbf{1} + i\overline{\mathbf{K}}\right] \qquad (180)
$$

and, finally

$$
\mathbf{T}_{oo} = -\frac{2i\mathbf{P}_o\overline{\mathbf{K}}}{\mathbf{1} - i\overline{\mathbf{K}}} \qquad (181)
$$

where

$$
\overline{\mathbf{K}} \equiv \frac{\mathbf{1}}{\overline{\mathbf{N}} - \mathbf{1}}\,\overline{\mathbf{J}}. \qquad (182)
$$

3.5 IOS T-Matrix Calculation

It is useful to note here that the method which will be used to obtain the IOS solution has already been used in the section where the central δ-shell potential was considered. To understand why this is so it is necessary to consider the two types of operators in the Schrödinger equation (ie., (29)) that bring about the directional coupling.

If the interaction potential is diagonal in orbital and rotor angular momentum representation, ie., it no longer couples different angular momentum states λ and λ' (and this is the case when there is only a central potential $V(R)$) then all

operators in the Schrödinger equation can be thought of as diagonal in angular momentum representation which leads to radial solutions parameterized by only one λ, ie.:

$$\frac{\hbar^2}{2\mu}\left[\frac{1}{R^2}\frac{d}{dR}R^2\frac{d}{dR}-\frac{\lambda(\lambda+1)}{R^2}+k^2\right]\psi_\lambda(kR)=V(R)\psi_\lambda(kR) \qquad (183)$$

where $k^2 = (2\mu/\hbar^2)E$. Conversely, if the angular momentum operators are replaced by quantities which are diagonal in orientation representation (and this is the case in the IOS approximation where *operator* Λ^2 is replaced by the *parameter* $\lambda_0(\lambda_0+1)$ so that all operators in the Schrödinger equation can be thought of as diagonal in orientation representation which leads to a set of uncoupled differential equations (as opposed to matrix radial solutions in the exact case) which is similar in form to (183) , ie.:

$$\frac{\hbar^2}{2\mu}\left[\frac{1}{R^2}\frac{d}{dR}R^2\frac{d}{dR}-\frac{\lambda_0(\lambda_0+1)}{R^2}+k_0^2\right]\psi_{\lambda_0}(k_0R,\theta)=V(R,\theta)\psi_{\lambda_0}(k_0R,\theta) \qquad (184)$$

except that there is the extra constant parameter θ classifying the solution $\psi_{\lambda_0}(k_0R,\theta)$. (Here $k_0^2=(2\mu/\hbar^2)\left[E-j_0(j_0+1)\hbar^2/2I\right]$ where j_0 is some chosen parameter.) Further, there is no longer the restriction that λ_0 be an integer, as in (183). Hence the methods of solution of the radial part of (183) and (184) are similar – (183) gives solutions parameterized by λ and k while (184) gives solutions parameterized by λ_0, k_0 and θ.

To demonstrate the above, the potential given by (114) is inserted in the IOS

equation (ie., equation (74)) and the following expression is obtained:

$$\frac{\hbar^2}{2\mu}\left[\frac{1}{R^2}\frac{d}{dR}R^2\frac{d}{dR}-\frac{\lambda_0(\lambda_0+1)}{R^2}+k_0^2\right]\psi_{\lambda_0}(k_0R,\theta)= V_\delta\left[1+b_2P_2(\cos\theta)\right]\delta(R-a)\psi_{\lambda_0}(k_0R,\theta). \quad (185)$$

In terms of the above discussion, the radial solution to (185) is dependent only on θ and hence the directional couplings which required matrix manipulations are avoided and (185) is solved for in the same manner as was (97).

Since the only integration done in solving (97) is over R, the addition of the θ term in the potential and the θ parameter dependence of the wave function makes no difference to the method of solution. So following the same steps as were used to solve for (97), a θ dependent T-matrix is obtained:

$$T_{\lambda_0k_0}(\theta)=\frac{-2i\xi_o g(\theta)j_{\lambda_0}^2(k_0a)}{1-i\xi_o j_{\lambda_0}(k_0a)h_{\lambda_0}(k_0a)} \quad (186)$$

where

$$\xi_o=k_0a \quad (187)$$

and

$$g(\theta)=-\frac{2\mu}{\hbar^2}V_\delta\left[1-b_2P_2(\cos\theta)\right]. \quad (188)$$

As was discussed in a previous section on IOS cross sections, the quantity $T^L_{\lambda_0k_0}$ must be calculated in order to obtain the $\sigma_{j\leftarrow j'}$ quantities. By inversion of (75), $T^L_{\lambda_0k_0}$ is given by:

$$T^L_{\lambda_0k_0}=\sqrt{2L+1}\int_0^{\frac{\pi}{2}}T_{\lambda_0k_0}(\theta)P_L(\cos\theta)\sin\theta d\theta. \quad (189)$$

Thus to get $\sigma_{j \leftarrow j'}$ cross sections, $T_{\lambda_0 k_0}(\theta)$ is calculated as given by (186) for appropriate values of λ_0, k_0 and θ. Next, using numerical methods this $T_{\lambda_0 k_0}(\theta)$ is integrated over all θ as given by (189) in order to get values for the $T^L_{\lambda_0 k_0}$'s. Finally (80) is used to get the resulting $\sigma_{j \leftarrow j'}$ cross sections.

4 CALCULATIONS AND RESULTS

4.1 Parameter Determination

4.1.1 Atom and Diatom Parameters

As mentioned in an earlier section, the molecular parameters are chosen so that the diatom is a model of nitrogen and so that the atom is a model of argon.

Hence the reduced mass μ is set to $2.734 \times 10^{-26} kg$. For the rotor, the atom separation is chosen to be $1.094 \times 10^{-10} m$. [38] which gives a moment of inertia I for nitrogen as $1.392 \times 10^{-46} kg - m.^2$, or a characteristic rotational temperature $\hbar^2/2Ik_B$ for nitrogen of 2.894K where k_B is the Boltzmann constant.

4.1.2 Choice of Energy

At temperature T the most probable energy for each of translational and rotational motion is $k_B\mathrm{T}$. In this thesis the major computation has been carried out at 300K. At this temperature $j = 6$ is the j-even state closest to a rotational energy of $k_B\mathrm{T}$ while the wave number

$$k = \sqrt{\frac{2\mu k_B \mathrm{T}}{\hbar^2}} \tag{190}$$

has the value $14.27 \times 10^{-10} m.^{-1}$ For this choice of rotor state (j =6) and translational energy k_BT, the total energy is $5.82 \times 10^{-21} J$. This is the total energy used for the cross section calculations in the following section. Corresponding to this energy, rotor states up to $j = 10$ are open and $j \geq 11$ closed. An analogous choice of energy parameters is used in section 4.3 for a calculation at 1000K. Note that the potential, (51), does not couple j-even and j-odd states, so the choice in this thesis is to restrict the calculation to j-even states.

4.1.3 Range of Partial Waves

In both of eqs. (81) (the IOS cross section) and (65) (the exact cross section) it is necessary to set an upper limit on λ, the maximum orbital angular momentum that significantly contributes to the sums over partial waves.

The largest λ value considered to contribute significantly to the scattering cross sections is that which corresponds to a particle just passing by the outer edge of the delta-shell, ie., the λ where the incoming particle approached a distance a from the scattering centre.

To determine this λ, it is necessary to associate the angular momentum as expressed in the quantum mechanical equation

$$L^2 = \lambda(\lambda + 1)\hbar^2 \tag{191}$$

which for large λ can be approximated as

$$L \approx (\lambda + \frac{1}{2})\hbar \tag{192}$$

with the angular momentum as expressed in the classical expression

$$L = \mu b v \tag{193}$$

where b is the impact parameter (see Figure 2 on page 63) and v is the particle velocity given by

$$v = \frac{\hbar k}{\mu}. \tag{194}$$

Equating (192) and (193) gives

$$\mu b v = (\lambda + \frac{1}{2})\hbar. \tag{195}$$

Since the maximum range of the potential is a, this gives

$$ka = (\lambda + \frac{1}{2}) \approx \lambda. \tag{196}$$

For a given translational and rotational energy the calculation for maximum λ was done as follows: the total energy (the kinetic and translational) was converted to a k value, then multiplied by a to arrive at a given λ. All λ beyond approximately twice this value did not contribute significantly to the cross sections.

4.1.4 Inverse Power Potential Comparisons

Since the aim of this study is to compare exact and IOS results using a delta-shell potential, the choice of potential parameters is arbitrary — just as long as the same parameters are used in both the exact and IOS calculations. However arbitrary this choice of parameters may be, it is nonetheless desirable that the parameters chosen yield cross sections which are comparable to cross sections

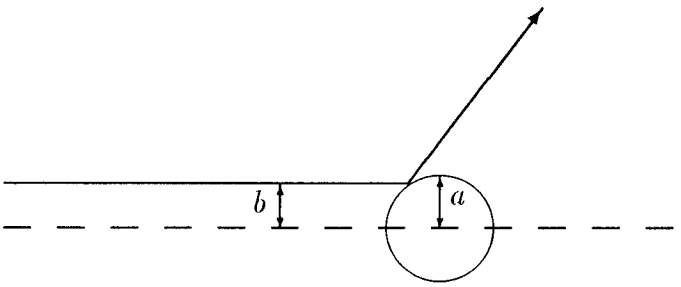

FIGURE 2: Impact parameter b is "the distance of the asymptotic path of the particle from the line of head on collision" [31].

obtained for a realistic system. In order to accomplish this, an IOS calculation using a realistic smooth repulsive potential was performed and then several choices of the delta-shell potential parameters were tried in equation (114) to see if these results could approximately reproduce the realistic results.

The potential chosen for comparison was the repulsive part of the Pattengill et. al. [39] potential

$$\begin{aligned} V(R,\theta) &= \frac{2.2\times 10^{-12}}{R^{12}}[1+0.5P_2(\cos\theta)] \\ &\quad -\frac{1.2\times 10^{-21}}{R^{6}}[1+0.13P_2(\cos\theta)] \end{aligned} \tag{197}$$

expressed in SI units, specifically the inverse power potential corresponding to the positive term

$$V(R,\theta)=\frac{2.2\times 10^{-12}}{R^{12}}[1+0.5P_2(\cos\theta)]\,. \tag{198}$$

Cross sections were calculated for this potential using the procedure reported by Snider and Coombe [40]. Phase shifts $\eta_{\lambda\kappa}(\cos\theta)$ were calculated using the WKB approximation

$$\eta_{\lambda k}(\cos\theta)=k\int_{r_c}^{\infty}\left(\sqrt{1-\frac{b^2}{R^2}-\frac{2\mu V(R,\theta)}{\hbar^2k^2}}-\sqrt{1-\frac{r_c^2}{R^2}}\right)dR+\frac{1}{2}k(b-r_c)\pi \tag{199}$$

where b is the impact parameter $(\lambda+\frac{1}{2})/\kappa$ $\left(\text{see } (196)\right)$ and r_c is the largest classical turning point.

By definition, the phase shifts are related to the S matrix by

$$S^{\lambda k}(\theta)=\exp\left[2i\eta_{\lambda k}(\cos\theta)\right]. \tag{200}$$

Since the potential is even in $\cos\theta$, it follows that the S-matrix can be expanded in even Legendre functions,

$$S^{\lambda k}(\theta) = \sum_{L(\text{even})} \sqrt{2L+1} S_L^{\lambda k} P_L(\cos\theta). \tag{201}$$

The expansion coefficients $S_L^{\lambda\kappa}$ are given by the inverse of (201), ie.

$$S_L^{\lambda k} = \sqrt{2L+1} \int_0^1 P_L(\cos\theta) \exp\left[2i\eta_{\lambda k}(\cos\theta)\right] d(\cos\theta). \tag{202}$$

To carry out this integration the phase shifts are fitted to an expansion in even Chebyshev polynomials:

$$\eta_{\lambda k}(\cos\theta) = A + BT_2(\cos\theta) + CT_4(\cos\theta) + DT_6(\cos\theta) \tag{203}$$

where the T_n's are Chebyshev polynomials and A, B, C and D are the fitting coefficients. A 60 point Gauss-Chebyshev integration scheme was then used to evaluate the $S_L^{\lambda\kappa}$ values.

The T-matrix expansion coefficients are then obtained according to

$$T_L^{\lambda k} = \delta_{0L} - S_L^{\lambda k} \tag{204}$$

and these were then substituted into (83) to obtain the $\sigma_{L\leftarrow 0}$ cross sections. The results are shown in Table 1.

For various values of the delta-shell potential parameters, ie., V_δ, b_2 and a, the IOS cross sections $\sigma_{L\leftarrow 0}$ were calculated, giving a wide range of results. For each choice of parameters, the θ dependent matrices were calculated using (186) and then using (189) integrated via a 40 point Gauss Legendre integration to

give the $T_L^{\lambda\kappa}$'s. The $\sigma_{L\leftarrow 0}^{IOS}$ were calculated using (80). After comparison with the results of the repulsive r^{-12} potential, parameters were chosen to give a reasonable fit. The best fit delta-shell potential is

$$V(R,\theta) = 3.697 \times 10^{-32} Jm \left[1 + 1.50 P_2(\cos\theta)\right] \delta(R-a) \qquad (205)$$

where $a = 5.5 \times 10^{-10} m$.

The leading coefficient for the potential is not directly comparable to the leading coefficient for the r^{-12} repulsive potential in (198) since the units and form are different. In the delta-shell $V_\delta = 3.697 \times 10^{-3} J. - m.$ has units of Joule-meters, whereas for the r^{-12} repulsive potential the coefficient has units of Joule-meters^{12}. Nonetheless, a form of comparison for these two parameters will be offered later in the discussion.

Table 1 gives a comparison of the cross sections for the two potentials:

Table 1: A Comparison of the Delta-Shell and r^{-12} Potentials

All cross sections in Å^2 $\kappa = 14.2717$ Å , $\lambda_{max} = 120$

L value	IOS with repulsive r^{-12}	IOS with delta shell
L=0	115.15	113.75
L=2	25.32	23.30
L=4	12.09	6.41
L=6	3.16	1.98
L=8	0.50	0.68
L=10	0.06	0.25

It is noted that the delta shell has a much higher anisotropy parameter but still gives smaller inelastic cross sections.

4.2 Cross Sections at 300K

4.2.1 Exact Cross Sections Including Only Open States

An exact calculation was done using as initial state, the thermally most probable rotor state and velocity corresponding to a temperature of 300K $\Big($equation $(190)\Big)$. For this temperature, j'=6, $k' = 14.27 \times 10^{-10} m.^{-1}$, and the maximum rotor state into which the molecule can scatter is $j = 10$. The present calculation was restricted to including only the open rotor states in solving the Schrödinger equation, thus $j_{\max} = 10$. $k'a \approx 77$ and $\lambda_{\max}$ was chosen to be 120. Since all the T-matrix elements are obtained from the calculation, all cross sections at this total energy are readily available. These are reported in Table 2.

Table 2: Exact Cross Sections

All cross sections in Å^2 *, Total Energy=5.82* $\times$ 10^{-21} *J.*

T.E.[1]	j'=0 421K	j'=2 404K	j'=4 364K	j'=6 300K	j'=8 213K	j'=10 103K
j =0	117.52	4.78	0.35	0.03	0.00	0.00
j =2	22.93	126.24	6.06	0.55	0.05	0.00
j =4	2.71	9.83	130.25	7.73	0.76	0.05
j =6	.32	1.06	9.21	143.19	8.75	0.66
j =8	.03	0.09	0.84	8.13	159.03	6.45
j =10	.00	0.00	0.03	0.36	3.86	197.47

1. TE = Translational Energy expressed as an equivalent temperature $(E = k_B \mathrm{T})$.

From the detailed calculations it was found that significant contributions to the cross sections fell off (ie., were of the order of 10^{-6} Å^2) for the j'=6 column at J=93 which corresponded to λ contributions ranging from λ=83 to λ=103. From J=93 to J=130 the contributions to the cross sections strictly decreased. Checks were maintained on the accuracy of the matrix inversion by a calculation of the condition number[1] for both the $\mathbf{K}^2+\mathbf{1}$ and $\mathbf{W}-1/\mathbf{jn}$ inversions as required by equations (140) and (141). The worst condition numbers found were of the order of about 2×10^4 for $\mathbf{W} - 1/\mathbf{jn}$ and 2×10^7 for $\mathbf{K}^2 + \mathbf{1}$. A further check as to the reliability of both inverses was performed by an actual multiplication of the matrix by its inverse and determining how close the result was to the unit matrix. For the product of the $\mathbf{W} - 1/\mathbf{jn}$ matrix (the matrix having condition number of 2×10^4) and its inverse, the largest off-diagonal term was of the order of 10^{-11} and the largest off-diagonal term for the product of the $\mathbf{K}^2 + \mathbf{1}$ matrix (the matrix having condition number of 2×10^7) and its inverse were of the order of 10^{-8}. Hence the inversion proved reliable for this set of initial conditions.

One trend is noted: as the kinetic energy decreases (and j' goes up), the elastic $j \leftarrow j'$ cross sections all increase.

[1]The condition number was calculated automatically by the inversion routine INV available as part of the support software at the UBC computing centre. According to reference [41] the condition number is a form of Turing's N-condition number[42]. Generally, the larger the condition number, the poorer the inverse. Well conditioned matrices will have a condition number of the order of N where N is the dimension of the matrix. At the other end of the scale, one of the most poorly conditioned matrices is the Hilbert matrix which has a condition number of order EXP(3.5N) [41]. For this run N=36.

4.2.2 Exact Cross Sections With Inclusion of Closed States

A calculation was run using the closed state calculation of (181) and then compared with a calculation done under similar conditions using the open state calculation of (133). Close-state calculations require the use of modified spherical Bessel functions (MSBF), and the values used in these calculations were obtained from a fitting of a table of values for MSBF for a given argument to a polynomial third order in λ. Two closed states, j' =10 and j' =12 were included in the calculations which are displayed in Table 3.

Table 3: Effect of Including Closed States

Part A: Using only open states. Total energy corresponds to translational energy of 300K and rotational state of 0. Units are in Å^2. *j' denotes the initial state, j the final state.*

	j'=0	j'=2	j'=4	j'=6	j'=8
j=0	126.95	5.00	0.49	0.06	0.01
j=2	23.56	142.98	7.39	0.80	0.09
j=4	3.59	11.39	145.24	8.08	0.84
j=6	0.43	1.31	8.60	164.04	7.76
j=8	0.04	0.10	0.61	5.21	202.36

Part B: Inclusion of closed states. Total energy corresponds to translational energy of 300K and rotational state of 0. Units are in Å^2. *j' denotes the initial state, j the final state.*

	j'=0	j'=2	j'=4	j'=6	j'=8
j=0	126.94	5.00	0.49	0.06	0.01
j=2	23.57	142.97	7.39	0.80	0.07
j=4	3.58	11.40	145.31	8.09	0.69
j=6	0.43	1.31	8.61	166.11	6.41
j=8	0.03	0.08	0.49	4.31	208.20

From the above table it is concluded that closed states only affect the calculations for those cross sections involving high rotor states (10←8, 8←10, 10←10). These differences can be of the order of about 20% but are confined to cross sections in the lower right hand corner of the above table of values (ie., high rotor states).

4.2.3 IOS $0 \rightarrow L$ Cross Sections

The IOS calculations are carried out in two steps. First, the $\sigma_{L \leftarrow 0}$ cross sections are calculated as given by (83) and then used along with the scaling relations as given by (84) to give the particular $j \leftarrow j'$ transition cross section. The first of these steps, the results of the calculation of the $\sigma_{L \leftarrow 0}$ cross sections, are given and compared with the exact results in this section.

Before any calculations using the IOS approximation can be performed, it is necessary to choose values for the parameters λ_0 and k_0. In equation (83), λ_0 was chosen to be an average of the λ and λ' values associated with the particular T-matrix element calculated. Hence for each combination of λ and λ' that gives a different λ_0 value, another T-matrix element was calculated.

The same choices for k_0 are available — one can choose k_0 as being equal to the k value corresponding to the j' state or to the k value corresponding to the j state or as being an average of both. For the $L \leftarrow 0$ calculations, both k_0 corresponding to the j' state and k_0 corresponding to the j state were used.

A Gauss Legendre angular integration scheme using 40 points was performed for the integration of the T-matrix as given by (189). Sums were done up to λ=120 and L=30 with contributions trailing off in significance (ie. giving cross section contributions of less than 10^{-6} Å^2) at λ=87 for $k_0 = 14.27 \times 10^{-10} m.^{-1}$

The unitarity of the S-matrix summing from L=0 to L=30, ie.,

$$\sum_{L=0}^{L=30} \left| S_L^{\lambda_0 k_0} \right|^2 = 1.00000 \tag{206}$$

was verified to 5 significant figures. The following results were obtained:

Table 4: IOS $\sigma_{L\leftarrow 0}$ Cross Sections

All cross sections in Å ^{2}

Final State L	Final k in Å^{-1}	Trans. Energy (T.E.)	Using $k_0 = k_{\text{init}}$ (16.92Å $^{-1}$) T.E.=421.5K	Using $k_0 = k_{\text{final}}$	Using $k_0 =$ 14.27 Å^{-1} T.E.=300K	Exact Results, $k =$ 16.92 Å^{-1} T.E.=421.5K
L =0	16.92	421.5K	101.90	101.90	113.75	117.52
L =2	16.57	404.2K	23.58	23.09	23.30	22.93
L =4	15.71	363.7K	5.85	5.50	6.41	2.71
L =6	14.27	300.0K	1.64	1.98	1.98	0.32
L =8	12.03	213.2K	0.52	0.80	0.68	0.03
L =10	8.37	103.2K	0.18	0.38	0.25	0.01
L =12			0.07		0.10	
L =14			0.03		0.04	
L =16			0.01		0.02	
L =18			0.01		0.01	

The general trend to be noted is that the IOS calculations underestimate the elastic 0←0 transitions and overestimate the inelastic cross sections. This can be explained by recognizing that a difference in energy between two states serves to hinder the excitation of the higher state. Hence with an approximation such as the IOS, which treats all rotational states as degenerate, it would be expected that the IOS would give higher inelastic cross sections than the exact results.

Another more classical explanation of these results is that at high L the rotor is moving more quickly with respect to the incoming atom than at say L =0. Hence the collision is less sudden at high L and it would be expected the IOS approximation to be less accurate for large angular momentum transfer. This

trend would be expected for transitions for $j' \neq 0$ since all other cross sections are dependent on these $\sigma_{L \leftarrow 0}$ values by (84).

One other effect arises because the IOS treats all rotational states as degenerate. This is that energetically inaccessible states are allowed, in particular, in the present calculation, transitions are allowed from L=0 to rotational states higher than L=10. The cross sections for these transitions however are so low that they may be effectively neglected. The next section contains some IOS results where energetically forbidden transitions are fairly significant.

Finally, the results above show that choosing the k_0 parameter to be either the initial or final k value does not significantly change the results. The only difference the k_0 choice seems to make is in the elastic cross section, where a choice of k_0=14.27 Å^{-1} gives a value closer to the exact value than choosing k_0=16.92 Å^{-1} , the actual initial k value for this transition.

The above trends apply to the $\sigma_{L \leftarrow 0}$ calculations. Since the $\sigma_{j \leftarrow j'}$ cross sections are calculated from these $\sigma_{L \leftarrow 0}$ cross sections, the differences between exact and IOS calculations noted here will be further examined after the scaling relations are applied to better determine how the IOS and exact calculations compare.

4.2.4 IOS Scaling Relations

4.2.4.1 Using IOS $\sigma_{L\leftarrow 0}$ Cross Sections

Since the IOS T-matrix was θ dependent it was expanded in Legendre polynomials in equation (75). This expansion subsequently led to a scaling relationship (84) which expresses $j \leftarrow j'$ cross sections in terms of $L \leftarrow 0$ cross sections. This relationship is used in this section to calculate the IOS $\sigma_{j\leftarrow j'}$ cross sections.

The previous section compared the IOS $\sigma_{L\leftarrow 0}$ and exact $\sigma_{L\leftarrow 0}$ cross sections. Whether their differences and similarities carry over to the $\sigma_{j\leftarrow j'}$ cross sections is examined here in order to determine how successful the scaling relation (84) is in predicting $j \leftarrow j'$ cross sections, once given the $L \leftarrow 0$ cross sections. As well, different k_0 choices are examined in light of the scaling relations .

For each of the three choices of k_0, $k_0 = k_{\text{initial}}$, $k_0 = k_{\text{final}}$ and k_0=14.92 Å^{-1}, the IOS $\sigma_{j\leftarrow j'}$ cross sections were calculated using the $\sigma_{L\leftarrow 0}$ cross sections from Table 4 and equation (84). The sum in (84) was taken up to the maximum allowed L value.

For the choice of $k_0 = k_{\text{initial}}$, the cross sections are given in Table 5:

Table 5: IOS Cross Sections at 300K Using $k_0 = k_{\text{initial}}$

Part A: Units are in Å^2. *j' denotes the initial state, j the final state.*

	j'=0	j'=2	j'=4	j'=6	j'=8	j'=10
j=0	101.90	4.62	0.61	0.15	0.05	0.02
j=2	23.58	111.03	7.48	1.40	0.37	0.13
j=4	5.85	13.86	113.22	8.54	1.63	0.46
j=6	1.64	3.17	11.65	120.97	8.43	1.70
j=8	0.52	0.89	2.47	11.60	132.19	7.41
j=10	0.18	0.29	0.64	2.70	10.65	155.32
j=12	0.07	0.10	0.19	0.78	2.64	8.96
j=14	0.03	0.04	0.06	0.26	0.81	2.50

Part B: Ratio of IOS to exact cross sections.

	j'=0	j'=2	j'=4	j'=6	j'=8	j'=10
j=0	0.87	0.97	1.75	4.48	15.9	154
j=2	1.03	0.88	1.23	2.55	6.92	46.7
j=4	2.15	1.41	0.87	1.11	2.14	9.80
j=6	5.21	2.99	1.27	0.85	0.96	2.59
j=8	20.4	9.36	2.93	1.43	0.83	1.15
j=10	297	98.3	20.6	7.40	2.76	0.79

The same trend is observed for cross sections with higher initial j-state as was observed for the j'=0 initial state cross sections — IOS inelastic cross sections are larger than the exact values while the elastic cross sections are lower. The results actually seem to get better for larger j' on using the scaling relationship but this is basically due to the nature of the summation. For example, the j'=6 column depends less on the large L-valued $\sigma_{L\leftarrow 0}$ cross section than the j' =0 columns. That is, to get the 10←0 cross section, only $\sigma_{L\leftarrow 0}$ for L=10 is used,

which is 297 times the exact $\sigma_{L\leftarrow 0}$ value. To get the 10←6 term, the $\sigma_{L\leftarrow 0}$ cross sections for the L=4, L=6, . . ., L=16 terms are used. And for L=4, the IOS $\sigma_{L\leftarrow 0}$ is only 2.15 times the exact $\sigma_{L\leftarrow 0}$ value. Not only are the lower-L $\sigma_{L\leftarrow 0}$ values more accurate, but they also contribute more in equation (84) relative to the other terms which also leads to better results for cross sections in the mid-table region.

With these points in mind, the $L \leftarrow 0$ results should be compared with the $j \leftarrow j'$ results in terms of how many rotor states the initial state is from the elastic transition. For instance, the 0←4 should be compared with the 2←6 transition. On this basis, the scaling law given by (84) preserves the ratios of the IOS to exact cross sections for the $L \leftarrow 0$ transitions when it is used to calculate the $j \leftarrow j'$ transitions.

The scaling relation also allows energetically forbidden cross sections and these may be of significant size. For example, the IOS 12←10 transition is calculated at 8.96 Å^2 but is 0 (ie., not allowed) for the exact calculation.

The cross sections using the choice $k_0 = k_{\text{final}}$ are given in Table 6.

Table 6: IOS Cross Sections at 300K Using $k_0 = k_{\text{final}}$

Part A: Units are in Å^2 *. j' denotes the initial state, j the final state.*

	j'=0	j'=2	j'=4	j'=6	j'=8	j'=10	j'=12	j'=14
j=0	101.90	4.72	0.65	0.13	0.03	0.01	0.00	0.00
j=2	23.09	111.03	7.70	1.22	0.26	0.07	0.02	0.01
j=4	5.50	13.46	1 13.22	8.06	1.31	0.27	0.07	0.02
j=6	1.98	3.64	12.33	120.97	8.87	1.67	0.40	0.12
j=8	0.80	1.24	3.07	11.02	132.19	8.62	1.79	0.47
j=10	0.38	0.53	1.07	2.75	9.16	155.32	7.53	1.81

Part B: Ratio of IOS to exact cross sections.

	j'=0	j'=2	j'=4	j'=6	j'=8	j'=10
j=0	0.87	0.99	1.86	3.71	10.3	72.7
j=2	1.01	0.88	1.27	2.22	4.94	25.1
j=4	2.03	1.37	0.87	1.04	1.72	5.86
j=6	6.29	3.44	1.34	0.85	1.01	2.55
j=8	31.4	13.1	3.65	1.36	0.83	1.34
j=10	627	183	34.5	7.53	2.37	0.79

Compared with the $k_0 = k_{\text{initial}}$ choice the $k_0 = k_{\text{final}}$ choice was better (although only of the order of about 5% for values about 1.0 times the exact value) in 17 cases and the $k_0 = k_{\text{initial}}$ was better in 13 cases with the two being the same for the elastic cross sections. The following table shows which of the two choices is best for each transition:

Table 7: Comparison of k_{initial} and k_{final} IOS Cross Sections

The best agreement with the exact cross sections is : I *if Initial state,* F *if Final state or* E *if equal. j' notes initial state, j the final state.*

	j'=0	j'=2	j'=4	j'=6	j'=8	j'=10
j=0	E	F	I	F	F	F
j=2	F	E	I	F	F	F
j=4	F	F	E	F	F	F
j=6	I	I	I	E	F	F
j=8	I	I	I	F	E	I
j=10	I	I	I	I	F	E

Rather than analyzing the above trend in terms of initial or final state parameter k_0, it is useful to analyze the results in terms of choice of $k_{\max}$ or $k_{\min}$. Table 8 demonstrates the trend for the best k_0 value being $k_0 = k_{\max}$ for large $|\Delta j|$ transitions and $k_0 = k_{\min}$ generally being the best choice for transitions where $|\Delta j|$=2.

Table 8: Comparison of $k_{\max}$ and $k_{\min}$ IOS Cross Sections

The best agreement with the exact cross sections is: Max *if* $k_0 = k_{\max}$, Min *if* $k_0 = k_{\min}$ *or* E *if equal.* j' *notes initial state,* j *the final state*

	j'=0	j'=2	j'=4	j'=6	j'=8	j'=10
j=0	E	Max	Min	Max	Max	Max
j=2	Min	E	Min	Max	Max	Max
j=4	Min	Min	E	Max	Max	Max
j=6	Max	Max	Max	E	Max	Max
j=8	Max	Max	Max	Min	E	Min
j=10	Max	Max	Max	Max	Min	E

The above two tables can be rationalized as follows: Since the total energy in a collision is conserved, a *downward* transition (going from a high rotor state to a low rotor state) corresponds to a $k_{\min}$ to $k_{\max}$ transition while an *upward* transition corresponds to a $k_{\max}$ to a $k_{\min}$ transition. Now for the $\sigma_{L\leftarrow 0}$ cross sections the $k_{\min}$ value is always the final k_0 choice and the $k_{\max}$ value is always the initial k_0 choice. Regarding Table 4 it is noted that for $\sigma_{2\leftarrow 0}$ and $\sigma_{4\leftarrow 0}$ the k_{final} or $k_{\min}$ choice is best while for $\sigma_{6\leftarrow 0}$, $\sigma_{8\leftarrow 0}$ and $\sigma_{10\leftarrow 0}$, k_{initial} or $k_{\max}$ is best. By the scaling relationship in (84), transitions are governed mainly by the $\sigma_{L\leftarrow 0}$ value corresponding to $L = |j' - j|$ since this is the largest term. Assuming that more accurate $\sigma_{L\leftarrow 0}$ values will give more accurate $\sigma_{j\leftarrow j'}$ values, then downward transitions (ie. going from a low k_0 to a high k_0) with $|\Delta j|$ greater than or equal to 4 would tend to favour a k_{final} choice or $k_{\max}$. Upwards transitions (going from a high k_0 to a low k_0) with $|\Delta j|$ greater than or equal

to 4 would favor the $k_{\max}$ choice as well but this now corresponds to the k_{initial} choice. For transitions with $|\Delta j|$=2, downward transitions would favour k_{initial} or $k_{\max}$ (as is the case in the 0←2, 4←6 and 4←8 transitions) and upward transitions would favour k_{final} or $k_{\min}$ (as is the case in 2←0, 4←2, 8←6, and 10←8).

Finally, to complete the study of k_0 values, one fixed energy was chosen, k_0=14.27 Å^{-1} . The cross sections using this choice of k_0 are given in Table 9:

Table 9: IOS Cross Sections At 300K Using $k_0 = 14.27$ Å^{-1}

Part A: Units are in Å^2 *. j' denotes the initial state, j the final state.*

	j'=0	j'=2	j'=4	j'=6	j'=8	j'=10	j'=12	j'=14
j=0	113.75	4.66	0.71	0.15	0.04	0.01	0.00	0.00
j=2	23.30	122.24	7.93	1.40	0.33	0.09	0.03	0.01
j=4	6.41	14.27	121.25	8.54	1.57	0.38	0.11	0.03
j=6	1.98	3.64	12.33	120.97	8.87	1.67	0.40	0.12
j=8	0.68	1.11	2.97	11.60	120.87	9.08	1.74	0.43
j=10	0.25	0.38	0.88	2.70	11.22	120.82	9.23	1.79
j=12	0.10	0.14	0.30	0.78	2.55	10.98	120.80	9.33
j=14	0.04	0.06	0.11	0.26	0.73	2.47	10.83	120.78

Part B: Ratio of IOS to exact cross sections

	j'=0	j'=2	j'=4	j'=6	j'=8	j'=10
j=0	0.97	0.97	2.04	4.48	15.6	103
j=2	1.02	0.97	1.31	2.55	6.20	33.4
j=4	2.36	1.45	0.93	1.11	2.07	8.02
j=6	6.29	3.44	1.34	0.85	1.01	2.55
j=8	26.8	11.7	3.53	1.43	0.76	1.41
j=10	419	131	28.3	7.40	2.91	0.61

In comparison with the previous results, the k_0=14.27Å^{-1} choice works best in the elastic cross sections. This can be accounted for in that the largest term in the sum in (84) is the term involving the $\sigma_{0\leftarrow 0}$ value and this is estimated better when k_0 is chosen as $k_0 = 14.27$ Å^{-1} rather than k_{initial} or k_{final}. In the inelastic transitions, however, the k_{initial} and k_{final} choices are better. A further

investigation could study a k_{average} value where

$$k_{\text{average}} = \frac{k_{\text{initial}} + k_{\text{final}}}{2} \tag{207}$$

but since the results in the above three choices of k_0 differ much less among themselves than they do with the exact results, little change from what has already been given would be expected.

The main point to note about the scaling relations is that the discrepancies noted in the $\sigma_{L\leftarrow 0}$ cross sections are carried over into the $\sigma_{j\leftarrow j'}$ cross sections with the results getting neither better nor worse. This is important to note since it suggests these scaling laws can be applied to the exact results which is the topic of investigation in the next section.

4.2.4.2 Using Exact $\sigma_{L\leftarrow 0}$ Cross Sections

There are two parts to the prediction of $\sigma_{j\leftarrow j'}$ by means of the scaling law in (84) — the values of the $\sigma_{L\leftarrow 0}$ cross sections and the way these $\sigma_{L\leftarrow 0}$ cross sections are combined with the 3-j symbols — each affects the result. In particular, the question arises if the 3-j symbols predict the correct j, j' dependence of $\sigma_{j\leftarrow j'}$. This can easily be tested with the delta-shell potential by putting in the exact $\sigma_{L\leftarrow 0}$ values in (84) to determine how the resulting $j \leftarrow j'$ cross sections compare with their corresponding exact cross sections. The cross sections obtained using the exact $\sigma_{L\leftarrow 0}$ values of Table 4 are reported in Table 10.

Table 10: IOS Cross Sections At 300K Using Exact $\sigma_{L\leftarrow 0}$ Values

Part A: Units are in Å^2. *j' denotes the initial state, j the final state.*

	j'=0	j'=2	j'=4	j'=6	j'=8	j'=10	j'=12	j'=14
j=0	117.52	4.59	0.30	0.02	0.00	0.00	0.00	0.00
j=2	22.93	124.85	7.00	0.51	0.04	0.00	0.00	0.00
j=4	2.71	12.60	123.97	7.63	0.58	0.05	0.00	0.00
j=6	0.32	1.32	11.02	123.80	7.97	0.62	0.05	0.00
j=8	0.03	0.14	1.10	10.43	123.75	8.18	0.65	0.06
j=10	0.00	0.01	0.12	1.01	10.11	123.72	8.32	0.67
j=12	0.00	0.00	0.01	0.10	0.96	9.91	123.70	8.43
j=14	0.00	0.00	0.00	0.01	0.10	0.92	9.77	123.70

Part B: Ratio of IOS to exact cross sections.

	j'=0	j'=2	j'=4	j'=6	j'=8	j'=10
j=0	1.00	0.96	0.86	0.71	0.51	0.25
j=2	1.00	0.99	1.15	0.93	0.79	0.94
j=4	1.00	1.28	0.95	0.99	0.76	1.05
j=6	1.00	1.25	1.20	0.87	0.91	0.95
j=8	1.00	1.51	1.30	1.28	0.78	1.27
j=10	1.00	3.67	3.71	2.76	2.62	0.63

Two trends in the above table can be noted: downward transitions are calculated as somewhat lower than the actual value, and upward transitions are calculated as being higher. As well, the elastic cross sections become progressively less than the actual values as j' increases.

That the downward transitions are lower than upward transitions can be accounted for by considering that the IOS has replaced wave number k_j with

one fixed parameter k_0. One implication of this approximation can be seen in the detailed balance equation:

$$\sigma^{\text{Exact}}_{j\leftarrow j'}(E_{k_{j'}}+\epsilon_{j'}) = \frac{[j]}{[j']}\frac{k_j^2}{k_{j'}^2}\sigma^{\text{Exact}}_{j'\leftarrow j}(E_{k_j}+\epsilon_j) \tag{208}$$

where $[j] = 2j+1$ and k_j is the k value corresponding to the state with rotor quantum number equal to j. For the IOS case, with $k_j^2 = k_{j'}^2 = k_0^2$, (208) becomes:

$$\sigma^{\text{IOS}}_{j\leftarrow j'}(E) = \frac{[j]}{[j']}\sigma^{\text{IOS}}_{j'\leftarrow j}(E). \tag{209}$$

(The above could also be derived using (84) for each of $\sigma_{j\leftarrow j'}$ and $\sigma_{j'\leftarrow j}$ and equating the two expressions.) For downward transitions $k_{j'} < k_j$ so $k_j/k_{j'} > 1$ but by (209) the IOS approximates this term as 1. As well, in upward transitions the term $k_j/k_{j'} < 1$ is also approximated by 1. If for $j' > j$ (ie., a downward transition) the $\sigma_{j'\leftarrow j}$ term is very close to the exact term, then the resulting $\sigma_{j\leftarrow j'}$ cross section would then be lower than the exact value. Conversely, for an upward transition the $\sigma_{j\leftarrow j'}$ cross section would be higher than the exact value, as is the case in the above table. For downward transitions with final state 0, the trend for this type of study will always lead to lower than exact values since the $\sigma_{j'\leftarrow j}$ values *are* the exact values. For downward transitions with final state other than 0, this trend would not always be expected. For example, the $\sigma_{j'\leftarrow j}$ term may be very much higher than the exact $\sigma_{j\leftarrow j'}$ term which, in a downward transition could compensate for the lack of the $k_j/k_{j'} > 1$ term and give an accurate IOS downward transition.

The other trend — that elastic IOS cross sections become progressively less than the exact value for larger initial rotor state — can also be attributed partly to the IOS approximating k_j^2 with k_0^2. The k_0 value used for the cross section calculations was 16.92Å^{-1} . These in turn were used to calculate the $\sigma_{j\leftarrow j'}$ cross sections for $j' = 6$ where k=14.27Å^{-1} . If the *exact* $\sigma_{L\leftarrow 0}$ values corresponding to k_{initial} =14.27Å^{-1} are used, the following values (shown in comparison to the k_{initial}=16.92Å^{-1} values) are obtained:

Table 11: Effect Of Using Different k Values In Exact $\sigma_{L\leftarrow 0}$ Values on the $\sigma_{j\leftarrow j'}$ Cross Sections

Exact $\sigma_{L\leftarrow 0}$ cross sections calculated at k=14.92 Å^{-1} and substituted into (84).Results are in Å^2 and are shown in comparison to the values given in Table 10:

Transition	k=14.92Å^{-1}	Ratio to exact results	k=16.92Å^{-1}	Ratio to exact results
0← 6	0.03	0.96	0.02	0.71
2← 6	0.67	1.23	0.51	0.93
4← 6	7.96	1.03	7.63	0.99
6← 6	133.54	0.93	123.80	0.87
8← 6	10.87	1.34	10.43	1.28

The elastic cross section does get better on using the proper energy but most of the other transitions do not. Hence while a proper accounting for different wave numbers among transitions may allow the scaling relation in (84) to better replicate elastic cross sections, inelastic cross sections may require even further types of corrections.

The results in Table 10 are now compared to results obtained using scaling relation (84) and IOS $\sigma_{L\leftarrow 0}$ values for an energy corresponding to 16.92Å^{-1} ; see Table 12.

Table 12: IOS Cross Sections At 300K Using k=16.92 Å^{-1}

Part A: Sums were done to maximum L using (84) *and the* $\sigma_{L\leftarrow 0}$ *values given for k=16.92* Å^{-1} *. Units are in* Å^2 *. j′ denotes the initial state, j the final state.*

	j'=0	j'=2	j'=4	j'=6	j'=8	j'=10	j'=12	j'=14
j=0	101.90	4.72	0.65	0.13	0.03	0.01	0.00	0.00
j=2	23.58	110.30	7.87	1.25	0.26	0.06	0.02	0.01
j=4	5.85	14.16	109.30	8.48	1.40	0.30	0.08	0.02
j=6	1.64	3.25	12.26	109.04	8.82	1.49	0.33	0.09
j=8	0.52	0.90	2.65	11.54	108.94	9.04	1.55	0.35
j=10	0.18	0.28	0.71	2.41	11.16	108.90	9.19	1.60
j=12	0.07	0.10	0.22	0.63	2.28	10.94	108.88	9.29
j=14	0.03	0.04	0.08	0.19	0.59	2.20	10.78	108.87

Part B: Ratio of IOS to exact cross sections.

	j'=0	j'=2	j'=4	j'=6	j'=8	j'=10
j=0	0.87	0.99	1.86	3.71	10.3	72.7
j=2	1.03	0.87	1.30	2.27	5.01	24.8
j=4	2.15	1.44	0.84	1.10	1.84	6.49
j=6	5.21	3.06	1.33	0.76	1.01	2.27
j=8	20.4	9.49	3.14	1.42	0.69	1.40
j=10	297	97.1	22.9	6.61	2.89	0.55

The major finding to note is that in all but the 6←8 and 0←2 transitions the cross sections obtained using the exact $\sigma_{L\leftarrow 0}$ values fared better than those

obtained using the IOS $\sigma_{L\leftarrow 0}$ values. This demonstrates that the scaling law works best with $\sigma_{L\leftarrow 0}$ values that are closer to the exact results. (It could have been that the scaling law corrected for inaccurate trends in the $\sigma_{L\leftarrow 0}$ cross sections — in which case using exact $\sigma_{L\leftarrow 0}$ cross sections would give worse results.)

Further, the errors due to the scaling laws are generally less than those attributed to the $\sigma_{L\leftarrow 0}$ values. For example, in the 4←6 transition, the use of an exact $\sigma_{L\leftarrow 0}$ value and the scaling law gives a 1% error but the use of the IOS $\sigma_{L\leftarrow 0}$ value and the scaling law gives a 10% error.

The derivation of the scaling law involved only the angular momentum coupling made possible through a θ parameterized T-matrix which was made possible by the assumption of suddenness. The calculation of the IOS $\sigma_{L\leftarrow 0}$ values, involve not only angular momentum simplifications but linear momentum simplifications associated with the assumption of suddenness. Since the scaling law at 300K is more accurate than the $\sigma_{L\leftarrow 0}$ values, it appears that the concept of suddenness for this collision may be better suited to studying the angular, rather than energy, or combination of energy and angular aspects of the collision.

4.2.5 Energy-Corrected Scaling Relation

As derived in (86), the Energy Corrected Scaling Relation requires a collision time τ. Since the shell of the potential is of negligible width (it takes no time to pass through the potential) τ might be considered to be 0. Nonetheless two

proposals for a finite value of τ are presented and then various τ values are tested to determine whether the Energy-Corrected Sudden scaling relation can improve the IOS results.

One possibility for the calculation of τ is to take the average time for a straight line trajectory through the sphere inside the Delta Shell potential at a given impact parameter b. Assuming the velocity v during the collision is constant, τ is calculated to be

$$\tau = \frac{2}{v}\left(\frac{1}{a}\right)\int_0^a \sqrt{a^2 - b^2}db = \frac{\pi a}{2v} \tag{210}$$

where a is the radius of the delta-shell. The value for v could correspond to the final or initial collision velocity or some average of the two. Table 13 gives the result of choosing the *lowest* velocity to calculate a τ value for the correction. The IOS $\sigma_{L\leftarrow 0}$ cross sections, on the other hand, were calculated using the initial state k value, whether this corresponded to the lowest velocity or not.

Table 13: ECIOS Cross Sections At 300K Using $\tau = \pi a/(2v_{\min})$ and Exact $\sigma_{L\leftarrow 0}(E_{k_{\text{initial}}})$ Values

Part A: Units are in Å^2 *. j' denotes initial state, j the final state.*

	j'=0	j'=2	j'=4	j'=6	j'=8	j'=10
j=0	101.90	2.38	0.02	0.00	0.00	0.00
j=2	12.14	111.03	0.65	0.00	0.00	0.00
j=4	0.17	1.21	113.22	0.13	0.00	0.00
j=6	0.00	0.01	0.18	120.97	0.02	0.00
j=8	0.00	0.00	0.00	0.03	132.19	0.00
j=10	0.00	0.00	0.00	0.00	0.00	155.32

Part B: Ratio of ECIOS to exact cross sections.

	j'=0	j'=2	j'=4	j'=6	j'=8	j'=10
j=0	0.87	0.50	0.05	0.01	0.00	0.00
j=2	0.53	0.88	0.11	0.01	0.00	0.00
j=4	0.06	0.12	0.87	0.02	0.00	0.00
j=6	0.01	0.01	0.02	0.85	0.00	0.00
j=8	0.00	0.00	0.00	0.00	0.83	0.00
j=10	0.00	0.00	0.00	0.00	0.00	0.79

Aside from the elastic cross sections, which are not affected by the ECIOS scaling relation, all cross sections have been practically reduced to 0 by this choice of τ. Clearly this choice of τ is too large. This does however demonstrate how the ECIOS scaling relation works. The IOS, by assuming a 0 collision time, overestimates inelastic cross sections. The worse this assumption (ie., the less sudden the collision) the more the IOS will overestimate the inelastic cross sections. Introducing a correction term inversely proportional to a collision time, as is done in the ECIOS scaling relation, reduces inelastic collision cross sections.

Further studies were done on finding a better τ value. If a factor f is defined so that

$$\tau = f\frac{a}{v} \tag{211}$$

then Table 13 displays the results obtained using f=1.57. It was found that an f value of 100 completely reduces all inelastic cross sections to 0.00 Å^2 while an f value of 1x10^{-5} does not change any of the IOS cross sections. In the investigation as to which τ value worked best for the ECIOS scaling relation it was found that while one choice of f was sufficient to get a column (ie. a set of cross sections with the same initial state) of IOS upwards transitions within 55% of exact values, this same value of f was not suitable for any other column. Table 14 reports the ECIOS cross sections for upward transitions which best fit the exact results as well as the f value used to obtain these results. Upward transitions can be calculated using detailed balance and would then give the same ratio to exact cross sections as their respective downward transition.

Table 14: ECIOS Cross Sections At 300K Using $\tau = fa/v_{\min}$ and IOS $\sigma_{L\leftarrow 0}\ (E_{k_{\max}})$ Values

Part A: Cross sections are in Å^2 *. j' denotes initial state, j the final state.*

	j'=0	j'=2	j'=4	j'=6	j'=8	j'=10
j=0	101.90					
j=2	22.91	111.03				
j=4	4.22	12.60	113.22			
j=6	0.43	1.64	10.01	120.97		
j=8	0.02	0.11	0.94	8.63	132.19	
j=10	0.00	0.00	0.03	0.37	4.57	155.32
f value	0.300	0.225	0.165	0.145	0.145	0.79

Part B: Ratio of ECIOS to exact cross sections.

	0	2	4	6	8	10
j=0	0.87					
j=2	1.00	0.88				
j=4	1.55	1.28	0.87			
j=6	1.37	1.54	1.09	0.85		
j=8	0.84	1.15	1.12	1.06	0.83	
j=10	0.75	0.89	0.89	1.03	1.18	0.79

It can be seen from Table 14 that the actual time that is needed to make the scaling relation work best is actually about 1/10th to 1/5th that calculated when it was assumed that the interaction lasts for the *whole* time it takes for the atom to traverse the diatom potential shell.

Another result brought to light by this study is the fact that the correction, which uses τ corresponding to the *least* velocity works best on an IOS result that calculates the $\sigma_{L\leftarrow 0}$ values based on the *highest* velocity and hence highest

energy. DePristo et. al. [32] recommend the minimum k value for the calculation of $\sigma_{L\leftarrow 0}$. This is based on the assumption that if the collision is sudden at the minimum kinetic energy value, it will be sudden at the maximum value as well. However a study of rate constants by Chapman and Green [43], essentially a Boltzmann average of cross sections, found that using the initial energy for upward $j \leftarrow 0$ transitions and the initial energy for downward $0 \leftarrow j'$ transitions gave best results. The present study comes to the same conclusion.

If, however, the minimum k value is used in *both* the calculation of the $\sigma_{L\leftarrow 0}$ cross sections and the ECIOS scaling relation then it is not possible to get the results to all agree within a 50% deviation of the exact results, as is demonstrated in Table 15, where the cross sections for initial rotor state equal to 10 are reported. The f value used was that which gave results that deviated least from the exact cross sections.

Table 15: ECIOS Cross Sections at 300K Using $\tau = 0.16a/v_{\min}$ and IOS $\sigma_{L\leftarrow 0}\ (E_{k_{min}})$ Values

Transition	Cross Section in Å^2	Ratio to Exact Results
0←10	0.00	3.8
2←10	0.00	1.4
4←10	0.02	0.46
6←10	0.18	0.28
8←10	2.75	0.43
10←10	155.32	0.79

The resulting $\sigma^{IOS}_{j\leftarrow j'}(E_{k_{\min}})$ cross sections with scaling could not be fitted to the exact results as closely as were the $\sigma^{IOS}_{j\leftarrow j'}(E_{k_{\max}})$ cross sections. The ratio of results:exact ranged by an order of 10 using minimum k value for the $\sigma_{L\leftarrow 0}$ cross sections and ranged by an order of about 1.5 using the maximum k value. A possible interpretation of why different k values work best in the scaling relation and $\sigma_{L\leftarrow 0}$ cross sections is that the IOS calculates the sudden part of the collision where the $k_{\max}$ value would be dominant while the ECIOS scaling relation calculates the non-sudden part of the collision where the $k_{\min}$ value would be dominant.

Table 14 may be further understood by considering the actual collision time, once τ is calculated using the f value which worked best. Table 16 shows both the k value used to calculate the $\sigma_{L\leftarrow 0}$ cross sections and the actual τ value used (obtained by multiplying f times a, divided by the least velocity) that gave the results in Table 14.

Table 16: $\sigma_{L\leftarrow 0}$ k Values and ECIOS τ Values Used In Table 14

For each entry, the upper number is the k value in Å^{-1} used to calculate the $\sigma_{L\leftarrow 0}$ cross sections while the lower number is the collision time τ in fs (10^{-15} s.). Elastic cross sections are not corrected by the ECIOS scaling relations and so there are no collision times for these values. j' denotes initial state, j the final state.

	j'=0	j'=2	j'=4	j'=6	j'=8	j'=10
j=0	16.92					
j=2	16.92	16.57				
	258.3					
j=4	16.92	16.57	15.71			
	272.3	204.2				
j=6	16.92	16.57	15.71	14.27		
	299.8	224.8	164.9			
j=8	16.92	16.57	15.71	14.27	12.03	
	355.6	266.7	195.6	171.9		
j=10	16.92	16.57	15.71	14.27	12.03	8.37
	511.0	383.3	281.1	247.0	247.0	
Factor	0.300	0.225	0.165	0.145	0.145	

If the τ value is regarded as a reliable measure of the time of interaction then the collision time seems to be proportional to the difference in rotor states between initial and final states. For example, transitions where $|\Delta j|$=2 seem to require about 200 fs. whereas those with $|\Delta j|$=8 require about 370 fs. This could explain why using the least τ value in the correction works so well, as well as why a different factor must be used for each j' value. If the same τ value was used for the j'=0 and j'=2 columns then the 4←0 and 4←2 would have the same τ value. But because the j'=0 column requires a larger f value than the

j'=2 column, the τ values for the 4←0 and 4←2 transitions are 272 and 204 fs. respectively. Hence the outcome of calculating τ based on final velocity and f based on initial state gives a set of actual values that increase with $|\Delta j|$. Note that the same sort of effect *could not* be achieved by using a τ value dependent on the average of initial and final velocities. For example, using an average τ velocity for the 10←0 transition ($|\Delta j|$=10) would give a τ value much less than using an average velocity for the 10←8 transition ($|\Delta j|$=2).

One final point was investigated — whether using the different k values in the calculation of the $\sigma_{L\leftarrow 0}$ cross sections affected the choice of collision time. It turns out that while certain combinations seem to work best (ie., largest k value for the calculation of the $\sigma_{L\leftarrow 0}$ cross sections and least velocity value for the calculation of τ in the ECIOS scaling relation) there does not appear to be a direct relationship between the two possible choices. Table 17 demonstrates that if the $\sigma_{L\leftarrow 0}$ cross sections are calculated at a lower k value, then a higher τ term in the ECIOS scaling relation *is not* always needed to compensate for this.

Table 17: How f Varies According To the k Used in the Calculation of the $\sigma_{L\leftarrow 0}$ Cross Sections

The f values chosen so that the 6←4, 8←4 *and* 10←4 *ECIOS cross sections are within 15% of the exact values.*

k Used to Calculate $\sigma_{L\leftarrow 0}$ in Å^{-1}	f Value Giving Best Results
16.92	0.170
15.71	0.165
8.37	0.190

The lack of correlation between the $\sigma_{L\leftarrow 0}$ value and ECIOS scaling relation velocity can be accounted for in that the IOS, regardless of choice of k value, assumes an instantaneous collision. Any correction accounting for collision time, such as the ECIOS scaling relation, would not be directly correlated to the k value used in the IOS $\sigma_{L\leftarrow 0}$ cross section calculations.

In summary, then, the results in this section recommend for the calculation of IOS $\sigma_{L\leftarrow 0}$ cross sections the use of the highest k value and then the use of these cross sections to calculate upward transitions. These cross sections are then to be used with the ECIOS scaling relations, where best results are obtained when the least velocity weighted by a factor dependent on the initial state is used for the τ value. The net effect of this method of calculating cross sections is to allow for a collision time in the IOS, and further, for this collision time to be dependent on the magnitude of $|\Delta j|$ for the transition.

Finding that τ increases as does $|\Delta j|$ or ΔE appears to violate the uncertainty principle. This seems to imply that interpreting τ as *only* a collision time may

be too narrow a definition of τ. Since $\epsilon_j - \epsilon_{j'}$ *is also* dependent on $|\Delta j|$ via

$$\epsilon_j - \epsilon_{j'} = (j - j')(j + j' + 1)\frac{\hbar^2}{2I} \tag{212}$$

it could well be that instead of interpreting $(\epsilon_j - \epsilon_{j'})\tau$ in the ECIOS correction factor as an energy-collision time term it is found out that an (energy)^2 term gives a better approximation to the exact cross sections.

4.2.6 General S-Matrix Scaling Relation

4.2.6.1 Using IOS $\sigma_{L\leftarrow 0}$ Cross Sections

In this section the General S-Matrix Scaling Relation (GSMSR, Equation (89)) is studied with regards to how well it can correct the IOS $\sigma_{L\leftarrow 0}$ cross sections. That is, even though exact $\sigma_{L\leftarrow 0}$ values are intended to be used in the GSMSR, it is investigated whether the GSMSR can improve the regular IOS results.

In replacing the exact $\sigma_{L\leftarrow 0}(E_k + \epsilon_L)$ with IOS $\sigma_{L\leftarrow 0}(E_{k_0})$, there is some arbitrariness as to the choice of E_{k_0} since in the IOS all rotational states are degenerate. The choice is made to interpret the $[L]\sigma^{\text{Exact}}_{0\leftarrow L}(E_k + \epsilon_L)$ term as $\sigma^{\text{IOS}}_{0\leftarrow L}(E_{k_0})$. That is, the choice of the k_0^2 value which will replace operator k^2 will correspond to the kinetic energy E_k with the ϵ_L term ignored. With this substitution Equation (89) becomes

$$\sigma_{j\leftarrow j'}(E_k+\epsilon_{j'}) = (2j+1)\sum_L \begin{pmatrix} j & j' & L \\ 0 & 0 & 0 \end{pmatrix}^2 \left[\frac{6 + [(\epsilon_L - \epsilon_0)\tau/2\hbar]^2}{6 + [(\epsilon_{j'} - \epsilon_j)\tau/2\hbar]^2}\right]^2 \sigma^{\text{IOS}}_{L\leftarrow 0}(E_k). \tag{213}$$

As well, the optimal choice of τ was involved using for each j', an f value and the minimum collision velocity. This resulted in the cross sections listed in Table 18.

The cross sections were calculated using (213) and the values where $E_{k_{j'}}$ is the translational energy associated with rotor state j' from Table 5. The τ value is calculated using the minimum collision velocity, the value for f reported below and equation (211).

Table 18: GSMSR Cross Sections At 300K Using IOS $\sigma_{L\leftarrow 0}$ Values

Part A: j' denotes initial state and j the final state. All cross sections are in Å^2 .

	$j'=0$	$j'=2$	$j'=4$	$j'=6$	$j'=8$	$j'=10$
$j=0$	101.90	4.62	0.61	0.15	0.05	0.02
$j=2$	23.58	111.55	7.25	1.27	0.32	0.11
$j=4$	5.85	13.53	115.11	7.92	1.27	0.32
$j=6$	1.64	2.73	9.98	122.88	7.52	1.14
$j=8$	0.52	0.72	1.44	9.64	134.71	6.33
$j=10$	0.18	0.23	0.30	1.48	9.30	158.25
f Value	[1]	0.25	0.30	0.20	0.15	0.10

[1]The τ value cancels out for these transitions

Part B: Ratio of GSMSR to exact cross sections.

	$j'=0$	$j'=2$	$j'=4$	$j'=6$	$j'=8$	$j'=10$
$j=0$	0.87	0.97	1.7	4.5	16	$1.5\text{x}10^2$
$j=2$	1.0	0.88	1.2	2.3	6.1	40
$j=4$	2.2	1.4	0.88	1.0	1.7	6.9
$j=6$	5.2	2.6	1.1	0.86	0.86	1.7
$j=8$	20	7.6	1.7	1.2	0.85	1.0
$j=10$	$3.0\text{x}10^2$	79	9.7	4.0	2.4	0.80

For transitions with j'=0, (213) reduces to

$$\sigma^{\rm GSM}_{j\leftarrow 0}(E_k+\epsilon_{j'}) = \sigma^{\rm IOS}_{j\leftarrow 0}(E_k) \tag{214}$$

and for those with j=0, (213) reduces to

$$\sigma^{\rm GSM}_{0\leftarrow j'}(E_k+\epsilon_{j'}) = \frac{1}{[j']}\sigma^{\rm IOS}_{j'\leftarrow 0}(E_k) \tag{215}$$

so there is no change in these values from Table 5. The other values report a marginal improvement over Table 5 (ie., the IOS Scaling Relation with IOS $\sigma_{L\leftarrow 0}$ values) in that elastic cross sections are increased and inelastic cross sections are decreased, more in keeping with exact results. The τ values which worked best tend to decrease as j' increases but this is not a definite trend as the j'=2 column demonstrates.

An alternative for these calculations is to convert (89) using the equation for detailed balance (equation (208)) to

$$\begin{aligned}&\sigma^{GSM}_{j\leftarrow j'}(E_k+\epsilon_{j'})\\ &= (2j+1)\sum_L \begin{pmatrix} j & j' & L \\ 0 & 0 & 0 \end{pmatrix}^2 \left[\frac{6+[(\epsilon_L-\epsilon_0)\tau/2\hbar]^2}{6+[(\epsilon_{j'}-\epsilon_j)\tau/2\hbar]^2}\right]^2 \left(\frac{E_k+\epsilon_L}{E_k}\right)\sigma^{\rm Exact}_{L\leftarrow 0}\end{aligned} \tag{216}$$

and replace $\sigma^{\rm Exact}_{L\leftarrow 0}$ with $\sigma^{\rm IOS}_{L\leftarrow 0}$. This results in

$$\begin{aligned}&\sigma^{GSM}_{j\leftarrow j'}(E_k+\epsilon_{j'})\\ &= (2j+1)\sum_L \begin{pmatrix} j & j' & L \\ 0 & 0 & 0 \end{pmatrix}^2 \left[\frac{6+[(\epsilon_L-\epsilon_0)\tau/2\hbar]^2}{6+[(\epsilon_{j'}-\epsilon_j)\tau/2\hbar]^2}\right]^2 \left(\frac{E_k+\epsilon_L}{E_k}\right)\sigma^{\rm IOS}_{L\leftarrow 0}.\end{aligned} \tag{217}$$

Comparing (217) with (216) reveals that the effect of this treatment would be to multiply all cross sections by a factor of $(E_k+\epsilon_L)/E_k > 1$ which would

lead to even poorer agreement with the exact cross sections. Other ways of approximating the $\sigma^{\mathrm{EX}}_{L\leftarrow 0}(E_k + \epsilon_L)$ term by a $\sigma^{\mathrm{IOS}}_{L\leftarrow 0}(E_{k_0})$ value would not be expected to significantly improve these results owing to the fact that the values of $\sigma^{\mathrm{IOS}}_{L\leftarrow 0}(E_{k_0})$ change only slightly with respect to a change in k_0 (Table 4).

It may be concluded that the GSMSR, even though intended for use with exact $\sigma_{L\leftarrow 0}$ values does have an advantage over the ECIOS (one intended for IOS $\sigma_{L\leftarrow 0}$ values) in increasing elastic cross sections. With regards to inelastic cross sections, however, the ECIOS does a better job than the GSMSR of scaling down the high $\sigma^{\mathrm{IOS}}_{j\leftarrow j'}$ values to match exact $\sigma_{j\leftarrow j'}$ cross sections.

4.2.6.2 Using Exact $\sigma_{L\leftarrow 0}$ Cross Sections

The GSMSR was tested as to how well it applied to reproducing the exact results. In order to calculate the column of cross sections with j'=10, the GSMSR required the calculation of $\sigma_{L\leftarrow 0}\ (E_k\ +\ \epsilon_L)$ cross sections for E_k corresponding to 103K and ϵ_L for L=0,2,4,6,8,12,14 in order to get enough terms in (89) to have the resulting $\sigma_{j\leftarrow j'}$ cross sections converge to two significant figures. Table 19 lists the details of this calculation, ie., the input values required for the calculation of cross sections for the GSMSR. E_k is the energy according to the most probable translational energy at 103K. $J = \lambda + j$ is the total angular momentum. The last contributing J value is that value of J for which there was a contribution of at least 1×10^{-7} Å^2 to the cross section.

Table 19: Input $\sigma_{L\leftarrow 0}(E_k+\epsilon_L)$ Values for the GSMSR at 300K for j'=10

Cross Section	Largest condition number[1]	Max. rotor state	Max. λ	Max. J	Contributing J	Calc. time (sec)[2]	Cross Section in Å^2
$\sigma_{0\leftarrow 0}(E_k+\epsilon_0)$	2.2x10^3	4	80	84	55	3.3	1.77x10^2
$\sigma_{0\leftarrow 2}(E_k+\epsilon_2)$	1.4x10^5	4	80	84	59	3.3	4.71x10^0
$\sigma_{0\leftarrow 4}(E_k+\epsilon_4)$	8.5x10^5	6	90	96	67	6.7	4.32x10^{-1}
$\sigma_{0\leftarrow 6}(E_k+\epsilon_6)$	9.5x10^6	8	100	108	78	14.5	6.50x10^{-2}
$\sigma_{0\leftarrow 8}(E_k+\epsilon_8)$	1.1x10^7	8	110	118	90	16.2	3.55x10^{-3}
$\sigma_{0\leftarrow 10}(E_k+\epsilon_{10})$	1.9x10^7	10	120	130	104	68.9	1.17x10^{-4}
$\sigma_{0\leftarrow 12}(E_k+\epsilon_{12})$	6.1x10^5	12	140	152	118	81.2	3.11x10^{-6}
$\sigma_{0\leftarrow 14}(E_k+\epsilon_{14})$	3.5x10^6	14	150	164	132	162.1	1.50x10^{-7}

1. Not all the conditions numbers checked for the 0←10 transition (Calculations for the 0←10 transition done on an Amdahl 470 V8)
2. The calculation time is that required for the Amdahl 5840.

The GSMSR also requires the calculation of a collision time τ. Using an average τ value with minimum v resulted in inelastic cross sections that were too low and an elastic cross section that was too high. If, however, τ is decreased, it is found that this scaling relationship decreases elastic cross sections since the coefficient in each term in the sum in (89) becomes

$$\left[\frac{6+[L(L+1)\hbar\tau/(4I)]^2}{6}\right]^2. \tag{218}$$

Not only does a decrease in τ decrease elastic cross sections, but it also increases inelastic cross sections since the coefficient in each term for these cross sections

in (89) becomes

$$\frac{6+\left[L(L+1)\hbar\tau/(4I)\right]^2}{6+\left[\left[j'(j'+1)-j(j+1)\right]\hbar\tau/(4I)\right]^2} \tag{219}$$

and for L small (where most of the contribution occurs) and j'=10 and j=2,4,6,8

$$j'(j'+1)-j(j+1) > L(L+1). \tag{220}$$

A τ value of 1.28×10^{-13} seconds was then found to bring all results to within 25% of the exact results as is shown in Table 20.

Table 20: GSMSR at 300K Using Exact $\sigma_{L\leftarrow0}(E_k+\epsilon_L)$ Values

The $\sigma_{L\leftarrow0}(E_k+\epsilon_L)$ values used are from Table 19. $\tau = 1.28\times10^{-13}$ s.

Transition	Cross Section in Å^2	Ratio to Exact Results
0 ← 10	0.00	1.00
2 ← 10	0.00	1.25
4 ← 10	0.06	1.24
6 ← 10	0.49	0.75
8 ← 10	6.73	1.04
10 ← 10	184	0.93

The results in Table 20 demonstrate that the GSMSR, with its allowance of a collision time, is about as accurate in predicting cross sections as the regular IOS Scaling Relation (Table 10), where no collision times were taken into account. (The j'=0 is a special case for the GSMSR in which (89) reduces to

$$\sigma_{j\leftarrow j'}(E_k+\epsilon_{j'}) = \sigma_{L\leftarrow0}(E_k+\epsilon_{j'}) \tag{221}$$

with $j = L$). The success of the GSMSR then seems to come not so much in accounting for a collision time but in that it makes use of the IOS scaling relationship.

One further result from Table 20 is that the τ value was found to have the same magnitude as in the ECIOS case, again suggesting the actual time of interaction to be about 1/10th the time it takes for a particle going at minimum collision velocity to traverse a shell with radius a=5.5Å . There are, however, some limitations to interpreting this τ value as an actual time of collision. This is demonstrated by adjusting the τ value for each transition in order for the cross section to fit with exact results. Table 21 lists the τ values required to get cross sections that are within 1% of the value of the exact results.

Table 21: τ Values Required to Match the GSMSR with Exact Results at 300K

The τ reported below is that value required by the GSMSR to give cross sections to within 1% of the exact values.

Transition	τ value in seconds
$2 \leftarrow 10$	1.79×10^{-13}
$4 \leftarrow 10$	1.53×10^{-13}
$6 \leftarrow 10$	0.89×10^{-13}
$8 \leftarrow 10$	1.36×10^{-13}
$10 \leftarrow 10$	8.52×10^{-13}

The τ value required to fit the elastic cross section to exact results is 5-10 times higher than the τ value required for inelastic cross sections but there

does not appear to be any physical reason why this should be so. As well, no direct relationship appears between the τ value and the type of transition (eg. decreasing τ with increasing j) which cautions one to not make too literal an interpretation of the τ value as being an accurate measure of the collision time.

4.2.7 Accessible States Scaling Relation

4.2.7.1 Using IOS $\sigma_{L\leftarrow 0}$ Cross Sections

In the previous section, the GSMSR used the assumptions of the IOS to relate $\sigma_{j\leftarrow j'}(E_k+\epsilon_{j'})$ values with $\sigma_{0\leftarrow L}(E_k+\epsilon_L)$ cross sections. In the Accessible States Scaling Relation (ASSR), the assumptions involve a simplification of angular coupling coefficients, neglect of quantum tunnelling and a statistical treatment of transition probabilities [33]. This leads to an alternative relationship between $\sigma_{0\leftarrow L}(E_k+\epsilon_L)$ values with $\sigma_{j\leftarrow j'}(E_k+\epsilon_{j'})$ cross sections. In this section several cross sections are calculated using the ASSR in order to determine how well it can reproduce exact cross sections.

The difference of the ASSR with the GSMSR is that the ASSR uses only one $\sigma_{0\leftarrow L}(E_k+\epsilon_L)$ value for each $\sigma_{j\leftarrow j'}(E_k+\epsilon_{j'})$ cross section calculated whereas the GSMSR involves a sum of $\sigma_{0\leftarrow L}(E_k+\epsilon_L)$ values for calculation of the $\sigma_{j\leftarrow j'}(E_k+\epsilon_{j'})$ cross section. For this reason the ASSR calculations are easier and less costly to obtain than the GSMSR calculations. As mentioned above, since the ASSR is similar to the GSMSR in that it relates $\sigma_{j\leftarrow j'}(E_k+\epsilon_{j'})$ cross sections with cross sections of a different energy, namely the $\sigma_{0\leftarrow L}(E_k+\epsilon_L)$ cross section.

Although the ASSR is intended to be used with exact $\sigma_{L\leftarrow 0}(E_k+\epsilon_L)$ values, a study is made in this section as to how good a scaling relation the ASSR is with the IOS $\sigma_{L\leftarrow 0}$ values. Comparing these results with exact results, it will be determined how compatible the assumptions that lead to the IOS cross sections are with the assumptions that lead to the ASSR.

As in the GSMSR when IOS $\sigma_{L\leftarrow 0}$ values were used, the choice is made to interpret the quantity $[j'-j]\sigma^{\rm EX}_{0\leftarrow|j'-j|}(E_k+\epsilon_{|j'-j|})$ as $\sigma^{\rm IOS}_{L\leftarrow 0}(E_{k_0})$. With this substitution, equation (91) becomes

$$\sigma^{\rm AS}_{j\leftarrow j'}(E_k+\epsilon_{j'})=\frac{[j]}{[j']}\frac{N(E_k+\epsilon_{j'-j})}{N(E_k+\epsilon_{j'})}\sigma^{\rm IOS}_{|j'-j|\leftarrow 0}(E_{k_0}). \qquad (222)$$

Table 22 lists the cross sections calculated from (222) using the IOS cross sections of Table 5.

Table 22: ASSR Cross Sections at 300K Using IOS $\sigma_{L\leftarrow 0}$ Values

Part A: Accessible States Cross Sections using $\sigma_{L\leftarrow 0}(E_{k_{j'}})$. j' denotes initial state and j the final state. All cross sections are in Å^2 .

	j'=0	j'=2	j'=4	j'=6	j'=8	j'=10
j=0	101.90	4.62	0.61	0.15	0.05	0.02
j=2	117.88	102.81	11.35	2.24	0.58	0.18
j=4	57.39	41.56	96.54	13.20	2.82	0.72
j=6	25.24	16.15	29.51	93.07	12.13	2.11
j=8	11.18	5.97	10.38	24.93	91.29	6.71
j=10	5.13	2.76	3.82	9.42	19.59	67.94

Part B: Ratio of above to the exact cross sections

	j'=0	j'=2	j'=4	j'=6	j'=8	j'=10
j=0	0.87	0.97	1.7	4.5	16	1.5 x 10^2
j=2	5.1	0.81	1.9	4.1	11	66
j=4	21	4.2	0.74	1.7	3.7	15
j=6	80	15	3.2	0.65	1.4	3.2
j=8	4.4x10^2	63	12	3.1	0.57	1.0
j=10	8.5x10^3	9.4x10^2	1.2x10^2	26	5.1	0.34

Downward transitions appear more accurate than upward transitions at the same j' and $|\Delta j|$. Elastic cross sections underestimate exact results and become increasingly lower as j' increases.

For transitions with j=0, (222) reduces to the expression

$$\sigma^{\text{AS}}_{0\leftarrow j'}(E_k + \epsilon_{j'}) = \frac{1}{[j']}\sigma^{\text{IOS}}_{j'\leftarrow 0}(E_{k_0}) \tag{223}$$

and so for these transitions the ASSR using IOS $\sigma_{L\leftarrow 0}$ values is the same as the IOS scaling relation using $\sigma^{\text{IOS}}_{L\leftarrow 0}$ values. For all other transitions, however, these

ASSR cross sections prove much more inaccurate than the IOS scaling relation using $\sigma^{\rm IOS}_{L\leftarrow 0}$ values in that the ASSR reports higher inelastic and lower elastic cross sections than the IOS results. An alternative calculation, ie., use in (91) the exact relation

$$[j'-j]\sigma^{\rm Exact}_{0\leftarrow|j'-j|}(E_k+\epsilon_{|j'-j|}) = \left[\frac{E_k+\epsilon_{|j'-j|}}{E_k}\right]\sigma^{\rm Exact}_{|j'-j|\leftarrow 0}(E_k+\epsilon_{|j'-j|}) \quad (224)$$

and then approximate $\sigma^{\rm Exact}_{|j'-j|\leftarrow 0}(E_k+\epsilon_{|j'-j|})$ by $\sigma^{\rm IOS}_{L\leftarrow 0}(E_{k_0})$ as outlined in (216) to (217) for the General S-Matrix Scaling relation, leads to all cross sections being multiplied by a factor of $(E_k+\epsilon_{|j'-j|})/E_k > 1$. This would increase the already high inelastic cross sections.

From the results in this section it appears important to retain the angular coupling coefficients (the 3-j symbols) when relating $\sigma^{IOS}_{j\leftarrow j'}$ cross sections with $\sigma^{IOS}_{L\leftarrow 0}$ values since the scaling relations based on the 3-j symbols (the regular IOS and ECIOS scaling relations) prove better than the ASSR. The ASSR, by assuming these coefficients to be functions of differences in j and j' only, is not compatible with the $\sigma^{\rm IOS}_{L\leftarrow 0}$ values since it does not correct for and in fact amplifies the inaccuracies resulting from using the $\sigma^{\rm IOS}_{L\leftarrow 0}$ values, namely, low elastic and high inelastic cross sections.

4.2.7.2 Using Exact $\sigma_{L\leftarrow 0}$ Cross Sections

Accessible states cross sections have been calculated for j'=10 and j'=6. For j'=10 the input cross sections are given in Table 19 while the j'=6 while the j'=6 input cross sections appear in Table 23. The same $\sigma_{0\leftarrow L}(E_k+\epsilon_L)$ values

given in Table 19 are then used for cross sections with initial rotor state of 10. As well, the $\sigma_{0\leftarrow L}(E_k + \epsilon_L)$ values given in Table 23 are used to calculate cross sections with initial rotor state of 6.

In Table 23 E_k is the energy according to the most probable translational energy at 300K, and $\epsilon_L = L(L+1)\hbar^2/2I$. $J = \lambda + j$ is the total angular momentum. The last contributing J value is that value of J for which there was a contribution of at least 1×10^{-7} Å^2 to the cross section. The time for calculations is that required for the Amdahl 5840.

Table 23: Input $\sigma_{0\leftarrow L}(E_k + \epsilon_L)$ Values for the ASSR at 300K for $j' = 6$

Cross Section	Largest Condition Number[1]	Max. Rotor State	Max. λ	Max. J	Contributing J	Calc. Time[2] (sec.)	Cross Section in Å^2
$\sigma_{0\leftarrow 0}(E_k + \epsilon_0)$	1.2x10^7	8	110	118	89	20.138	0.126952 x 10^3
$\sigma_{0\leftarrow 2}(E_k + \epsilon_2)$	1.8x10^5	8	110	118	91	19.737	0.507163x10^1
$\sigma_{0\leftarrow 4}(E_k + \epsilon_4)$	2.1x10^5	10	120	130	96	39.148	0.404343x10^0
$\sigma_{0\leftarrow 6}(E_k + \epsilon_6)$	1.9x10^7	10	120	130	104	68.934	0.340958x10^{-1}

1. Not all the conditions numbers checked for the 0←6 transition
2. Calculations for the 0←6 transition done on an Amdahl 470 V8

The values from Tables 19 and 23 were then substituted into equation (91) and the resulting cross sections are displayed in Table 24.

Table 24: ASSR Cross Sections Using Exact $\sigma_{0\leftarrow L}(E_k+\epsilon_L)$ Values for 300K

The $\sigma_{0\leftarrow L}(E_k+\epsilon_L)$ values used are from Tables 19 and 23 .

Transition	Cross Section in Å^2	Ratio to Exact Results	Transition	Cross Section in Å^2	Ratio to Exact Results
0←6	0.03	1.00	0←10	0.00	1.00
2←6	1.27	2.32	2←10	0.00	4.32
4←6	14.36	1.86	4←10	0.03	5.62
6←6	126.95	0.73	6←10	1.31	2.00
8←6	25.36	3.34	8←10	8.67	1.34
10←6	3.64	14.7	10←10	80.58	0.41

The calculations in Table 22 are also more inaccurate than the ASSR using $\sigma^{\text{Exact}}_{0\leftarrow|j'-j|}(E_k+\epsilon_{|j'-j|})$ values (Table 24).

On the basis of these results, the ASSR calculates elastic cross sections that are lower and inelastic cross sections that are higher than the exact cross sections. (The special case where j=0 reduces (91) to

$$\sigma_{0\leftarrow j'}(E_k+\epsilon_{j'})=\sigma_{0\leftarrow L}(E_k+\epsilon_L) \tag{225}$$

with $j'=L$ and so the 0←10 and 0←6 ASSR cross sections are exact). As well, as $|j-j'|$ increases, so too does the error. In the j'=6 column the cross section for a downward transition with a given $|j-j'|$ is much closer to the exact value than is the upward transition cross section for the same $|j-j'|$.

In the paper where the ASSR is introduced some calculations [32] using the ASSR for Ar-N_2 using the potential of Pattengill, LaBudde, Bernstein and Curtiss [39], it was found that error increases as $|j-j'|$ increases. In these calculations

it was also found that the error for transitions for the Ar-N_2 system increases as j' increases but this is not the case for the results in Table 24 . For example, the ratio of the 4←6 transition cross section to exact results is 1.9 but for the 8←10 transition is more accurate, with a ratio to exact results of 1.3.

It was also found in the calculations by DePristo [33] that the ASSR for some transitions where $|j - j'|$=4 can overpredict by a factor of 2 (as is the case in this study for the 2←6 and 6←10 transitions) and the ASSR for $|j - j'|$=6 can overpredict by as much as 11 times (here, for the 4←10 transition, the ASSR overpredicts by only about 5.5 times).

In comparison to the ASSR cross sections, the IOS cross sections which use the IOS $\sigma_{L\leftarrow 0}$ values (Table 5) are better for all the j'=6 transitions and for the j'=10 transitions for $|j - j'|$=0 and 2 (ie. the 10←10 and 8←10 transitions). The two are similar in that they become worse with increasing $|j - j'|$ and this error in both scaling relations grows to about the same magnitude as the transition becomes more inelastic. For example, the errors in the IOS for the 8←10, 6←10 and 4←10 transitions are 15%, 160% and 880% and for the ASSR are 34%, 100% and 460% respectively. DePristo further notes [33] that using pure statistical theory (ie. treating all rotational states as degenerate) to relate the $\sigma_{0\leftarrow L}(E_k + \epsilon_L)$ values with the $\sigma_{j\leftarrow j'}(E_k + \epsilon_{j'})$ cross sections leads to even greater inelastic cross sections and hence even poorer results. It seems possible then that the reason for the overestimation of the inelastic collisions comes from the statistical assumptions made in each scaling relation, the ASSR when it

assumes that the transition probability is inversely proportional to the number of accessible states, and the IOS, when it replaces operator k_j^2 with one parameter k_0^2 and in doing so treats all rotational states as energetically equivalent.

One further note on DePristo's work [33] which may have some relevance on this work is that DePristo found that his scaling theory worked best for systems with a lower reduced mass, such as a He-CO system, for which the reduced mass is about 3.5 atomic mass units (amu). Less accurate results were found by DePristo for the Ar-N_2 system, which has a reduced mass of 16.5 amu.

Finally, in comparing the ASSR cross sections (which vary by as much as 1500% from the exact results) with the GSMSR cross sections (which vary by at most only 25% from the exact results (Table 20)), it may be concluded that the manner in which the GSMSR relates the $\sigma_{0\leftarrow L}(E_k + \epsilon_L)$ values with the $\sigma_{j\leftarrow j'}(E_k + \epsilon_{j'})$ cross sections appears to be more reliable. In the ASSR, the combined assumptions of degeneracy, the Effective Hamiltonian having angular coupling coefficients dependent on energy differences and neglect of quantum tunnelling lead to errors of the same magnitude found in IOS scaling relations with IOS $\sigma_{L\leftarrow 0}$ values even though $exact$ input cross sections are used. One possibility for decreasing this error of the ASSR is to modify or remove its assumption that on statistical grounds that the transition probability is proportional to the number of accessible states.

4.3 Cross Sections at 1000K

4.3.1 The Exact Cross Sections

An exact calculation for 1000K was carried out. This requires changing certain parameters from the values used for the 300K calculation. Specifically, at 1000K, the thermally most probable rotor state is 12.64 (which was taken to be 12 since this study considers only the even rotor states) and the maximum rotor state for N_2 with a translational energy of 1000K (ie. using (190)) and initial rotational state of 12 is 20. This gives a total energy of $E = k_B\mathrm{T} + \epsilon_{12} = 2.004 \times 10^{-20} J$. If all the energy from the initial conditions is converted to kinetic energy then the maximum k value possible is $3.14 \times 10^{11} m.^{-1}$ Using (196) the maximum partial wave contributing is estimated at 173 so contributions from 190 partial waves were kept. All other parameters — those for the potential and N–N distance — were kept at the same values as used in the 300K calculations. As this study is focussed on the utility of the IOS approximation and its variants to calculate rotational cross sections, any aspects of vibrational motion have been ignored. The calculated cross sections retaining only open states are listed in Table 25.

Table 25: Exact Cross Sections at Energy=1000K

j' denotes initial state and j the final state. All cross sections are in Å^2 .

	j'=0	j'=2	j'=4	j'=6	j'=8	j'=10
j=0	70.07	3.13	0.19	0.01	0.00	0.00
j=2	15.44	73.92	5.24	0.27	0.02	0.00
j=4	1.68	9.16	75.64	4.96	0.30	0.02
j=6	0.16	0.66	6.83	80.03	5.52	0.32
j=8	0.01	0.06	0.51	6.75	79.69	6.01
j=10	0.00	0.00	0.03	0.44	6.76	85.11
j=12	0.00	0.00	0.00	0.03	0.44	6.70
j=14	0.00	0.00	0.00	0.00	0.03	0.36
j=16	0.00	0.00	0.00	0.00	0.00	0.02
j=18	0.00	0.00	0.00	0.00	0.00	0.00
j=20	0.00	0.00	0.00	0.00	0.00	0.00

	j'=12	j'=14	j'=16	j'=18	j'=20
j=0	0.00	0.00	0.00	0.00	0.00
j=2	0.00	0.00	0.00	0.00	0.00
j=4	0.00	0.00	0.00	0.00	0.00
j=6	0.02	0.00	0.00	0.00	0.00
j=8	0.37	0.02	0.00	0.00	0.00
j=10	6.38	0.35	0.02	0.00	0.00
j=12	90.09	6.63	0.39	0.03	0.00
j=14	6.49	98.79	7.00	0.50	0.03
j=16	0.34	6.28	108.63	8.05	0.49
j=18	0.02	0.35	6.28	127.48	7.05
j=20	0.00	0.01	0.22	4.00	171.52

For the inversion of matrix $\mathbf{K}^2 + \mathbf{1}$ the largest condition number was found to be of the order of 1×10^7. For the inversion of matrix $\mathbf{W} - 1/\mathbf{nj}$ the largest condition number was found also to be about 1×10^7.

A comparison of the 300K cross sections (Table 2) with the 1000K cross sections reveals that all inelastic and elastic cross sections are reduced as the temperature increases.

4.3.2 The IOS $\sigma_{L\leftarrow 0}$ Cross Sections

As noted in the literature, the Energy Sudden [30] and Centrifugal Sudden [44] approximations improve for higher collision energies. Thus it is expected that the IOS, a combination of the ES and CS, should improve at a higher collision energy.

The IOS calculation was carried out for 1000K keeping all the parameters the same as described for the 300K calculation except: contributions from 190 instead of 120 partial waves were included and the $k_0 = k_{\text{init}}$ value was calculated as that value which would give a total energy corresponding to

$$\frac{\hbar^2 k_{\text{init}}^2}{2\mu} + j_{\text{initial}}(j_{\text{initial}}+1)\frac{\hbar^2}{2I} = 2.004\text{x}10^{-20} J \qquad (226)$$

where 2.004x10^{-20} J. is the total energy appropriate for 1000K. Again the λ_0 value was chosen to be the average of λ and λ'. The calculated IOS cross sections are listed in Table 26.

Table 26: IOS Cross Sections at 1000K Using $k_0 = k_{\text{initial}}$

Part A: j' denotes initial state and j the final state. All cross sections are in Å^2 .

	j'=0	j'=2	j'=4	j'=6	j'=8	j'=10
j=0	62.40	3.97	0.34	0.05	0.01	0.00
j=2	19.79	69.14	6.16	0.62	0.10	0.02
j=4	3.05	11.18	69.04	6.77	0.73	0.13
j=6	0.59	1.59	9.67	70.28	7.15	0.84
j=8	0.14	0.30	1.29	9.24	71.98	7.52
j=10	0.04	0.07	0.23	1.22	9.07	75.00
j=12	0.01	0.02	0.05	0.22	1.20	9.11
j=14	0.00	0.01	0.01	0.05	0.22	1.25
j=16	0.00	0.00	0.00	0.01	0.05	0.24
j=18	0.00	0.00	0.00	0.00	0.01	0.06
j=20	0.00	0.00	0.00	0.00	0.00	0.02

	j'=12	j'=14	j'=16	j'=18	j'=20
j=0	0.00	0.00	0.00	0.00	0.00
j=2	0.01	0.00	0.00	0.00	0.00
j=4	0.03	0.01	0.00	0.00	0.00
j=6	0.16	0.04	0.01	0.01	0.01
j=8	0.95	0.19	0.06	0.03	0.02
j=10	7.80	1.10	0.24	0.09	0.05
j=12	78.95	8.40	1.25	0.33	0.14
j=14	9.16	85.18	8.62	1.52	0.47
j=16	1.32	9.65	92.63	9.00	1.81
j=18	0.26	1.46	9.74	105.03	8.75
j=20	0.06	0.29	1.60	10.03	127.47

Table 26 – Continued

Part B: Ratio of IOS to exact cross sections

	j'=0	j'=2	j'=4	j'=6	j'=8	j'=10
j=0	0.89	1.3	1.7	3.6	9.8	52
j=2	1.3	0.94	1.2	2.3	4.9	20
j=4	1.8	1.2	0.91	1.4	2.4	7.6
j=6	3.8	2.4	1.4	0.88	1.3	2.7
j=8	10	5.2	2.5	1.4	0.90	1.3
j=10	48	19	7.4	2.8	1.3	0.88
j=12	$3.1\text{x}10^2$	$1.0\text{x}10^2$	30	8.5	2.7	1.4
j=14	$1.3\text{x}10^3$	$4.5\text{x}10^2$	$1.2\text{x}10^2$	33	8.4	3.4
j=16	$1.2\text{x}10^4$	$4.3\text{x}10^3$	$1.0\text{x}10^3$	$2.0\text{x}10^2$	48	14
j=18	$1.3\text{x}10^5$	$3.7\text{x}10^4$	$6.1\text{x}10^3$	$1.2\text{x}10^3$	$2.4\text{x}10^2$	71
j=20	$1.9\text{x}10^7$	$2.2\text{x}10^6$	$3.3\text{x}10^5$	$3.6\text{x}10^4$	$5.4\text{x}10^3$	$1.3\text{x}10^3$

	j'=12	j'=14	j'=16	j'=18	j'=20
j=0	$4.1\text{x}10^2$	$1.7\text{x}10^3$	$2.5\text{x}10^4$	$4.8\text{x}10^5$	$1.6\text{x}10^6$
j=2	$1.3\text{x}10^2$	$5.5\text{x}10^2$	$8.0\text{x}10^3$	$1.2\text{x}10^5$	$1.4\text{x}10^7$
j=4	36	$1.5\text{x}10^2$	$1.8\text{x}10^3$	$1.8\text{x}10^4$	$1.8\text{x}10^6$
j=6	8.8	36	$2.7\text{x}10^2$	$2.4\text{x}10^3$	$1.1\text{x}10^5$
j=8	2.6	8.4	55	$3.7\text{x}10^2$	$1.1\text{x}10^4$
j=10	1.2	3.1	13	78	$1.6\text{x}10^3$
j=12	0.88	1.3	3.2	13	$1.6\text{x}10^2$
j=14	1.4	0.86	1.2	3.1	18
j=16	3.9	1.5	0.85	1.1	3.7
j=18	15	4.2	1.6	0.82	1.2
j=20	$1.9\text{x}10^2$	29	7.4	2.5	0.74

Contributions for $\lambda > 184$ for j=0 were found to be negligible (ie., affecting only the sixth significant figure).

The unitarity of the S matrix (equation (206)) again was verified to 6 significant figures for (206) summed up to $L = 30$. As well, a check was done

on the S-matrix integration procedure, using 96 as well as 40 points for Gauss-Legendre integration. The 96 point integration procedure agreed with the 40 point procedure to 6 significant figures.

Table 26 demonstrates that in 28 of the 36 transitions for j and j' ranging from 0 to 10 the ratios of the IOS cross sections to exact cross sections at 1000K are closer to one than the corresponding ratios at 300K (Table 5).

4.3.3 ECIOS $\sigma_{L\leftarrow 0}$ Cross Sections

One of the most attractive features of the ECIOS scaling law is that it corrects for the large IOS values for highly inelastic collisions. This warranted investigation at higher temperatures, where there is the possibility for even higher energy inelasticity. Will the ECIOS be able to correct for this as well?

Table 27 gives a comparison between exact, IOS, and ECIOS values at 1000K. The f value chosen for the ECIOS calculation is 0.5.

Table 27: ECIOS Cross Sections at 1000K

Transition	Calculation	Cross Section	Ratio to Exact
0←0	Exact	70.07	
	IOS	62.40	0.89
	ECIOS	62.40	0.89
2←0	Exact	15.4	
	IOS	19.8	1.3
	ECIOS	19.4	1.3
4←0	Exact	1.68	
	IOS	3.05	1.8
	ECIOS	2.40	1.4
6←0	Exact	0.157	
	IOS	0.589	3.8
	ECIOS	0.232	1.5
8←0	Exact	0.0137	
	IOS	0.138	10
	ECIOS	0.0167	1.2
10←0	Exact	7.73×10^{-4}	
	IOS	3.72×10^{-2}	48
	ECIOS	1.11×10^{-3}	1.4
12←0	Exact	3.57×10^{-5}	
	IOS	1.11×10^{-2}	310
	ECIOS	7.86×10^{-5}	2.2
14←0	Exact	2.80×10^{-6}	
	IOS	3.56×10^{-3}	1300
	ECIOS	5.97×10^{-6}	2.1
16←0	Exact	1.01×10^{-7}	
	IOS	1.19×10^{-3}	12000
	ECIOS	4.60×10^{-7}	4.6
18←0	Exact	3.20×10^{-9}	
	IOS	4.12×10^{-4}	130000
	ECIOS	3.15×10^{-8}	10
20←0	Exact	7.74×10^{-12}	
	IOS	1.46×10^{-4}	19000000
	ECIOS	1.29×10^{-9}	167

The results in Table 27 seem to indicate that the corrections invoked by the ECIOS are mathematically valid; the ECIOS follows the behaviour of the exact calculations even to values as low as 1×10^{-7} Å^2.

4.4 Changing Parameter C_{V_δ}

In the calculations parameter C_{V_δ} is the unitless constant

$$C_{V_\delta} = \frac{2\mu}{\hbar^2} a V_\delta \tag{227}$$

and so an increase in C_{V_δ} corresponds to increasing value V_δ, or "height" of the shell. It was investigated whether an increase in this value would make the collision more "sudden" and hence bring about better agreement between the IOS and exact calculations.

Table 28 displays the results of this calculation. Initial conditions were set with j'=0 and translational energy equivalent to 300K

Table 28: Exact and IOS Cross Sections at 300K for C_{V_6} =1000

Part A: Exact Results. Units are in Å^2 *. j' denotes initial state, j the final state.*

	j'=0	j'=2	j'=4	j'=6	j'=8
j=0	198.63	0.59	0.07	0.01	0.001
j=2	2.80	203.92	0.70	0.09	0.01
j=4	0.52	1.08	202.36	0.35	0.04
j=6	0.08	0.15	0.37	202.12	0.17
j=8	0.006	0.01	0.03	0.12	205.62

Part B: IOS Results.

	j'=0	j'=2	j'=4	j'=6	j'=8
j=0	199.87	0.54	0.16	0.022	0.0029
j=2	2.19	201.74	1.21	0.16	0.021
j=4	0.92	1.91	202.42	0.64	0.087
j=6	0.47	0.86	1.93	201.97	0.39
j=8	0.29	0.46	0.94	0.86	202.46

Part C: Ratio of IOS to exact cross sections.

	j'=0	j'=2	j'=4	j'=6	j'=8
j=0	1.006	0.90	2.36	2.06	2.50
j=2	0.78	0.989	1.73	1.77	2.17
j=4	1.76	1.77	1.000	1.81	2.46
j=6	5.65	5.89	5.17	0.999	2.22
j=8	48.40	42.04	37.40	7.36	0.985

While the values in Table 28 indicate that changing parameter C_{V_δ} does not improve agreement for inelastic cross sections, it does show that the IOS elastic cross sections do improve in their agreement with exact results. In Table 5 with C_{V_δ} =100, elastic cross sections are out by about 20%, whereas in Table 28, with C_{V_δ} =1000, the IOS elastic cross sections agree to within about 1% with exact values.

Note also that increasing parameter C_{V_δ} increases elastic cross sections and decreases inelastic cross sections in general.

4.5 Changing Parameter a

It was investigated whether reducing the parameter a, the delta-shell radius, would increase the agreement between IOS and exact results. The motivation behind this investigation is that a smaller radius would correspond to a shorter time of interaction between the atom and diatom and make for a more sudden collision.

The initial conditions were chosen with j'=0 and the translational energy corresponding to 300K. The results are shown in Table 29.

Table 29: Exact and IOS Cross Sections at 300K for a=0.55Å^{-1}

Part A: Exact Results. Units are in Å^2 *. j' denotes initial state, j the final state.*

	j'=0	j'=2	j'=4	j'=6	j'=8
j=0	2.29	0.0063	0.00076	0.00011	0.0000051
j=	0.030	2.33	0.0091	0.0013	0.000068
j=4	0.0056	0.014	2.29	0.0026	0.00025
j=6	0.00082	0.0021	0.0028	2.35	0.0018
j=8	0.000026	0.000075	0.00018	0.0012	2.47

Part B: IOS Results.

	j'=0	j'=2	j'=4	j'=6	j'=8
j=0	2.21	0.0068	0.00089	0.00062	0.000064
j=2	0.018	2.22	0.0081	0.0040	0.00046
j=4	0.0076	0.027	2.28	0.014	0.0017
j=6	0.0044	0.016	0.013	2.31	0.0069
j=8	0.0033	0.010	0.0039	0.018	2.35

Part C: Ratio of IOS to exact cross sections.

	j'=0	j'=2	j'=4	j'=6	j'=8
j=0	0.96	1.1	1.16	5.82	13
j=2	0.61	0.95	0.89	3.08	6.8
j=4	1.4	1.9	0.99	5.23	6.9
j=6	5.4	7.2	4.5	0.98	3.72
j=8	126	139	22	15	0.95

The first observation to be made from Table 29 is that cross sections in both the exact and IOS calculations are drastically reduced, about 2 orders of magnitude for both elastic and inelastic collisions from their values when a =5.5 Å^{-1} . Yet even at these reduced values the IOS still overestimates inelastic collisions. Elastic collisions agree to within about 5%.

The results of the last two tables indicate that something more complex than reaction time considerations may be required to further improve the IOS reliability for inelastic cross sections. Another useful investigation involving adjusting a collision parameter would be to decrease the anisotropy parameter b_2. Yet another would be to calculate cross sections for a lighter system, eg., He-N_2.

5 DISCUSSION

5.1 Time Savings of the IOS

One of the most attractive features of the IOS approximation is its computational efficiency. Matrix manipulation is greatly reduced and the programs required for calculations are shorter and much quicker than those for the exact calculations. Table 30 lists the computer time required for the IOS and exact calculations presented in this study. It lists the times in seconds required for program compilation and execution for the cross sections calculated in the previous chapter. The 300K calculation was done on an Amdahl 470V8 and the 1000K calculation on an Amdahl 5840.

Table 30: Computer Time Required for IOS and Exact Calculations

Temperature	IOS Calculation	Exact Calculation
300K	30.0	67.3
1000K	64.0	1000.0

As previously noted, the IOS becomes more accurate at higher collision energies [30], [44]. This feature of the IOS, coupled with the fact that at higher

energies the exact solution requires a far greater amount of calculation make the IOS a very attractive alternative to close-coupled calculations at high energies.

5.2 Possible Improvements to the IOS

In replacing values k_j and λ by parameters k_0 and Λ_0 in (29), the IOS allows for an easier method of calculation which, depending on the conditions of the collision process, may or may not be an accurate reflection of the exact results. Certain modifications to the IOS are proposed in this section which may serve to enhance the accuracy of the approximation.

One promising result is that the ECIOS proved to correct high IOS inelastic cross sections. A possible extension to this study could be to:

1) improve the calculation of the τ value, and,

2) extend the ECIOS correction to include a Centrifugal Sudden correction where τ would be dependent on λ as well as j.

A correction to the ECS proposed by Richard and DePristo [45] does not improve the agreement with exact cross sections. Even if it did improve the agreement, applying such a correction to the values presented in this work may not be as effective as correcting for the CS approximation, as was done by McLenithan and Secrest [46]:

$$\frac{\partial}{\partial \bar{l}_j}\mathbf{S}^{CS} = -\frac{1}{2i}\int_0^\infty \left[\psi^{CS}(R)\right]^T \frac{(2\bar{l}+1)}{R^2}\delta^j\psi^{CS}(R)dR + \frac{i\pi}{2}(\mathbf{S}^{CS}\delta^j + \delta^j\mathbf{S}^{CS}) \tag{228}$$

where $\mathbf{S}^{CS}$ is the CS S-matrix, $\bar{l}$ is λ_0 and δ^j is a null matrix, save for its jth

diagonal element, which equals unity. The above is essentially a first order perturbative correction to the CS scattering matrix, where that part of the Hamiltonian neglected by the IOS is calculated and then applied as a correction to the approximation. A first order correction has been shown to improve the CS results for cross sections involving m transitions [46].

Another way of correcting for the CS approximation could be to split the free motion Hamiltonian into a radial and angular part and from this get

$$H_{\text{free}} = H_{\text{radial}} + H_{\text{angular}} \tag{229}$$

in order to get a correction term something like

$$\sigma^{CCIOS}_{j \leftarrow j'} = \sum_{\lambda\lambda'} \frac{24\hbar^2}{24\hbar^2 + (\epsilon_{\lambda'} - \epsilon_{\lambda})^2\tau^2} \sigma^{IOS}_{\lambda \leftarrow \lambda'} \tag{230}$$

Equations (229) and (230) are at best very sketchy and the details remain to be worked out.

5.3 Applications of the IOS

Since its introduction in 1974 [3, 6] the IOS has been used in a variety of chemical systems and processes. Examples of its usefulness can be found in papers dealing with the Senftleben-Beenakker effect [47], calculation of pressure broadening cross sections [48], calculation of molecular fragmentation [49], angular momentum alignment due to collisions [50], and modeling potential parameters [51]. Two particular areas of study are mentioned, namely using the IOS for collisions

involving vibrational transitions and using the IOS in the calculation of reaction cross sections.

The Vibrational Infinite Order Sudden Approximation (VIOSA) is an approximation which deals with the vibrational quantum number n the same way the rotational quantum numbers j and λ are dealt with in the IOS. This idea was suggested by Pack in 1974 [3] and then formally derived by Pfeffer in 1985 [52]. Pfeffer obtains the following equation for the VIOSA:

$$\left[\frac{d^2}{dR^2}+\frac{2}{R}\frac{d}{dR}+k_{nj}^2-\frac{\lambda(\lambda+1)}{R^2}\right]\left\langle \hat{r},\hat{R}\middle|\chi_{nj\lambda}(r,R)\right\rangle=\frac{2\mu}{\hbar^2}V(\mathbf{r},\mathbf{R})\left\langle \hat{r},\hat{R}\middle|\chi_{nj\lambda}(r,R)\right\rangle \tag{231}$$

The only difference between (231) and (74) is that the parameter k_{nj}^2 has an extra subscript — n — that comes about by replacing operator k^2 with the parameter k_{nj}^2. This is equivalent to assuming that the duration of interaction is much less than the time required for a vibration of the diatom. Results are encouraging and give reasonable agreement with exact quantum results [52] .

The Reactive Infinite Order Sudden (RIOS) approximation was developed in 1980 by Bowman and Lee [53] and by Khare, Kouri and Baer [54]. Most work so far is on the atom – diatom system, eg. H and H_2. As an A+BC system, there are three arrangement channels to consider, A+BC (α arrangement), AC+B (β arrangement) and AB+C (γ arrangement), each with its own set of coupled equations and potential function. The goal in reaction theory is to solve for these three sets of coupled equations while matching the wave functions ψ_α, ψ_β and ψ_γ so that the functions and first derivatives are continuous at the boundaries.

The IOS is used in decoupling each of the three separate blocks of equations and since the angular momentum operators have been replaced by parameters, the matching conditions are simpler as well (eg. setting $\Lambda^2_{0\alpha} = \Lambda^2_{0\beta}$ on the matching surface) where $\Lambda^2_{0\alpha}$ is the parameter replacing the operator Λ^2 for the α set of coupled equations and $\Lambda^2_{0\beta}$ for the β set. Work is continuing on the RIOS theory, which is proving to be a valuable approach to study chemical reactions [55].

Work on the IOS approximation and the exploration of new areas where it may be applied is attractive not only because of the substantial saving in calculation time that the IOS affords but also because it is through comparison of exact and IOS results that a further understanding of the underlying details which make up the final results is achieved. Through work such as this it is hoped that a fuller knowledge of the dynamics of chemical systems may be developed.

5.4 Molecular Potentials

5.4.1 Time Savings of the Delta-Shell

Since use of the delta-shell potential allows an R-integration step to be avoided that would otherwise be needed if a continuous potential was used, computations using the delta-shell potential are much simpler and faster than those using a continuous potential. Table 31 compares the computer time needed in the calculation of the elastic cross sections reported in Table 1.

Table 31: Computer Time Required for IOS Calculations for a Continuous and Delta-Shell Potential

The calculations were done on an Amdahl 5840.

Type of Potential	Time in Seconds
Delta-Shell	2.446
Inverse Power	3.562

5.4.2 Comparison of Potential Parameters

For purposes of comparing the effect of modelling an inverse power potential with a delta-shell potential, a way of comparing the inverse power potential parameters and the delta-shell potential parameters used in this study is presented in this section.

There are two factors which must be taken into account in comparing the relative strengths of the potentials. Firstly the parameters are of different units, the inverse power potential having a parameter in units of J-m^{12} and the delta-shell potential having a parameter in units of J-m^{-1}. Further, the potentials go to infinity at different points, the delta-shell at a = 5.5x10^{-10}m. and the inverse power at R = 0m. One method of comparison is to integrate the delta-shell potential over the a region of space from R = 0m. to R = 5.5x10^{-10} m. Then the inverse power potential will be assigned a *constant* value, namely, that value it has at R = 5.5x10^{-10}m. and then integrated over the same region of space. The two resulting energy-distance values obtained will then be compared.

Equation (198) gives the following value for the inverse power potential at $R =$ 5.5x10^{-10}m.:

$$V^{\text{inverse power}}(5.5 \times 10^{-10} m., \theta) = 2.911 \times 10^{-23} \text{J}\,[1 + 0.5 P_2(\cos\theta)] \qquad (232)$$

Integration of this value over the region $R =$ 0m. to $R =$ 5.5x10^{-10}m. leads to the following energy-distance value:

$$\int_{r=0}^{r=a} V^{\text{inverse power}}(5.5 \times 10^{-10} m., \theta) = 1.6 \times 10^{-32}\,[1 + 0.5 P_2(\cos\theta)]\,J - m \qquad (233)$$

Integrating the delta-shell potential over the same region of space gives the following value for comparison:

$$\begin{aligned} \int_{r=0}^{r=a} V^{\text{delta shell}} dr &= \int_{r=0}^{r=a} 3.697 \times 10^{-32}\,[1 + 1.5 P_2(\cos\theta)]\,\delta(r-a) dr \\ &= 3.70 \times 10^{-32}\,[1 + 1.5 P_2(\cos\theta)]\,\text{J} - \text{m} \end{aligned} \qquad (234)$$

Hence the area under the delta-shell used in this investigation is roughly twice what one would obtain with a square well potential extending from $R =$ 0m. to $R =$ 5.5x10^{-10} m. having a height that is given by the inverse power potential at $R =$ 5.5x10^{-10}m.

Another parameter to consider is the value for a, the position of the delta-shell. This value will be compared with the point where the inverse power potential becomes equal to the kinetic energy of the relative motion of the atom-diatom. Equating

$$V^{\text{inverse power}} = \frac{2.2 \times 10^{-14} \times [10^{-10}]^{12}}{R^{12}} J - m^{12}\,[1 + 0.5 P_2(\cos\theta)] = \frac{\hbar^2 k^2}{2\mu} \qquad (235)$$

where k = 14.27x10^{10}m^{-1} and μ = 2.73x10^{-26} kg. gives a value for R of 3.63x10^{-10}m. This is to be compared with the value of a= 5.5x10^{-10}m. A possible algorithm to determine magnitudes for delta-shell parameters in order to model an inverse power potential with a delta-shell potential could be:

- choose a to be twice the distance where the inverse power potential is equal to the relative kinetic energy of the atom-diatom
- choose the strength parameter V_δ to be twice the product of the strength of the inverse power potential at a and the distance a.

The final comparison is that for the anisotropy parameter. The inverse power potential uses 0.5 while the delta-shell requires a parameter of 1.5 to give equivalent 0←0 and 2←0 cross sections.

The comparison presented offers a quick method of comparing the two types of potentials. As for future delta-shell potential modelling, many possibilities exist. Another repulsive shell could be added to determine if the higher transitions, eg. 0←4, 0←6, ... can be matched with the inverse power potential cross sections. One could try to model the attractive part of a molecular potential with a delta-shell. Finally, an attractive and repulsive delta-shell could be combined in order to give a reasonable approximation to an actual molecular potential. The fact that 0←0 and 2←0 cross sections from the inverse power and delta-shell potentials can be matched fairly closely (see Table 1) is a promising note for future development of how to make a delta-shell to replace a continuous potential.

5.5 Calculations on a PC

The advent of a world wide standard PC in 1981 has resulted in improved portability of computer programs and availability of computing resources. Once a program is debugged and running successfully it is no longer necessary to change the source code to conform to the standards of the mainframe of the institution that the scientist is working at or visiting.

One other advantage is in the area of numerics. Overflows of the order of 10^{67} that could not be handled by a mainframe are handled easily by Microsoft Fortran 5.1 (which can handle values up to 10^{387}).

There are however still disadvantages with using a PC. Two of the main concerns are limited memory and a slower CPU (depending on machines used for comparison).

6 CONCLUSIONS

Many useful and interesting results have come about from this investigation of the IOS and delta-shell potential. The following is a summary of the most important results, as well as a summary of what further investigations may be performed in light of these results.

It was found that cross sections from a θ dependent delta-shell can be computed that are comparable to a more realistic potential, such as an inverse-power potential. Further studies may include various combinations of repulsive and attractive delta shell potentials.

This work suggests future work in many areas may prove beneficial, such as further investigating how to model a continuous potential (such as a Lennard-Jones) with a delta-shell potential. Perhaps a hard sphere repulsive (since it is non-penetrable) and non-spherical attractive delta-shell may offer a combination of ease of computing and a fairly realistic model of certain systems.

Expressions for the T-matrices have been derived from the exact and IOS solutions for an atom-diatom system with a θ-dependent delta-shell potential. As well, the rotor transition cross sections have been calculated for a variety of energies. The exact and IOS cross sections were then compared. At translational

energies corresponding to 300K and 1000K the cross sections were found to be reasonable but at high rotational energy transfer the IOS consistently overestimated the values.

Several scaling laws aimed at improving the IOS cross sections were investigated. These all are based on the IOS $\sigma_{L\leftarrow 0}$ cross sections. The Accessible States Scaling Relation, an approximate scaling law based on angular momentum transfer of the rotor states was found not to be a significant improvement over regular IOS scaling laws at 300K. The General S-Matrix Scaling Law, based on a scaling based on reaction times and rotor energy separation was found to be useful in some cases in correcting for the large inelastic cross sections given by the IOS approximation.

The Energy Corrected Scaling Law, based entirely on correcting for the IOS S matrix with a reaction time parameter τ was found to correct very well for IOS differences from exact results for 300K. The τ values that worked best were found to be 1/10th to 1/5th that calculated for the time it takes an atom to traverse the diatom potential shell.

The scaling laws also were investigated as to how well they performed using exact $\sigma_{L\leftarrow 0}$ cross-sections. All four scaling laws performed very well at 300K. This suggests that there exists for the delta-shell potential a quick way of calculating other transitions from the $\sigma_{L\leftarrow 0}$ cross sections.

Various choices for the k_0 parameter were investigated as to whether they affected the IOS results, but it was found that changes in its value did not

significantly improve agreement with exact values.

Inclusion of closed channels was not found to significantly affect the results.

Increasing the parameter C_{V_δ} improved both elastic and downwards transitions but upwards transitions became worse.

Decreasing the parameter a brought about very good agreement between exact and IOS results on elastic cross sections, but not for inelastic cross sections.

The savings in computational time was found to be very significant in each of the approximations considered. Using a delta-shell was far simpler and quicker than using the standard Lennard Jones potential. And using the IOS approximation on this delta-shell potential was found to be much easier than using the exact calculations for the same situation. This suggests that investigations into further improvements to the delta-shell potential and IOS approximation may prove beneficial to shedding light on problems that have been impossible to solve with conventional potentials and computing procedures.

References

[1] A. M. Arthurs and A. Dalgarno. *Proc. R. Soc. London, Ser. A*, 256:540, 1960.

[2] W.A.Lester, Jr. The N coupled-channel problem. In W. H. Miller, editor, *Dynamics of Molecular Collisions, Part A*, pages 1–32, Plenum Press, New York, 1976.

[3] R. T. Pack. *J. Chem. Phys.*, 60:633, 1974.

[4] S. I. Drozdov. *Sov. Phys. JETP*, 1:591, 1955.

[5] D. M. Chase. *Phys. Rev.*, 104:838, 1956.

[6] T. P. Tsien and R. T. Pack. *Chem. Phys. Lett.*, 6:54, 1970.

[7] T. P. Tsien and R. T. Pack. *Chem. Phys. Lett.*, 6:400, 1970.

[8] T. P. Tsien and R. T. Pack. *Chem. Phys. Lett.*, 8:579, 1971.

[9] R. T. Pack. *Chem. Phys. Lett.*, 14:393, 1972.

[10] T. P. Tsien, G. A. Parker, and R. T. Pack. *J. Chem. Phys.*, 59:5373, 1973.

[11] P. McGuire and D. J. Kouri. *J. Chem. Phys.*, 60:2488, 1974.

[12] G. A. Parker and R. T. Pack. *J. Chem. Phys.*, 68:1585, 1978.

[13] K. Takayanagi. *Prog, Theoret. Phys. (Kyoto) Suppl.*, 25:40, 1963.

[14] H. Rabitz. *J. Chem. Phys.*, 57:1718, 1972.

[15] G. A. Parker and R. T. Pack. *J. Chem. Phys.*, 66:2850, 1977.

[16] Y. Shimoni and D. J. Kouri. *J. Chem. Phys.*, 65:3372, 1976.

[17] Y. Shimoni and D. J. Kouri. *J. Chem. Phys.*, 66:675, 1977.

[18] Y. Shimoni and D. J. Kouri. *J. Chem. Phys.*, 65:3958, 1976.

[19] L. Monchick and E. A. Mason. *J. Chem. Phys.*, 35:1676, 1961.

[20] D. Secrest. *J. Chem. Phys.*, 62:710, 1975.

[21] L. W. Hunter. *J. Chem. Phys.*, 62:2855, 1975.

[22] C. F. Curtiss. *J. Chem. Phys.*, 49:1952, 1968.

[23] L. D. Knutson. *Phys. Rev. C*, 18:1032, 1978.

[24] L. P. Kok, J. W. de Maag, H. H. Brouwer, and H. van Haeringen. *Phys. Rev. C*, 26:2381, 1982.

[25] S.M. Blinder. *Phys. Rev. A*, 18:853, 1978.

[26] P. Lloyd. *Proc. Phys. Soc.*, 86:825, 1965.

[27] A. R. Edmonds. *Angular Momentum in Quantum Mechanics.* Princeton University Press, Princeton, New Jersey, 1960.

[28] R. F. Snider. *J. Chem. Phys.*, 76:3547, 1982.

[29] A. Das and A. C. Melissinos. *Quantum Mechanics: A Modern Introduction.* Gordon and Breach Science, Rochester, N.Y., 1986.

[30] D. J. Kouri, T. G. Heil, and Y. Shimoni. *J. Chem. Phys.*, 65:1462, 1976.

[31] Roger G. Newton. *Scattering Theory of Waves and Particles.* McGraw-Hill Book Company, New York, 1966. p.573.

[32] A. E. DePristo, S. D. Augustin, R. Ramaswamy, and H. Rabitz. *J. Chem. Phys.*, 71:850, 1979.

[33] A. E. DePristo and H. Rabitz. *Chemical Physics*, 24:201, 1977.

[34] P. A. M. Dirac. *The Principles of Quantum Mechanics.* Oxford University, Oxford, 1947. p.60.

[35] M. Abramowitz and I. A. Stegun. *Handbook of Mathematical Functions.* Dover, New York, 1972.

[36] D. Secrest. Vibrational excitation: quantal treatment. In R. B. Bernstein, editor, *Atom Molecule Collision Theory: A Guide for the Experimentalist*, page 388, Plenum, New York, 1979.

[37] P. Cress, P. Dirksen, and J. W. Graham. *Fortran IV with Watfor and Watfiv.* Prentice-Hall Inc., Englewood Cliffs, New Jersey, 1970. p.247.

[38] P. G. Kistemaker and A. E. deVries. *Chem. Phys.*, 7:371, 1977.

[39] M. D. Pattengill, R. A. LaBudde, R. B. Bernstein, and C. F. Curtiss. *J. Chem. Phys.*, 55:5517, 1971.

[40] R. F. Snider and D. A. Coombe. *J. Chem. Phys.*, 86:1164, 1982.

[41] Tom Nicol. *UBC Matrix: A Guide to Solving Matrix Problems.* University of British Columbia Computing Centre, Vancouver, 1982. p.40.

[42] A. M. Turing. *Quarterly Journal of Mechanics and Applied Mathematics*, 1:287, 1948.

[43] S. Chapman and S. Green. *Chem. Phys. Let.*, 112:436, 1984.

[44] Z. H. Top and D. J. Kouri. *Chem. Phys.*, 37:265, 1979.

[45] A. M. Richards and A. E. DePristo. *Chemical Physics*, 69:273, 1982.

[46] K. McLenithan and D. Secrest. *J. Chem. Phys.*, 80:2480, 1984.

[47] R. F. Snider. *J. Chem. Phys.*, 81:3482, 1984.

[48] G.C. Corey and F.R. McCourt. *J. Chem. Phys.*, 81:3892, 1984.

[49] O. Atabek, J.A. Beswick, and G. Delgado-Barrio. *J. Chem. Phys.*, 83:2954, 1985.

[50] V. Khare, D. J. Kouri, and D. K. Hoffman. *J. Chem. Phys.*, 74:2275, 1981.

[51] M. Keil and G. A. Parker. *J. Chem. Phys.*, 82:1947, 1985.

[52] G. A. Pfeffer. *J. Phys. Chem*, 89:1131, 1985.

[53] J.M. Bowman and K.T. Lee. *J. Chem. Phys.*, 72:5071, 1980.

[54] V. Khare, D. J. Kouri, and M. Baer. *J. Chem. Phys.*, 71:1188, 1979.

[55] J. Jellinek. *Chem. Phys. Let.*, 114:210, 1985.